LITHOFACIES, DEPOSITIONAL ENVIRONMENTS, BURIAL DIAGENESIS, AND DYNAMIC FIELD BEHAVIOR IN A CARBONIFEROUS SLOPE RESERVOIR, TENGIZ FIELD (REPUBLIC OF KAZAKHSTAN), AND COMPARISON WITH OUTCROP ANALOGS

JOEL COLLINS
ExxonMobil Development Company, 16945 Northchase Drive, GP 4, Rm 564, Houston, Texas 77060, USA
e-mail: joel.f.collins@exxonmobil.com

WAYNE NARR, PAUL M. (MITCH) HARRIS, AND TED PLAYTON
Chevron Energy Technology Company, 1500 Louisiana Street, Houston, Texas 77002, USA

STEVE JENKINS AND TERRELL TANKERSLEY
TengizChevroil, 3 Satpayev Street, 060011 Atyrau, Republic of Kazakhstan

AND

JEROEN A.M. KENTER*
Chevron Energy Technology Company, San Ramon, California 94583, USA
**Present address: Statoil ASA, Sandsliveien 90, 5254 Bergen, Norway*

ABSTRACT: Tengiz Field is a steep-sided, isolated carbonate platform in the Precaspian Basin, Kazakhstan, with hydrocarbon production from Carboniferous platform and slope facies. Systematic differences in reservoir pressure decline during production indicate that this reservoir consists of three subcompartments or material balance regions: (1) a central "platform reservoir" made up of cyclic platform-top facies that acts like a single, stratified, multistory reservoir; (2) a "wedge reservoir" formed by a prograding margin containing upper slope microbial facies; and (3) an "apron reservoir" containing allochthonous facies deposited in deep water around the base of the buildup. The facies in the apron reservoir accumulated during an early depositional stage and were subsequently partly to fully buried by prograding microbial slope facies of the wedge reservoir. The wedge and apron reservoirs together form a succession 800 to 1000 m thick within the Tengiz oil column.

The wedge reservoir shows uniform pressure decline with time and is well connected. Field data (cores and well logs) are insufficient to determine internal continuity of lithofacies and depositional environments or to quantify the pore network responsible for the high connectivity. An outcrop analog (Asturias, Spain) with facies matching those observed in Tengiz cores was used to predict that the microbial lithofacies form a distinct and continuous mechanical unit within the wedge reservoir. Tengiz microbial facies contain a high concentration of solution-enlarged, syndepositional and other early fractures oriented parallel and normal to depositional strike. Borehole image logs provide data on enlarged fracture apertures and local fracture density, but no data related to fracture height or length. An outcrop analog with early fractures in similar facies (Windjana Gorge, Australia) was used to obtain large-scale height and spacing data for solution-enlarged syndepositional fractures. Dissolution processes in the outcrop are different from those of Tengiz, but the fracture aperture and cavern sizes are comparable to their known counterparts in the Tengiz wedge reservoir, and application of the outcrop height data to geologic models of the Tengiz wedge subcompartment can account for its dynamic behavior. The apron reservoir shows a nonsystematic pressure decline with time and is less depleted than the wedge reservoir. The irregular decline indicates reduced internal connectivity within the apron reservoir, which is corroborated by core and borehole image data indicating high lithofacies heterogeneity and the absence of continuous microbial facies responsible for reservoir continuity in the wedge reservoir. A reservoir pressure increase of 1700 psi from the wedge reservoir to the apron reservoir observed in a single well penetration suggests reservoir communication between them may be reduced across a stratigraphic baffle.

The wedge and apron reservoirs both contain a late burial matrix diagenetic overprint represented mainly by co-precipitated bitumen and calcite cement and local development of matrix microporosity. Enlargement of the early fractures in the wedge reservoir also occurred during burial diagenesis based on the presence of diagenetic halos containing the burial overprint around the fractures and based on the presence of co-precipitated bitumen and calcite in the fractures. Scenarios and mechanisms for fracture enlargement are evaluated against the observations from field data and the outcrop analogs.

KEY WORDS: Carboniferous, carbonate slope, Kazakhstan, Tengiz Field, burial diagenesis

INTRODUCTION

Tengiz and other similar nearby buildups in the Primorsk Archipelago (Fig. 1) are significant hydrocarbon-bearing carbonate reservoirs of onshore and offshore Kazakhstan. The Tengiz buildup measures 15 by 8 km wide and occupies an area of approximately 112 sq km around the crest of the structure. Tengiz Field was discovered in 1979 and has been operated in-country by TengizChevroil (TCO) since 1993. The field has elevated levels of H_2S (13.4%) dissolved in the oil, and insoluble hydrocarbons (bitumen) affect reservoir quality in parts of the field. Weber et al. (2003) developed the stratigraphic framework, general lithofacies, porosity, platform architecture, and growth history of the Tengiz buildup based on an integrated interpretation of seismic logs, cores, and an early biostratigraphic

Deposits, Architecture and Controls of Carbonate Margin, Slope and Basinal Settings
DOI: 10.2110/sepmsp.105.11
SEPM Special Publication No. 105, Copyright © 2013
SEPM (Society for Sedimentary Geology), Print ISBN 978-1-56576-323-4, CD/DVD ISBN 978-1-56576-324-1, p. 50–83.

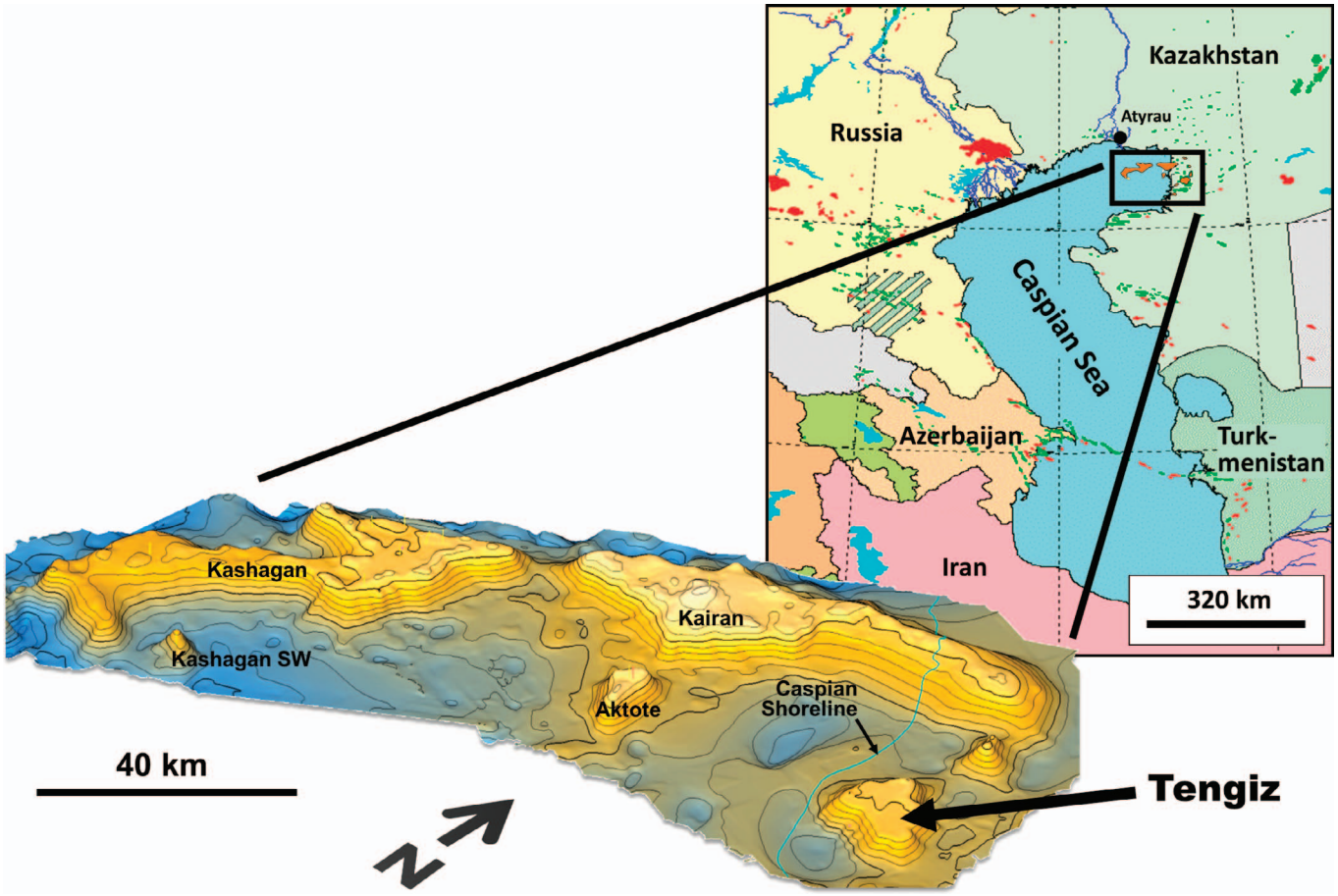

FIG. 1.—Oil/gas fields in the greater Caspian region, with an oblique structural view showing the location of the Tengiz buildup relative to Kashagan, Aktote, Kairan, and other carbonate buildups in the Primorsk Archipelago.

analysis of key wells (Brenckle and Milkina 2003). The distribution of facies and major controls on reservoir quality were subsequently described in more detail in Kenter et al. (2006) and Collins et al. (2006).

The Tengiz Field has historically been subdivided into the geographic regions of platform, rim, and flank (Fig. 2) based on systematic differences in well performance. The best rim and flank wells first lost circulation during drilling, then produced oil with multi-darcy flow. Platform wells typically produce through matrix permeability of 10 md (millidarcies) or less and encounter lost circulation only rarely. The rim, platform, and flank areas were defined by boundaries based on present-day relative structural elevation differences across the field. As their original intent was only to classify wells based on expected rate differences, they effectively amounted to vertical subsurface partitions that extend into the subsurface from the top of the buildup. For example, the rim defines the region of elevated structure along the margin of the buildup, but in the reservoir it includes all of the different lithofacies and stratigraphic intervals that underlie this elevation (Fig. 3). Similarly, the basinward-sloping flanks of the structure (which define the flank region) represent a different collection of lithofacies.

As development of the field proceeded dynamic reservoir data became available illuminating communication both within and between the platform, rim, and flank areas (e.g., King et al. 2012, Tursinbayeva et al. 2012). This article describes the dynamic behavior of three nonisolated reservoir subcompartments that form a connected hydrocarbon reservoir system within the field, the boundaries of which conform to the stratigraphic hierarchy and depositional system tracts of a large-scale, transgressive–regressive turnaround sequence. Two of these subcompartments (also called "material balance regions")—termed "wedge" and "apron"—are contained within the rim and flank regions and are the main focus of this study. Outcrop analogs were used to develop rules, paradigms, and concepts for interpreting reservoir quality distribution within and across the rim and flank material balance regions where existing core and well log data offer insufficient constraints. The remaining subcompartment, the platform material balance region, was defined based on pressure data from platform wells that demonstrated systematic pressure decline over a specific stratigraphic range within the platform area, and this subcompartment is discussed only in the context of its boundary and connection with the rim sub-compartments.

The remainder of this introductory section integrates and summarizes the geologic nature of the rim, flank, and adjacent platform areas of Tengiz. Because the controls on reservoir quality are complex, this section contains a somewhat-detailed description of diagenesis and reservoir burial history from previous Tengiz studies, which, for the purposes of this article, are treated largely as observations to support some of the conclusions presented later on

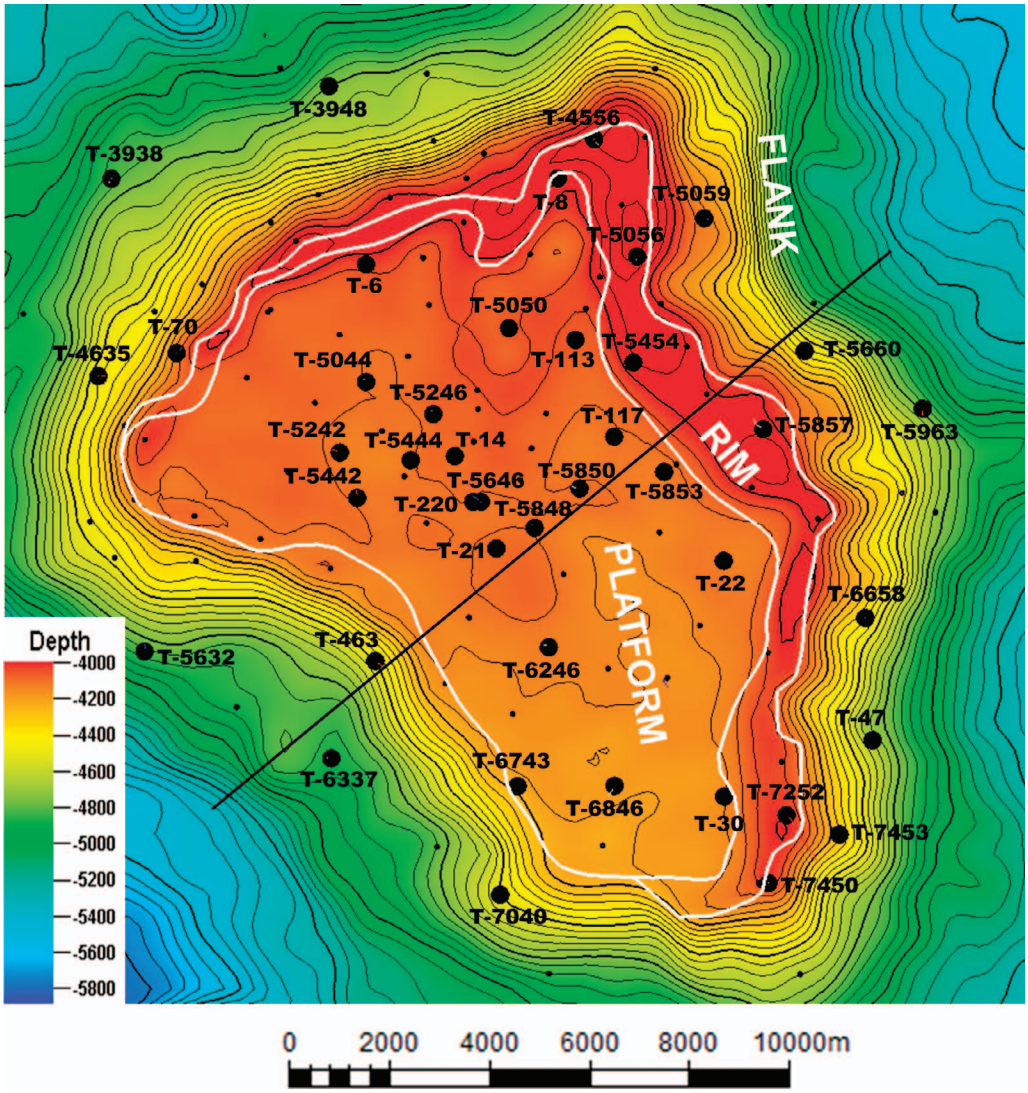

FIG. 2.—Structure map of the top of the Tengiz buildup showing the geographic distribution of the platform, rim, and flank areas and well locations discussed or illustrated in the article. The boundaries between these regions (white lines) generally follow structure contours. For example, the rim is a structurally elevated area of uneven width along the outer edge of the buildup. The black line indicates the location of the seismic profile in Figure 3. Depth scale in meters subsea.

in the "Discussion" section. The two sections following this introduction describe the subsurface characterization of the wedge and apron reservoir subcompartments with the aid of outcrop analogs. The "Discussion" section at the end ties together the burial diagenetic summary from the "Introduction" and the detailed descriptions of the wedge and apron subcompartments, with particular focus on fractures in the wedge reservoir subcompartment and its outcrop analog.

Rim–Platform Boundary and Stratigraphy

Seismic sequences in the Tengiz buildup are shown in Figure 3, corresponding to changes in platform size, geometry, and internal stratigraphy and facies. The late Visean and the Serpukhovian–Bashkirian sequences together form a large-scale transgressive–regressive system that partly controls the structural boundary between the rim and platform areas. The geographic rim–platform boundary is aligned with the margin of the late Visean seismic sequence. The late Visean sequence consists of aggradational cycles of platform-top facies (Kenter et al. 2006), while the Serpukhovian–Bashkirian sequence is a progradational margin that was deposited around the outer edge of the buildup and filled in more than 900 m of vertical relief and up to 2 km of lateral accommodation that resulted from backstepping above the Devonian and early Visean–Tournaisian sequences. The alignment between the rim elevation and the late Visean margin was interpreted to have formed during burial (Fig. 4) based primarily on two lines of evidence: (1) cores indicating the presence of an expanded Serpukhovian interval containing several hundred meters of early-lithified slope facies in the progradational

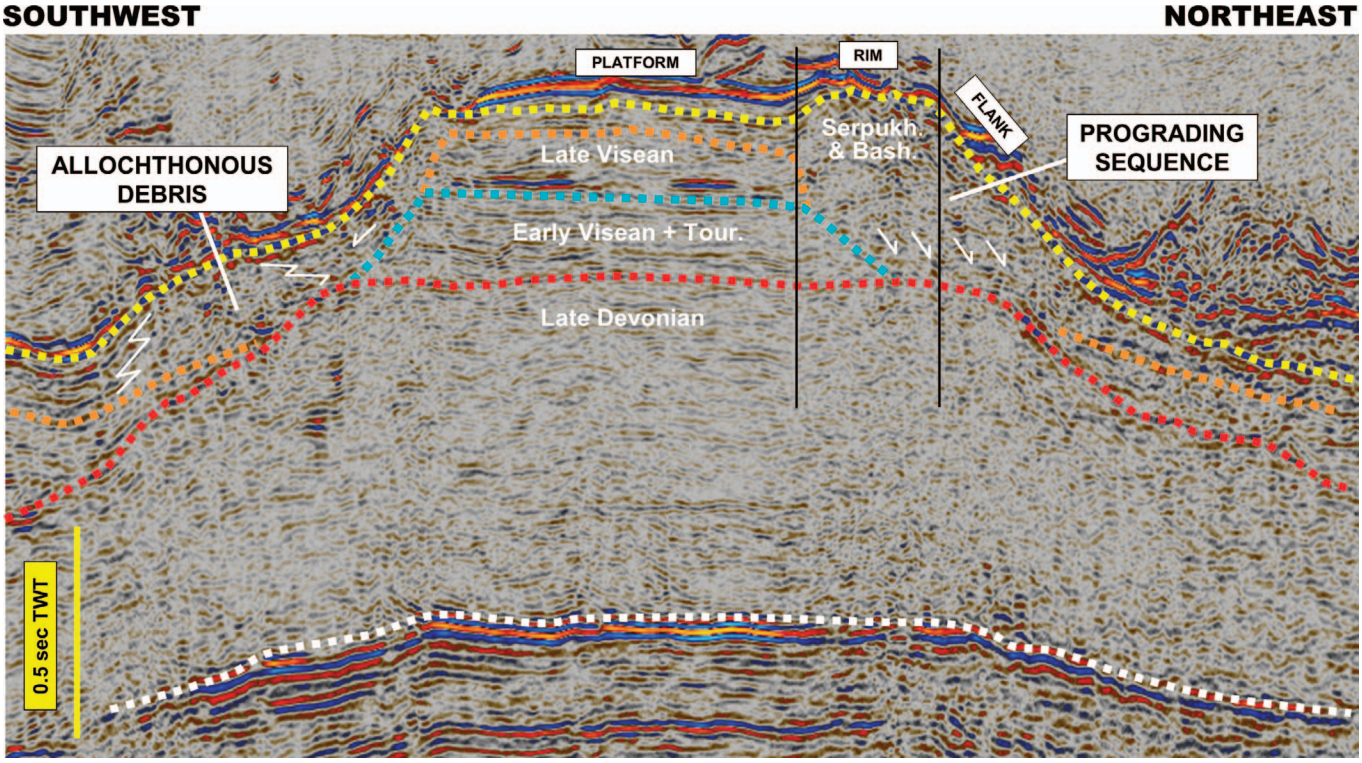

FIG. 3.—Seismic profile across the Tengiz buildup (see Fig. 2 for location) showing the major seismic sequences in the Tengiz buildup. Also shown are hypothetical boundaries (vertical black lines) corresponding to the platform, rim, and flank areas according to the structural configuration on top of the buildup. The rim overlies the Serpukhovian–Bashkirian sequence, and the rim–platform boundary aligns with the late Visean margin. The Serpukhovian–Bashkirian sequence is asymmetric around the buildup. It is dominated by allochthonous facies that form downslope bulges along the western margin and by progradation along the eastern margin (downlap arrows are inferred based on depositional facies observed in well data but are not visible in the seismic data).

sequence (Weber et al. 2003) that are not present in the adjacent platform region and (2) biostratigraphically correlative cycles of shallow marine facies in the Bashkirian, indicating that depositional surfaces were essentially flat across the buildup after progradation. The seismic data used for the original stratigraphic interpretation (e.g., Fig. 3) are not of sufficient quality to directly image a maximum flooding surface associated with the turnaround from aggradation to progradation. The trace of the elevation change between the platform and the rim areas was used to indirectly map the location of the late Visean platform margin and the inboard terminus of boundstone facies in the progradational sequence. As a result, the geographic boundary between the platform and elevated rim areas became synonymous with the margin of the late Visean platform sequence (Fig. 3).

Rim, Flank, and Platform Transition Zone (PTZ) Geology

Figure 4 shows that the Serpukhovian–Bashkirian sequence in the rim and flank area consists of three major depositional units: (1) late Visean– to Serpukhovian-aged debris aprons of allochthonous upper slope material that accumulated around the base of the buildup; (2) a mostly Serpukhovian-aged progradational system anchored by upper slope boundstone facies that partly to fully buried the debris aprons and forms a wedge; and (3) an aggradational Bashkirian platform sequence containing shallow marine platform-top and platform margin facies. These three systems tracts form a large-scale shallowing-upward succession representing water depths from more than a thousand meters to shallow high-energy conditions at sea level. As indicated in Figure 2, the width of the Serpukhovian–Bashkirian sequence comprising the rim varies unevenly around the field. It is widest along the eastern and northern margins of the buildup and narrow to absent along the western margin. The narrow sequence along the western margin is a consequence of large-scale slope failure and mass transport, the products of which are visible on Figure 3 as a distinct downslope bulge of allochthonous debris.

The lithofacies in the progradational sequence are distinct from those in the platform area; however, there is a common element of burial diagenesis related to the formation of bitumen in the field that links the rim, flank, and adjacent platform area together. The general diagenetic histories of the rim, flank, and platform regions are relatively well understood from numerous microscale observations of thin sections that are typically taken every 30 cm from Tengiz cores. This diagenesis was reviewed in Kenter et al. (2006) and Collins et al. (2006) in the context of reservoir burial history and demonstrated that Tengiz diagenesis can be broadly described in terms of two main stages relative to the formation of bitumen: an early or "pre-bitumen" phase and a later "burial overprint" that includes bitumen. Pre-bitumen diagenesis collectively includes a number of typical early marine, meteoric, and shallow burial carbonate cements, and the burial overprint collectively refers to distinctive matrix diagenetic textures observed in the presence of bitumen. Microscale textures associated with the burial overprint include (1) occlusion of primary and early diagenetic voids with equant calcite cement and bitumen; (2)

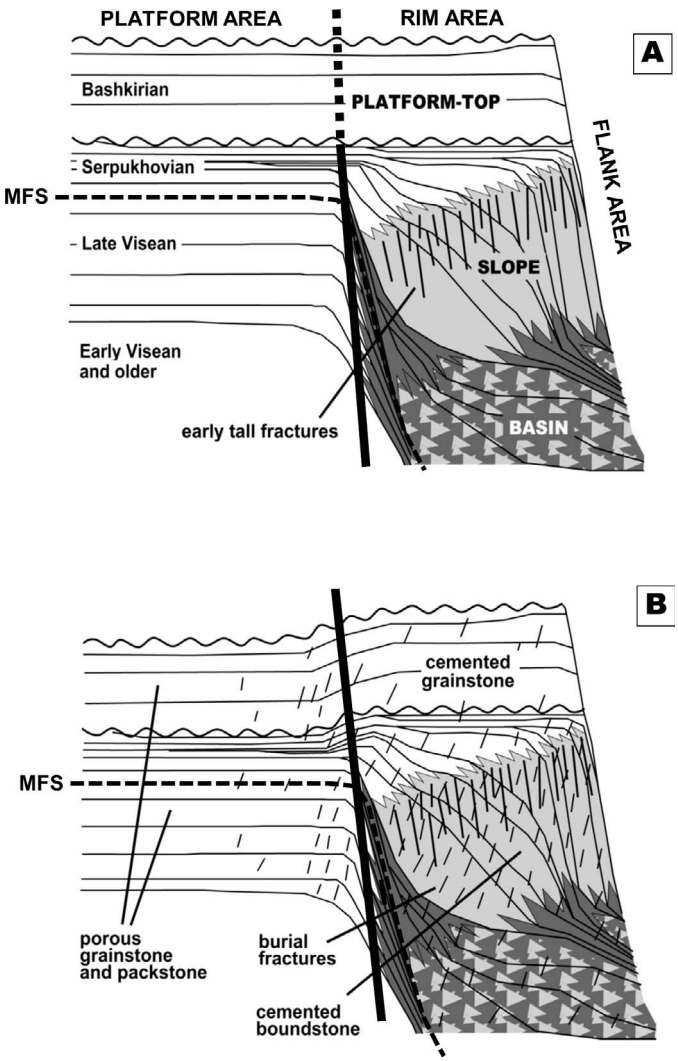

FIG. 4.—Major sequences and facies of the late Visean to Bashkirian sequences of Tengiz, shown before and after burial (not to true vertical scale): **A)** Depositional geometries for the aggradational late Visean sequence, the progradational Serpukhovian sequence, and the aggradational Bashkirian sequence. Note the Serpukhovian sequence consists of an early stage dominated by allochthonous deposition and a later stage dominated by in situ progradation of slope facies. **B)** Formation of the rim structural elevation during burial, as a result of differential compaction between early-lithified Serpukhovian slope facies and adjacent late Visean platform-top facies (see text for discussion).

occlusion of secondary microfractures with equant calcite cement and bitumen; (3) contemporaneous precipitation of calcite and bitumen; (4) corrosion of calcite where bitumen is present to form microporosity; and (5) postbitumen dissolution of calcite. In addition to the rim and flank regions, the area containing the matrix burial overprint also includes the outer margin of the adjacent platform region (Fig. 5), which is referred to as the PTZ. Like lithofacies, the area affected by the burial overprint indicated on Figure 5 represents another facet of the geology of the rim and flank area and is presented as a framework for discussions of burial diagenesis and fractures later in this article (pertaining to reservoir quality in the Tengiz reservoir subcompartments). Previous Tengiz studies also ascribe a specific timing and origin (reservoir depressurization) for the burial overprint in relation to reservoir burial history (see references on Fig. 6). A summary of the burial overprint, reservoir depressurization, and its timing is presented here as a preface to such discussions.

Burial Overprint and Matrix Porosity

The timing for the burial overprint was established from fluid inclusion data indicating precipitation temperatures of 90 to 100° C for equant calcites associated with bitumen (Collins et al. 2006). Assuming that calcite precipitation occurred at ambient reservoir temperatures, the burial overprint was temporally separated from pre-bitumen diagenesis by 100 my or more (Fig. 6). The calcite fluid inclusion data included two-phase hydrocarbon inclusions indicating that oil density increased during precipitation. Increasing oil–gas homogenization temperatures for the hydrocarbon inclusions were interpreted to indicate that one or more large reservoir pressure decreases from about 12,000 psi (approximately equal to present-day initial reservoir pressure) toward the oil bubble point (~4700 psi) occurred, resulting in increasing oil density and culminating in the formation of asphaltenes (bitumen) in the inclusions and in the reservoir (Pottorf et al. 2003, Tseng and Pottorf 2003). These studies attributed the pressure decline to a breach in the topseal and at least partial evacuation of an early hydrocarbon charge (Hallager et al. 1997, Schoellkopf and Hallager 1998, Warner et al. 2007) at the approximate timing established from ambient reservoir temperatures. The contemporaneous precipitation of bitumen and calcite commonly observed in thin sections supports this interpretation. Calcite solubility in carbonate reservoir groundwater generally increases with pressure, with variable possible impacts on porosity that depend on reservoir wettability, temperature, lithostatic vs. hydrostatic pressure controls, and other mineral reactions (Bathurst 1975, Moore 1989, Choquette and James 1990, Morse and Mackenzie 1990). A geologically sudden pressure decrease at constant temperature in the Tengiz reservoir would have favored calcite precipitation due mainly to a decrease in solubility of CO_2(g) at the same time as bitumen drop-out from oil. Subsequent repressurization at approximately constant temperature reversed this process, promoting calcite dissolution and temporarily halting bitumen formation. A series of such reservoir pressure fluctuations could thus account for the common juxtaposition of both calcite corrosion and precipitation textures adjacent to bitumen that characterizes the burial overprint.

The burial overprint can readily be identified in thin sections, cores, and in some cases on porosity logs. The diagnostic microscale textures are illustrated in Figure 7A through G. Thin sections have shown consistently that the burial overprint is present in the matrix of cored intervals containing solution-enlarged fractures. The solution-enlarged fractures are not always distinctly preserved, often generating rubble intervals, the angular pieces of which indicate a well intersection with a fracture swarm (Fig. 7H). In some cases, the rubble zones are thick (1 m or more) with rounded clasts (Fig. 7J). The burial overprint is absent from the central portion of the platform, except for the presence of stratigraphically controlled bitumen layers above certain sequence boundaries. The timing for bitumen formation in the platform (Kenter et al. 2006) is consistent with the timing established in the rim and flank areas. As indicated in Figure 5, the burial overprint has been recognized throughout the rim and flank area, in the facies of the allochthonous aprons, in the Serpukhovian progradational system, in the aggradational Bashkirian sequence, and in the PTZ along the outer margin of the late Visean platform sequence. The PTZ is based on cores containing fracture swarms and rubble zones with the burial overprint in the surrounding matrix from wells along the margin of the

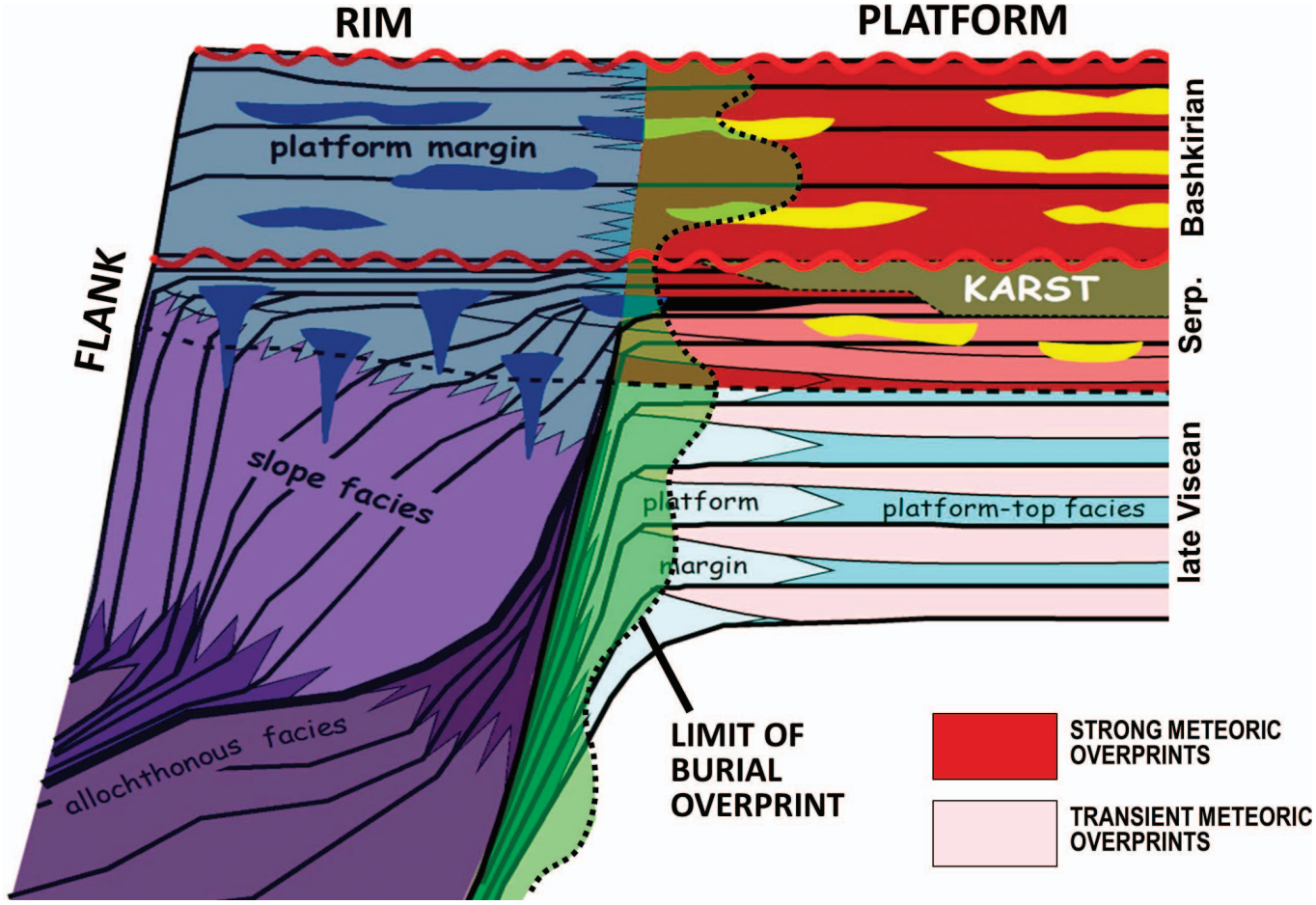

FIG. 5.—Extent of the burial overprint relative to stratigraphy, lithofacies, and large-scale diagenetic themes in the Tengiz buildup: The burial overprint occurs in the Serpukhovian apron and progradational slope facies of the rim and flank, in Bashkirian platform-top cycles in the rim, and in platform-top facies of the late Visean aggradational sequence adjacent to the rim. The burial overprint is superimposed over early marine and meteoric diagenetic patterns, including subaerial-exposure–related features (indicated with yellow- and blue-colored symbols) and is responsible for reduced matrix porosity and enlarged fractures in all three areas (see text for discussion).

platform area that also have a distinctive vertical pattern on porosity logs. Wells logs from the central portion of the platform have regular, cyclic vertical porosity variations (Fig. 8B). Logs from marginal platform wells generally display a poor relationship between porosity and depositional cycles, showing instead larger-scale vertical heterogeneity, such as intervals with anomalously high or low porosity, or pervasive porosity reduction over thick vertical intervals (Fig. 8A). Elevated radioactivity may be present as well, which spectral logs have shown is due to the presence of uranium. The anomalous log signatures are observed in platform-top facies for each of the late Visean, Serpukhovian, and Bashkirian intervals within the platform area. The observed association between the burial overprint in cores and the atypical well log signatures was used to map the PTZ for each of these intervals, but particularly for the late Visean platform sequence. The mapped PTZ forms a ring around the margin of the late Visean sequence a few hundred meters to a few kilometers wide (Fig. 9A) and reflects the spatial extent over which late burial diagenesis is also predicted to be present in the Bashkirian platform-top facies adjacent to the rim and flank (Fig. 9B).

Matrix porosity for the platform, PTZ, rim, and flank areas has been measured in cores and calculated from well logs. These data are plentiful in the platform overall, but cores with permeability data are limited from the PTZ. In the rim and flank areas, cores are an undersized, possibly unrepresentative data set relative to the total length of well penetrations, and well log porosity calculations are prone to uncertainty as a result of common zones with poor borehole conditions. The mapped PTZ is associated with a net reduction in average matrix porosity of ~3% compared to the central platform area for the late Visean interval (Fig. 9) and for the Bashkirian interval as well, where platform-top facies are present in both the platform and rim areas. The presence of the burial overprint across the PTZ contributes to porosity loss in the matrix, as indicated by the common presence in the core of bitumen and equant calcite in matrix voids from these areas (Collins et al. 2006). The PTZ and rim areas include some wells with above-average matrix porosity for the region (6.5–8.3%) in Bashkirian platform-top facies (Fig. 9B). The Serpukhovian slope and coarse allochthonous facies of the rim and flank both have pervasive low matrix porosity, with only local zones in certain wells indicating higher matrix porosity.

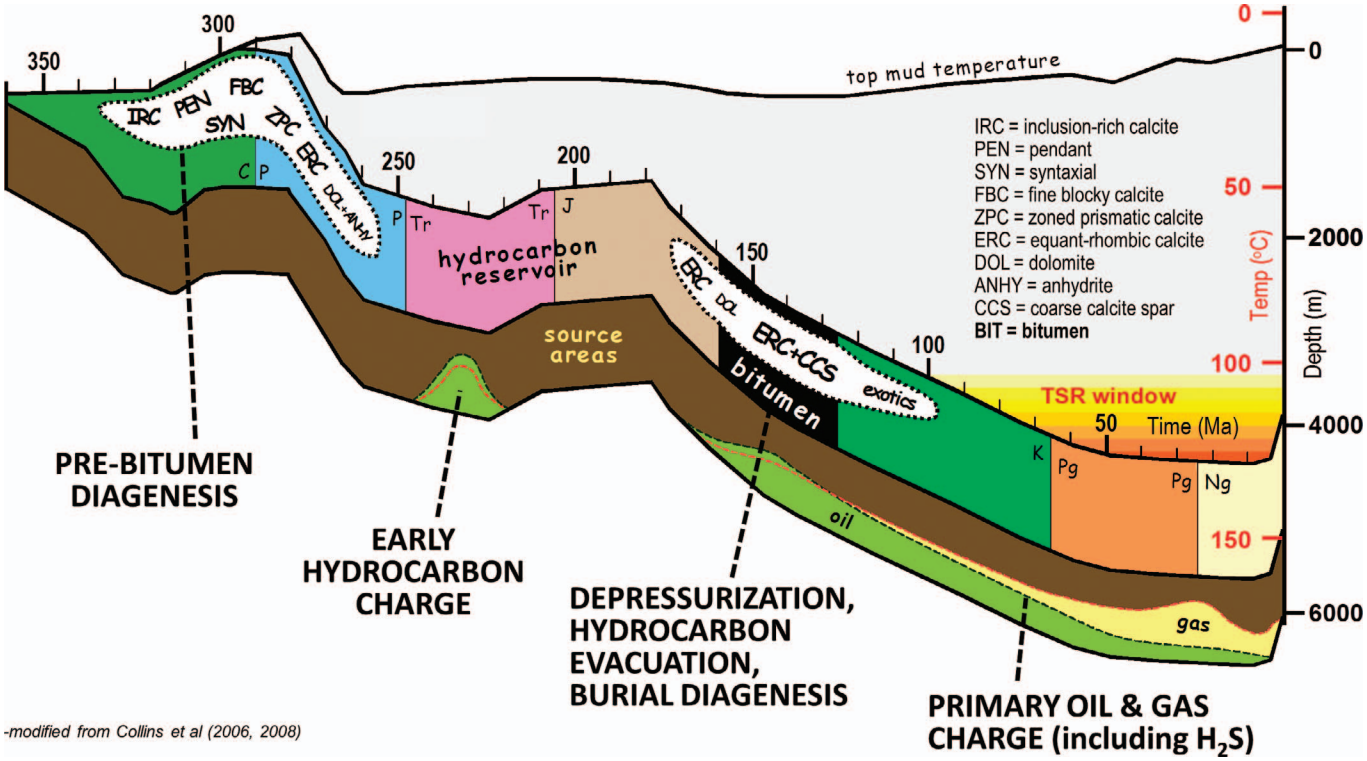

FIG. 6.—Key events in the burial and diagenetic histories of the Tengiz reservoir. Three burial curves are illustrated. The two shallow curves represent the top and base of the reservoir interval, and the deeper curve represents a range for possible local source rock depths. Time (Ma) is indicated above the upper curve, and geologic periods are shown as colored regions within the reservoir interval. Curves showing a generalized hydrocarbon flux history (modified from Pottorf et al. [2003]) are normalized relative to the width of the interval between the two deeper curves. Two major phases of Tengiz diagenesis are indicated along the burial profiles: (1) A pre-bitumen phase that encompasses early diagenesis in marine, meteoric, and shallow burial environments (with various cements present indicated by three-letter abbreviations) and (2) a later burial overprint phase associated with bitumen, equant calcite cement, and coarse calcite spar that formed during reservoir depressurization (see text for discussion). The H_2S buildup in the reservoir, interpreted to be sourced from thermochemical sulfate reduction in the basin, is shown associated with a late increase in gas charge flux.

Nonmatrix Porosity (Fractures and Caverns)

The Serpukhovian–Bashkirian sequence in the rim and flank area forms a naturally fractured reservoir (Narr et al. 2004, Carpenter et al. 2006). Our understanding of the occurrence and geometry of effective nonmatrix fractures comes mainly from borehole image (BHI) logs. Effective fractures (open fractures with significant hydraulic extent beyond the wellbore) are present in most wells drilled in the rim and flank. Cavernous porosity responsible for lost-circulation zones and bit drops during drilling operations in these regions is also recognizable on BHI logs. Open fractures and caverns, collectively referred to at Tengiz as "nonmatrix porosity" (porosity that is larger than the scale represented by cores and beyond the ability of cores or standard wireline logs to accurately quantify its volume), play an important role in the high productivity of rim and flank wells. Based on all available field data, fracture porosity in the Tengiz rim and flank is currently estimated at 0.4% (Tankersley et al. 2010). By contrast, only one well in the central platform area (T-14ST)—out of the nine platform wells studied (Fig. 10)—shows evidence of effective fractures. Effective fractures were noted in one additional well (T-6743) within the PTZ.

The BHI logs used to interpret Tengiz fractures are conventional microresistivity-based logs that were acquired in holes filled with oil-based mud; therefore, independent borehole data were used to distinguish oil-filled open fractures from fractures filled with resistive cement, such as dynamic responses at the wellbore (PLT log inflow, lost circulation), or responses on wireline logs, such as Stoneley-wave (Narr et al. 2006). Most Tengiz fractures appear to be of extensional origin (Mode I). Fracture strike trends correspond with the orientation of the local trend of the depositional margin (Fig. 10). Tengiz wells can be grouped into three sets based on dominant fracture strike direction observed in the well: wells with fractures that mostly strike parallel to the margin (e.g., wells T-70ST, T-5056, T-5963, and T-5632); wells with fractures that strike normal to the margin (wells T-463ST, T-5660, and T-6457); and wells with fractures that substantially disagree with either of these trends (wells T-3938 and T-6658). The correlation of fracture strike with the azimuth of the depositional margin implies that the stress field active at the time of fracture growth was controlled by the local topography of the margin, and we believe direct gravitational loading is the dominant source of induced stress. The high variability in fracture orientation at Tengiz suggests the stress-field orientation varied spatially or temporally as the fracture system developed. Variability in fracture azimuth may occur where

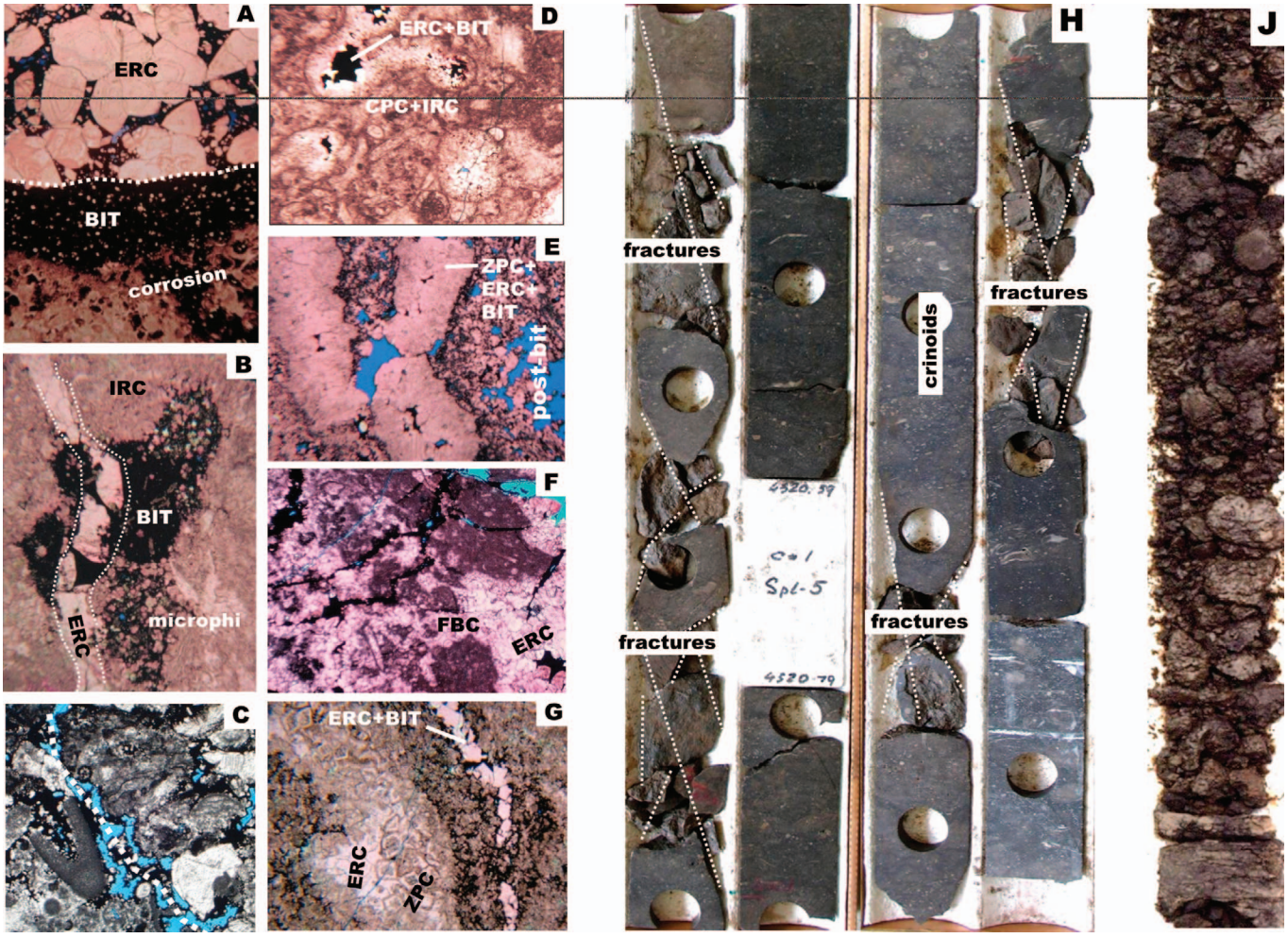

FIG. 7.—Examples of the late burial diagenetic overprint from Tengiz: **A)** Equant calcite crystals and bitumen precipitated in a geopetal void, with corrosion and microporosity present in the sediment layer and in the rock matrix adjacent to the void. **B)** Calcite and bitumen co-precipitation along a fracture. Euhedral calcite crystals inside the bitumen are aligned with earlier anhedral calcite filling a microfracture. Microporosity is present in the rock matrix associated with the bitumen, and the reprecipitated crystals within the bitumen are also slightly corroded along their outer surfaces. **C)** Postbitumen dissolution along a microchannel in low-porosity matrix with abundant interparticle bitumen. **D)** Bitumen and equant calcite precipitated as a final void fill. **E)** Postbitumen enhancement of matrix microporosity. Relict textures are voids filled with pre-bitumen cements and minor bitumen in the void centers. Bitumen is also present in microporous matrix around the voids. **F)** Bitumen precipitation in microfractures cross-cutting pre-bitumen void filling calcite cement. Note bitumen is also present in the center of a void at lower right. **G)** Co-precipitated equant calcite and bitumen in a microfracture. Bitumen and microporosity are present in the matrix adjacent to the fracture, surrounding an earlier void filled with pre-bitumen cements. **H)** Pervasive bitumen in the matrix surrounding corroded fracture-rubble (late Visean platform-top facies, T-6743). **J)** Bitumen-saturated core rubble zone due to intense fracturing and matrix corrosion (Bashkirian platform-top facies, T-5056). Thin-section photos represent low magnification (images are ~1–2 mm wide). Plug holes in cores are ~3.5 cm. Abbreviations for cements indicated are given on Figure 6.

local material heterogeneities are present, such as in the geometry of the depositional margin and related facies changes, thereby exerting control on fracture propagation, or where local variability in margin geometry induces similar variation in fracture orientation.

Successful core recovery of open fractures has been limited; hence, fracture studies in cores are biased toward those that are small or well cemented. Core material has been of value for providing details on fracture genesis and cement history and on the associations between lithofacies and fracture density. In a study of cores from 13 of the rim and flank wells shown in Figure 10, the highest fracture density occurs in microbial facies, including microbial boundstone, microbial boundstone breccia, or microbially stabilized packstone and grainstone. The cored fractures also demonstrate a relationship between degrees of fill and fill phases. Fractures containing sediments, pre-bitumen calcites, or bitumen are typically completely or almost completely closed (Fig. 11). The surfaces of most open (but not necessarily effective) fractures in cores are commonly coated only by coarse equant calcite and/or bitumen (Fig. 11E) and show other

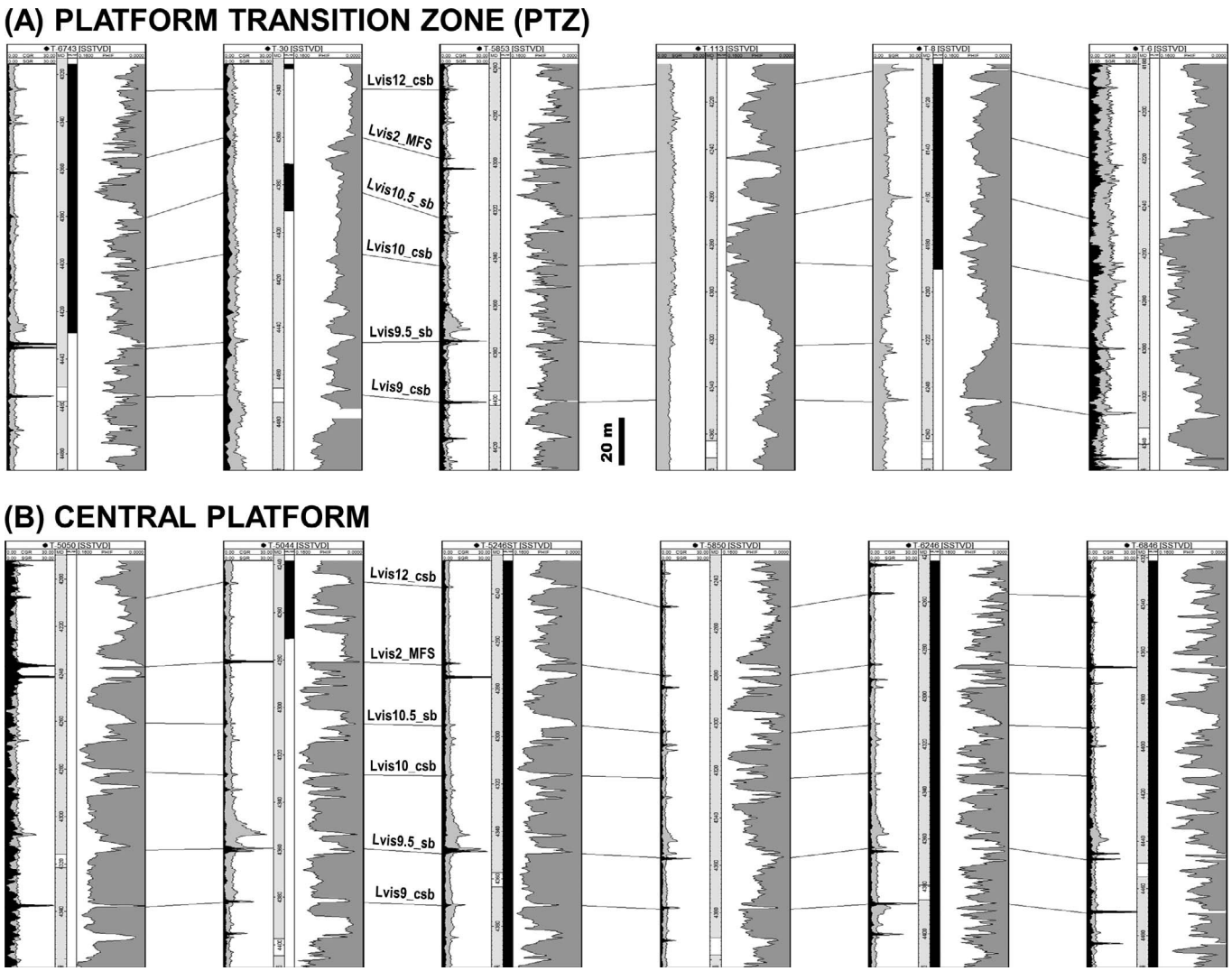

FIG. 8.—Cross sections showing selected wells from the PTZ and central part of the platform reservoir and comparing porosity (PHIE) and gamma ray (SGR and CGR) logs for fourth-order cycles in the late Visean platform sequence: **A)** Examples from the PTZ showing poor or inconsistent correlations between GR and PHIE patterns and depositional cycles; **B)** Examples from the central platform reservoir showing systematic vertical GR and PHIE patterns caused by parasequence stacking used to correlate the cycles. Note that low-porosity layers are generally associated with cycle boundaries. Cross-section locations are indicated in Figure 9A.

attributes of the burial overprint, such as corrosion or solution enlargement along their walls (Fig. 11D). Other fractures are planar, have small apertures, have no cement, or show no evidence of solution enlargement (Fig. 11F). Small caverns (Fig. 12) are likewise concentrated in microbial facies but are also known from Bashkirian platform-top and Serpukhovian allochthonous facies. Lithofacies control for cavern occurrences also comes from BHI logs (Collins et al. 2008, Poster 4), which are generally able to distinguish massive microbial facies (boundstone or breccia) from bedded facies (platform-top or allochthonous deposits).

Reservoir Subcompartments (Material Balance Regions)

The geographic terms "platform," "rim," and "flank," while still used for well classification, have become outdated for interpreting the increasing amount of dynamic data available from the field as production proceeds. Current reservoir surveillance began when the joint venture operated by TCO formed in 1993; however, at least 75 to 80 reservoir penetrations were drilled in the 14 years between field discovery in 1979 and formation of the joint venture. As a result of unsupervised production from these wells, not all new wells came on at original reservoir pressure. This circumstance actually proved useful for interpreting reservoir communication between drilled and undrilled portions of the rim and flank. Time-series reservoir pressure data collected after 1993 combined with initial pressure data show three baffled but connected reservoir subcompartments.

Two subcompartments corresponding to the rim and platform regions are revealed by datumed pressure data indicating separate uniform declines from ~11,750 psi between 1993 and 2010. A pressure decline of ~250 psi/yr is noted for wells drilled in the

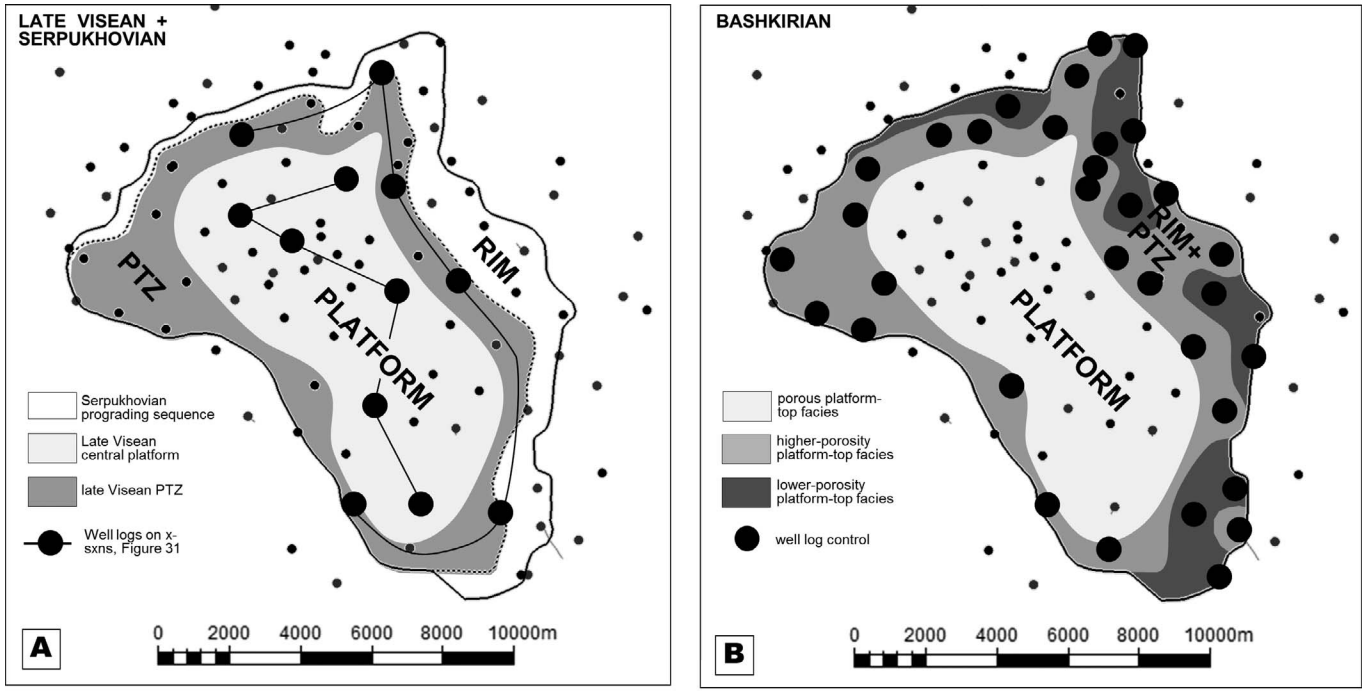

TENGIZ MATRIX POROSITY FROM IN CORE PLUGS

REGION	INTERVAL or FACIES	CORES avg phi	CORES fraction>6%	CONTROL	MAP
PLATFORM	LATE VISEAN AGGRADING PLATFORM	8.570	70.8	3082 plugs	A
PTZ	LATE VISEAN & SERPUKHOVIAN AGGRADING PLATFORM	5.646	44.4	525 plugs	A
RIM	SERPUKHOVIAN OUTER PLATFORM	4.310	24.8	637 plugs	A
RIM	SERPUKHOVIAN UPPER & MIDDLE SLOPE	3.051	10.0	1322 plugs	A
RIM & FLANK	COARSE ALLOCHTHONOUS FACIES	3.188	12.5	513 plugs	A
PLATFORM	BASHKIRIAN PLATFORM-TOP FACIES	8.026	54.0	886 plugs	B
PTZ + RIM	BASHKIRIAN PLATFORM-TOP FACIES	5.025	29.5	645 plugs	B

FIG. 9.—Distribution of the PTZ relative to the central platform and rim areas, based on well logs with the characteristics illustrated in Figure 8. **A)** Map showing the PTZ as a continuous zone of variable width around the margin of the late Visean aggradational sequence, the edge of which is located at the rim–platform boundary. **B)** Map showing the PTZ in the Bashkirian. It includes the rim area and is characterized by patchy variations in matrix porosity. The table compares matrix porosity in the different mapped regions calculated from core plugs. Porosity averages are indicated, as is the fraction of plugs with greater than 6% matrix porosity (a possible indicator net-to-gross reservoir based on an arbitrary 6% porosity cutoff).

platform region (Fig. 13B). Modular Dynamic Tester (MDT) pressure profiles define the stratigraphic interval represented by the platform decline as the late Visean B, late Visean A, Serpukhovian, and Bashkirian sequences of Weber et al. (2003) and Kenter et al. (2006). The platform decline trend shows an initial dispersion of ~1000 psi that has increased with time. Some of the dispersion is caused by the dominant internal heterogeneity within the platform region, namely vertical and lateral porosity variations controlled by depositional sequences, which also induces a slightly deviated tilt in reservoir pressure from the original oil gradient (Fig. 13C). Dispersion in the decline data is also caused by concentrated production from a cluster of wells in northern part of the platform, which creates a pressure gradient across the region. As a result, some of the later wells away from this area come on at higher pressures, but then decline at the same rate. The overall systematic decline for the late Visean, Serpukhovian, and Bashkirian intervals within the platform area define that volume as the material balance region representing the platform subcompartment. Because the different pressure behavior noted for rim and flank wells distinguishes them from platform wells, the same rim–platform boundary that aligns with the margin of the late Visean platform sequence is used for the outer boundary of the platform subcompartment (Fig. 13A).

Two different decline trends are noted for rim and flank wells. Wells that penetrated the structurally highest portion of the rim and flank areas have declined in an almost-linear fashion at a rate almost identical to that of the platform reservoir (Fig. 13B, D). The low pressure dispersion in this trend demonstrates an extraordinarily high degree of reservoir connectivity, given the geographic distribution of these wells and the variable rates at which they have produced oil (Fig. 13). Wells from the deeper portions of the rim/flank region, an area that was largely undeveloped prior to 2005, show a less systematic decline but still encountered initial pressures depleted by 1000 psi or more (Fig. 13B, E). Most of the wells on the deeper pressure trend were drilled along the western and northern flanks of the field through distally thickened seismic features like the example in Figure 3, representing allochthonous deposits. The T-5660 well on the eastern

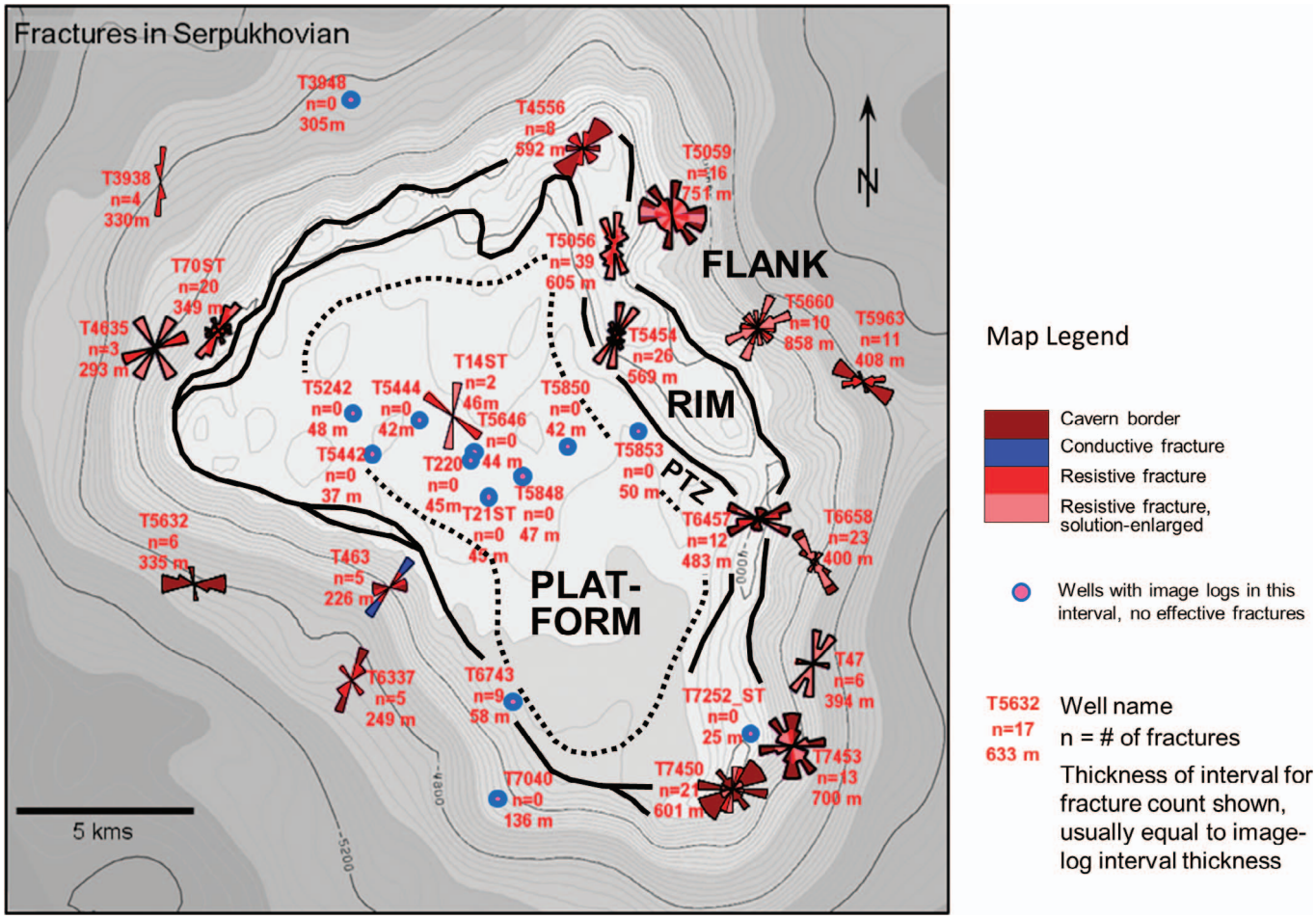

FIG. 10.—Fracture and cavern strike orientations and count data from the Serpukhovian interval plotted on a structure map of the Serpukhovian surface, relative to the PTZ, rim, and flank areas: Rose diagrams include orientations of cavern walls as well as open or enlarged (effective) fractures. Circles show the locations of wells with BHI logs that do not contain effective fractures.

flank (Fig. 14), however, encountered a pressure drop of 1700 psi between allochthonous facies and progradational slope facies (Fig. 15). The pressures recorded in the slope facies (~9600 psi) matched the contemporaneous datumed pressure trend for the structurally higher rim wells (Fig. 13B), while the higher pressures in the allochthonous facies (11,300 psi) matched the typically depleted initial pressures encountered in other flank wells. The bedded allochthonous facies in the high-pressure zone are indicated by BHI logs (Fig. 16), and cores demonstrate that the overlying low pressure zone is a shallowing-upward succession of lower to middle slope facies (Fig. 16C, D). The low porosity interval separating the two pressure regimes consists mainly of thin-bedded facies (Fig. 16C) interpreted as basinal to lower slope lithofacies at the bottom of the progradational system.

Based on this well, a plausible explanation for the different pressure trends in the rim and flank area is that two reservoir subcompartments are present: one compartment containing the allochthonous apron depositional system and a second compartment containing the overlying progradational depositional system. Two additional material balance regions were therefore identified on this basis for the rim and flank, termed the "wedge" and "apron" reservoirs (Fig. 14). In principle, the most likely source of a baffle that could form a pressure boundary between these subcompartments would be a theoretical downlap surface at the top of the allochthonous depositional system and the base of the progradational system. The depleted initial pressures in the apron material balance region most likely indicate communication with the overlying wedge reservoir; however, the high degree of data scatter in the pressure decline could indicate either variability in the degree of communication with the wedge or poor internal connectivity within the apron or both.

The base of the apron reservoir interval in T-5660 is a zone of high radioactivity containing abundant clay (Fig. 15) located above the well intersection with the Devonian and Tournaisian–early Visean sequences (see Fig. 14) known as the High Radioactivity Zone (HRZ). The HRZ, originally defined in Weber et al. (2003), forms the base of the MDT pressure profiles representing the platform material balance region. The platform HRZ can be correlated with the HRZ in wells from both the wedge and apron reservoirs (Collins et al. 2008, Poster 3). The HRZ is therefore recognized as the base of the reservoir system containing the platform, wedge, and apron subcompartments.

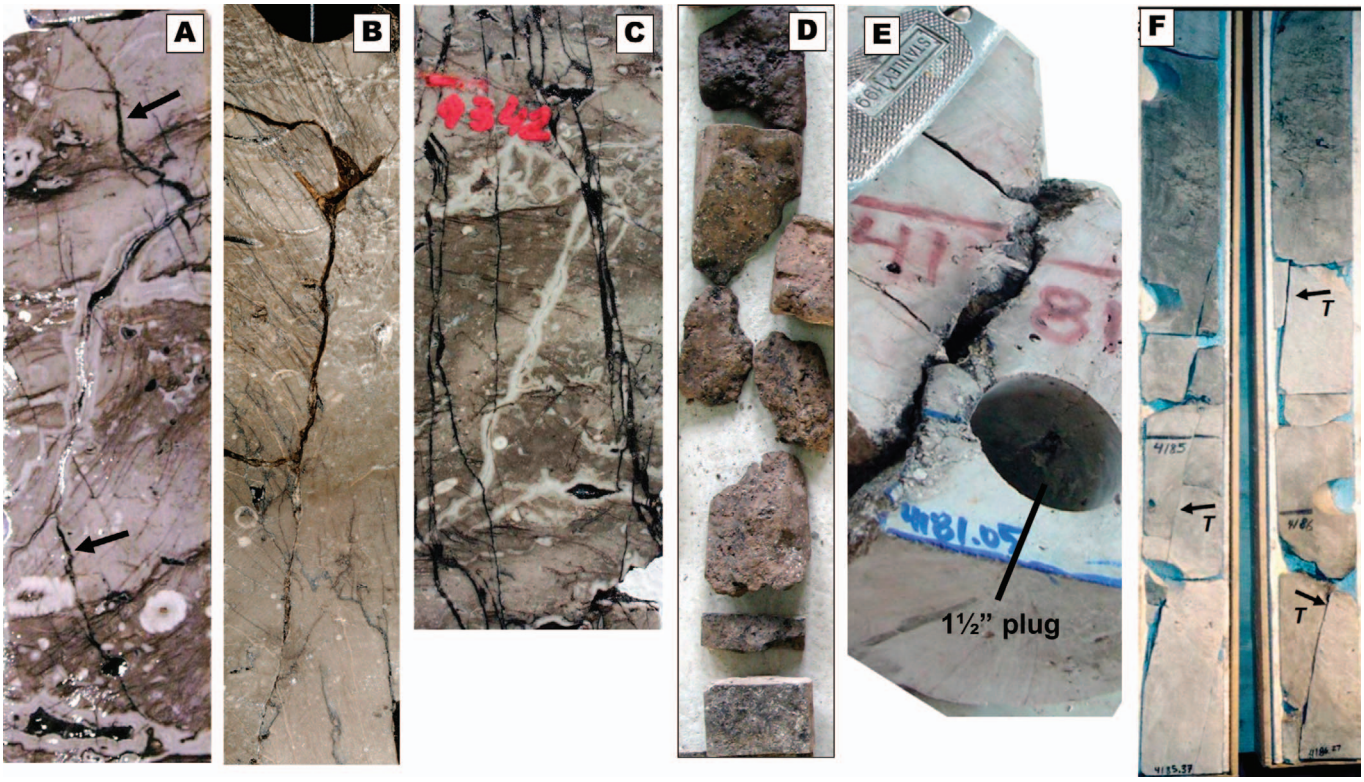

FIG. 11.—Examples of early and late fractures from the Tengiz rim and flank: **A)** Reactivated early fracture lined with early marine cement, indicating that reactivation occurred prior to or during bitumen precipitation. Secondary fractures (arrows) terminating at the early fracture are filled only with bitumen, and bitumen partly fills the reactivated early fracture. **B)** Fracture with evidence of shearing displacement, including lineated calcite (not shown) and antithetic secondary fractures. **C)** Probable burial fractures filled with bitumen cross-cutting early, marine-cemented fractures. Burial fractures often terminate at stylolites in core and commonly contain equant calcite and/or bitumen. **D)** Planar, solution-enlarged early fracture with corrosion visible on the fracture faces (flat surfaces of the core pieces). The associated rubble is typical of core recovery from intervals with effective fractures. This interval coincides with a significant inflow zone indicated on a production log. **E)** Solution-enlarged fracture containing incomplete fill by equant calcite and bitumen. The fracture is surrounded by a corrosion halo containing the burial diagenetic overprint. **F)** Planar, narrow-aperture tectonic fractures with little or no mineralization or corrosion that do not contribute significantly to fluid flow. Plug holes in cores are ~3.5 cm.

Synthesis and Outcrop Analog

The Tengiz Field is currently penetrated by 125 wells. Of these, 61 were drilled in the platform region, a few wells are too close to the rim–platform boundary to be classified with certainty, and the rest are classified as rim and flank wells. Almost 1600 m of core are available from 21 rim and flank wells, and BHI logs are available from an even larger subset. The platform, PTZ, wedge, and apron reservoir subcompartments each have large-scale internal matrix and nonmatrix reservoir characteristics, shown schematically in Figure 17, that determine their dynamic behavior. For example, the wedge reservoir is shown containing a series of horizontal diachronous lithofacies zones that influence the distribution of nonmatrix features. The apron reservoir is depicted with disorganized elements of matrix and nonmatrix porosity. The central platform reservoir is governed by cyclic variations in matrix porosity with minor internal stratigraphic baffles. In some cases, outcrop analogs were used to supplement well control and other field data in order to constrain these characteristics in geologic models of the field. As an example, the subcompartment boundaries discussed in the previous section are themselves poorly constrained by field data. The stratigraphic baffle interpreted between the wedge and apron reservoirs is based on hard data only from the T-5660 location, in which the wedge and apron subcompartments were identified by facies coupled with pressure data. For the wedge and platform subcompartments, there are no definitive well data across the boundary, only an indication of changing matrix and nonmatrix reservoir properties across the PTZ. The proxy relationship between the structurally elevated rim and the margin of late Visean platform aggradation is constrained only by well spacing and by the presence in cores and BHI logs from rim wells of slope microbial facies that are absent in platform wells.

Outcrop examples provided in this article were selected partly on the basis of "best fits" with the Tengiz data. The "Classic Face" outcrop from Windjana Gorge in the Canning Basin (Playford et al. 1989) is used as an analog on two occasions: in a later section as an analog for scaled fracture data beyond the ability of borehole data to measure, and here as a conceptual analog for the rim–platform boundary and the PTZ. The Classic Face demonstrates how a turnaround from aggradation to progradation can produce lateral juxtaposition of horizontally stratified platform-top facies and progradational slope geometries over a distance of 100 m or so

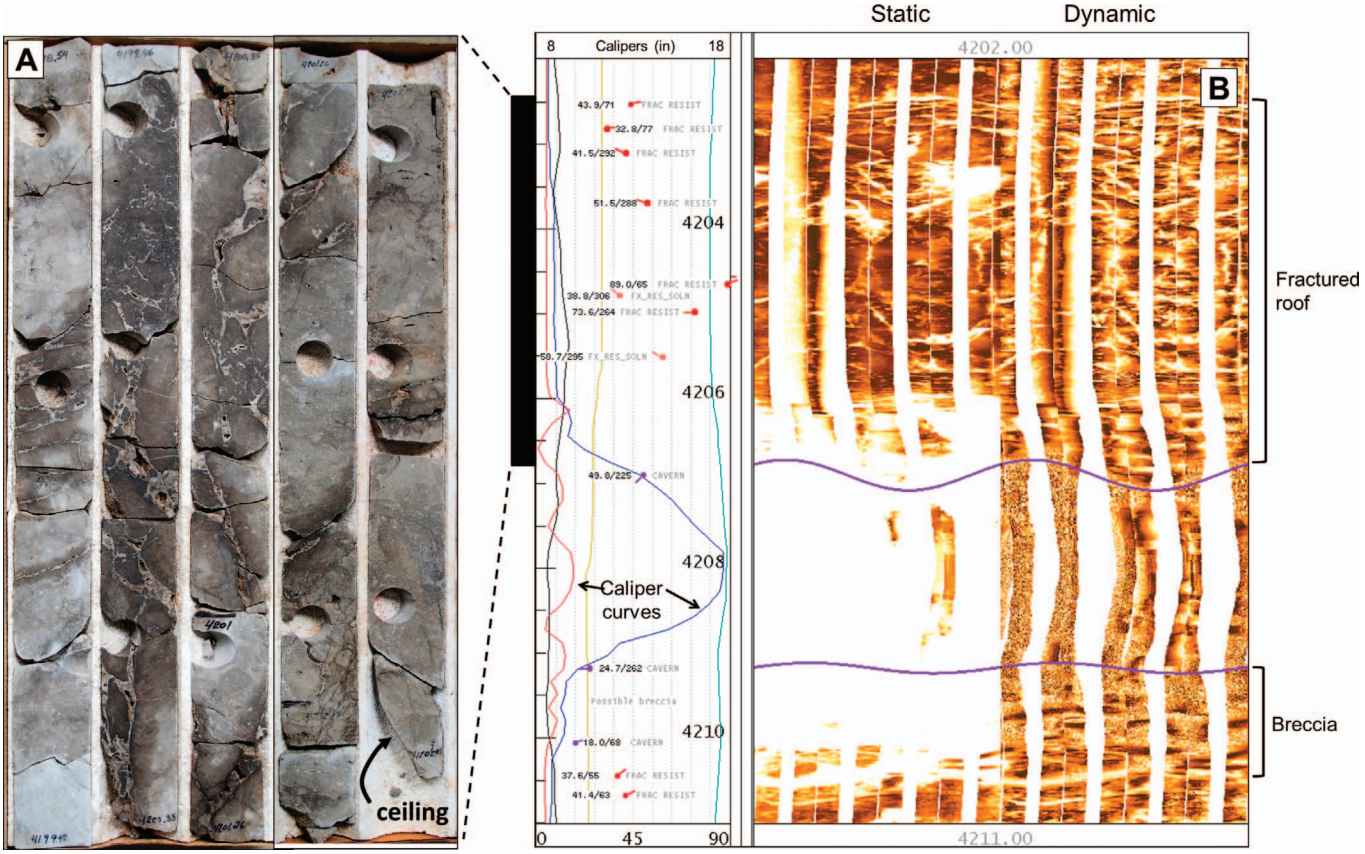

FIG. 12.—Irregular fractures incompletely filled by coarse calcite cement from T-5056 formed by roof collapse above a 2-m cavern. Fractures are surrounded by a diagenetic halo representing the burial overprint in the matrix **(A)**. The bottom of the core coincides with the cavern ceiling indicated on BHI logs **(B)**. Lost circulation of 200 bbls/hr (barrels of oil per hour) occurred after drilling into this cavern. The BHI log also shows a possible breccia accumulation on the cave floor. The core depth shift to log depth is about 4 m. Core plug holes are ~3.5 cm across. The static and dynamic BHI clips each represent the entire borehole circumference (note scale on caliper log).

(Fig. 18). The upper slope facies in these outcrops are also cemented, cavity-rich "cryptalgal," cyanobacterial, or microbial boundstones (Playford 1980, Kerans et al. 1986, Playford et al. 1989, Stephens and Sumner 2003). The best fit to Tengiz data is that collectively the facies identified in cores from rim and flank wells were consistent with the type of systematic progradation illustrated in Windjana Gorge adjacent to aggradational platform cycles.

Although the surface representing the top of the progradational system in Windjana Gorge is eroded, early lithification of the slope facies in the outcrop (Kerans et al. 1986) provides an immediate explanation for why a change in structural elevation that formed at Tengiz during burial compaction would be aligned with the transition from aggradation to progradation there. As will be demonstrated in subsequent sections of the article, Tengiz slope microbial facies also show evidence of early lithification, which is interpreted to have produced early mechanical resistance to compaction in the rim area. This alone should have been enough to justify using the rim elevation change at the top of the buildup to locate the margin of the adjacent late Visean platform sequence, but the clarity with which the transition is expressed in the outcrop analog helps make the data connections. The turnaround in the Classic Face outcrop was not a smooth transition, involving episodes of margin collapse and healing before systematic basinward slope progradation occurred (Playton 2008, Playford et al. 2009, Frost and Kerans 2010). For more widely applied uses of this analog, it would be worth knowing if the complexity associated with the turnaround is a normal part of transgressive–regressive behavior (a healing sequence?) in steep-sided platforms and thus to be expected in analogous subsurface reservoirs or whether it is something unique to the Lennard shelf system and should be discounted in most subsurface analogs. For example, if an analogous healing sequence is present at Tengiz, the associated lithologic complexity could be a partial explanation for the baffle between the wedge and platform reservoirs. The presence of the matrix burial overprint in the PTZ next to the wedge and apron reservoirs may signify an added diagenetic influence on communication between the platform and wedge subcompartments. Throughout the rest of this article, however, we focus on facies, outcrop analogs, and burial diagenesis of the wedge and apron subcompartments alone.

WEDGE RESERVOIR SUBCOMPARTMENT

The wedge reservoir contains the Serpukhovian–Bashkirian progradational depositional system, as shown in Figure 14. It has historically been problematic in the Tengiz rim and flank to calibrate facies from cores or BHI logs to standard well logs in order to improve lithofacies constraints in geologic models beyond the core control. Here we present five lithofacies groups or zones that have been extrapolated to well logs with the aid of an outcrop analog template

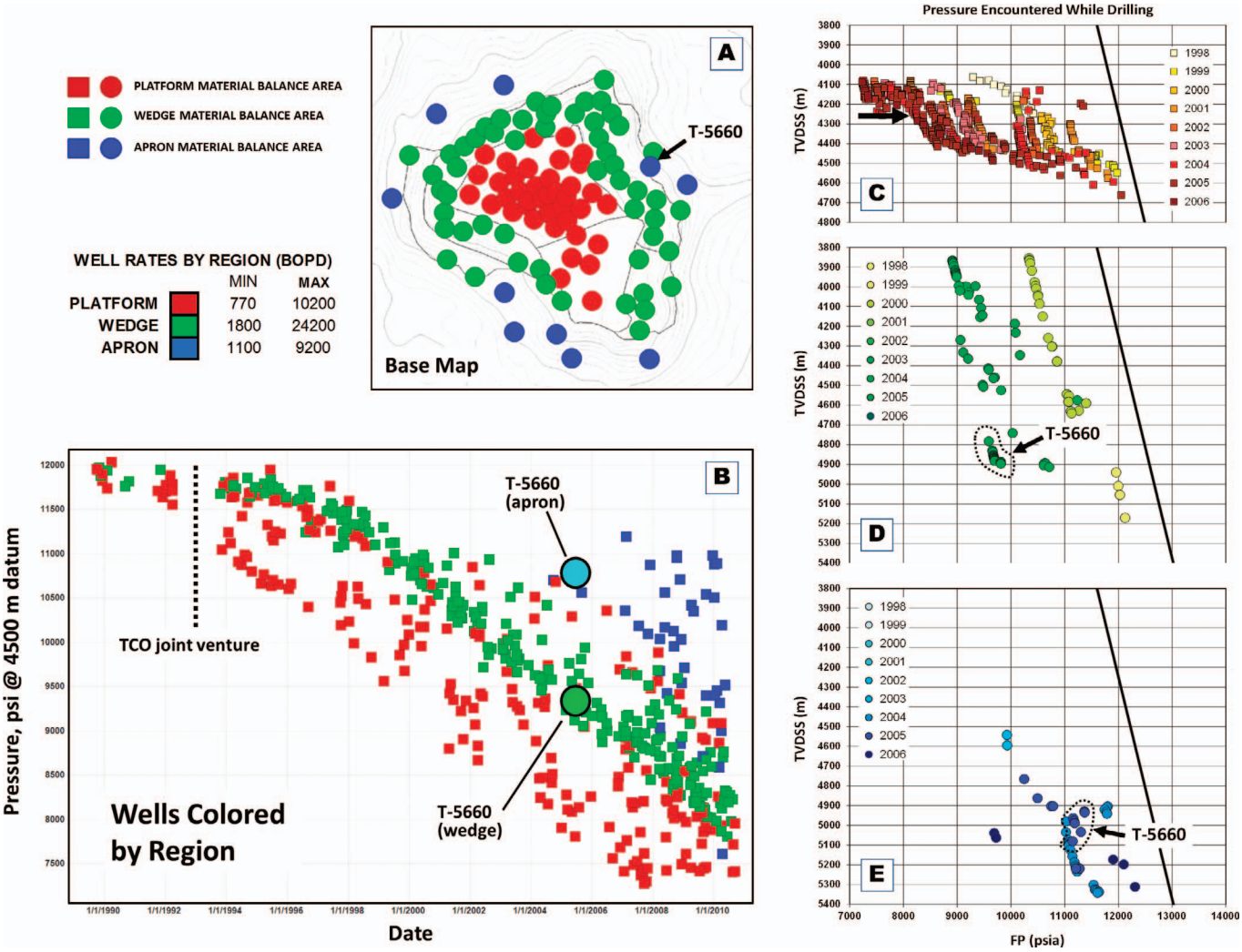

FIG. 13.—Dynamic pressure data from the platform, wedge, and apron reservoir subcompartments: **A)** Map showing the boundaries of the material balance regions and associated wells. Boundaries within the main regions indicate subregions used for history matching. **B)** Depletion trends for the platform, wedge, and apron subcompartments vs. time. The wedge reservoir shows rapid uniform depletion across a large area. The platform reservoir shows rapid depletion with pressure dispersion across the area. The apron reservoir shows depleted initial pressures followed by nonsystematic decline. **C)** MDT pressure profiles showing the systematic depletion with time in the platform reservoir between 1998 and 2006 and demonstrating the associated depth range (300–400 m) for the subcompartment. The original oil gradient (black line) has been slightly tilted by minor differential depletion across fourth-order stratigraphic surfaces, including a significant unconformity (arrow) at the top of the Serpukhovian. The subcompartment includes the Bashkirian, Serpukhovian, and upper part of the late Visean interval. **D)** MDT pressure profiles from selected wells in the wedge reservoir showing systematic depletion with time and oil gradients generally parallel to the original gradient. **E)** MDT pressure profiles from the apron reservoir showing depleted initial pressures, nonsystematic pressure decline, and spatial variations in the oil gradient. The T-5660 well is highlighted because it has pressure data from both the wedge and apron reservoirs at the same location.

that probably also have the requisite mechanical contrasts to influence the distribution of nonmatrix porosity in the subsurface. The extrapolation of these lithofacies to well logs where they aren't otherwise constrained could be used to reveal differences in average matrix porosity associated with them. Borehole image logs across these lithofacies zones may also help refine the distribution of fractures and other nonmatrix porosity.

Tengiz lithofacies in the wedge reservoir generally conform to a platform-to-basin faunal progression observed for Carboniferous ramp systems (e.g., Mamet 1992; Bridges et al. 1995; Gutteridge 1995; Madi et al. 1996, 2000; Martindale and Boreen 1997; Flugel 2004). The main differences between steep-sided margins like Tengiz and low-angle ramp systems are related to the abundance of microbial fabrics. The margins of steep-sided platforms are more likely to be preserved during times when euphotic reef builders were scarce, such as during the Carboniferous, if microbial binding played a significant role in anchoring the slope. In the Tengiz wedge reservoir, microbial boundstones are present to varying degrees in all lithofacies zones of

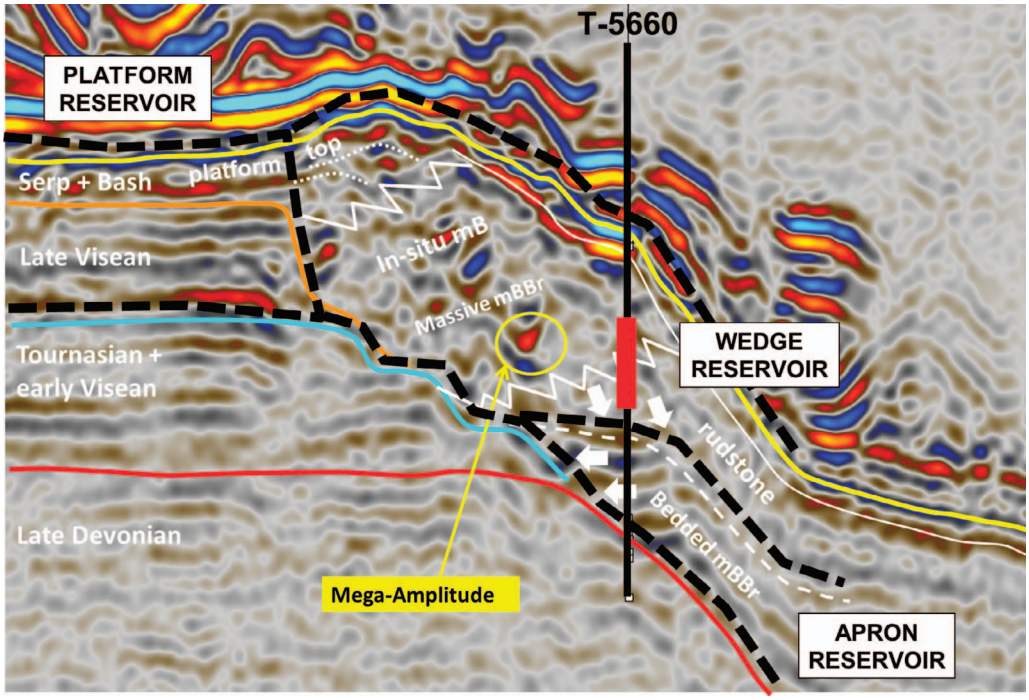

FIG. 14.—Seismic profile showing the wedge and apron reservoirs at the T-5660 location: The apron reservoir is stratified with updip onlap against the Devonian and Tournaisian–early Visean platform margins. The top is marked by a change to chaotic seismic character in the overlying wedge reservoir. Progradational clinoforms are not visible in the wedge, but local amplitude bursts interpreted as zones with enlarged fractures and cavernous nonmatrix porosity are visible. The platform subcompartment is shown as aligned with the margin of the aggradational late Visean sequence. The figure represents approximately the upper 1500 m of the buildup and is about 8 km wide. Dominant lithofacies are also indicated (mB = microbial boundstone; mBBr = microbial boundstone breccia).

the wedge reservoir, and their relationship to skeletal grain types is an important factor in recognizing the depositional environments they represent. For steep-sided platforms like Tengiz, shallow-water platform grains can be transported onto the slope and become entrained by microbial binding and mixed with in situ grain types. Care must be taken to consider such "out-of-context" lithofacies or faunal assemblages that can be mistaken for shallower environments than they truly represent. The definition of larger-scale lithofacies groups or zones with broader general characteristics largely avoids this problem.

Platform-Top Facies (Bashkirian)

Shallow marine platform-top facies occur in the Bashkirian of the wedge reservoir. Microfauna and grain types are similar to those described from the platform region by Kenter et al. (2006). They are dominated by grainstones but have higher proportions of intraclasts, crinoids, brachiopods, and algae. Bashkirian lithofacies in the wedge reservoir are generally interpreted as high energy (Fig. 19A) and include laminated to cross-bedded grainstones, coarse massive grainstones, brachiopod shell coquinas, bedded intraclast rudstones, and occasional rudstones with demosponge fragments. The coquinas, intraclast rudstones, and sponge rudstones are more common in Bashkirian cycles of the wedge reservoir compared to cycles in the platform. Microbial boundstone textures are locally present, but biomicrite is restricted to small encrusting masses in some skeletal-rich facies. The presence of corals and demosponges may indicate localized patch-reef development in some cycles. Intraclasts up to several centimeters in size are formed by rounded, reworked cemented grainstone fragments or occasionally by micritic to peloidal clasts representing reworked lagoonal facies.

Bashkirian–Serpukhovian Unconformity and Outer Platform Facies

The boundary between the Serpukhovian and Bashkirian is an unconformity with time missing mainly from the top of the Serpukhovian (Brenckle and Milkina 2003). The expression of the unconformity is highly variable in the wedge reservoir, but it is often associated with an abrupt basinward facies shift from shallow platform-top facies to deeper outer platform facies, most likely as a result of erosional removal of shallow Serpukhovian facies from the top of the interval. The Serpukhovian outer platform facies occupy a 75 to 200–m-thick interval below the unconformity in the wedge reservoir, where they form a poorly organized downward transition to upper slope microbial boundstone. The transition is lithologically complex and contains a mixture of skeletal rudstone, grainstone, wackestone, and skeletal-rich microbial boundstone. In terms of megafauna, outer platform facies contain large crinoids, abundant brachiopods, and occasional solitary corals. Grain types observed in thin-section microfacies include crinoids, algae, and a diverse assemblage of foraminifera. Biomicrite of probable microbial origin occurs in localized or patchy clotted and peloidal masses or as massive encrustations around individual grains or groups of grains. Outer shelf strata may be bedded with low-angle dips (Fig. 19B), which we interpret to be analogous to the "fall-in beds" described by Lloyd Pray

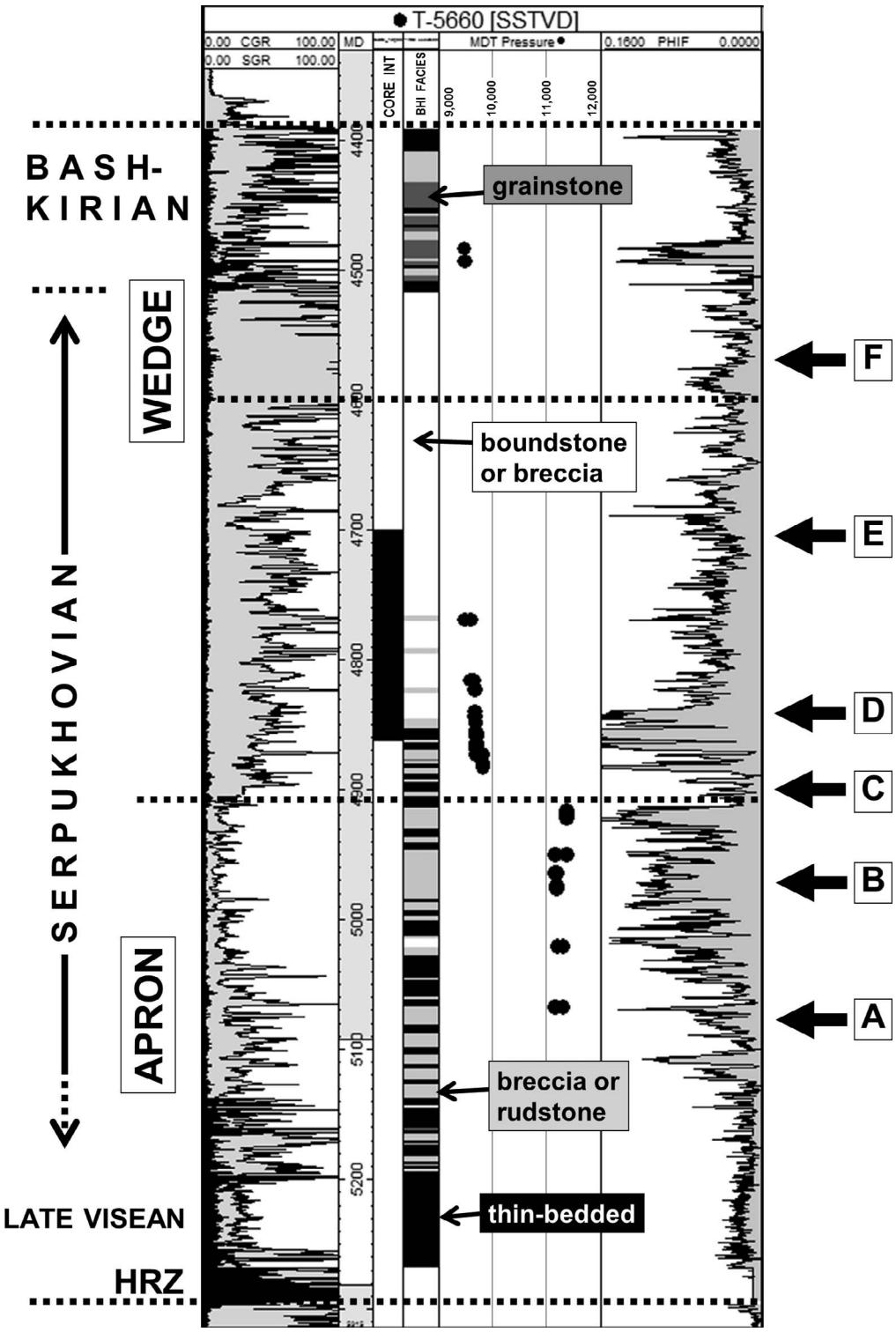

FIG. 15.—Wedge and apron reservoir intervals identified by lithofacies and MDT pressure data in T-5660: Pressures (black circles) drop from 11,300 to 9600 psi across a low-porosity zone at the base of the wedge interval. Note that the two Bashkirian pressure points fall on the same oil gradient as the deeper wedge interval pressures. Facies are interpreted from BHI logs covering the entire wedge and apron intervals and from core (interval indicated by black rectangle). Lithofacies are identified by gray shades (see indicated labels). Arrows indicate the locations of core photos and BHI clips shown in Figure 16. The vertical scale gives measured depth in meters for the well.

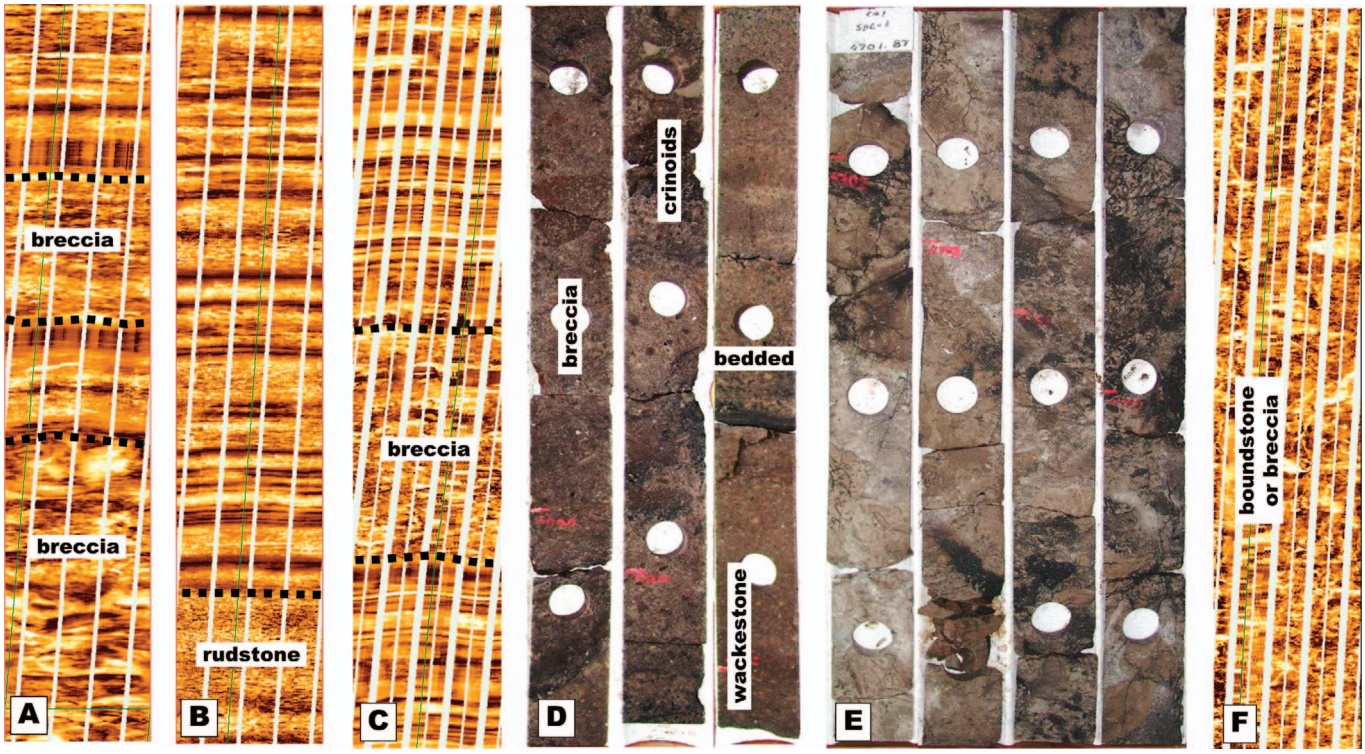

FIG. 16.—Facies from the wedge and apron reservoirs in BHI logs and cores, T-5660: **A)** BHI of coarse bedded facies (mainly breccia), apron reservoir (5071–5080 m), showing breccia beds up to 1 to 2 m thick. **B)** BHI of porous bedded rudstones, apron reservoir (4968–4977 m), interpreted based on a similar BHI expression for rudstones in the cored interval. **C)** BHI of thin-bedded basinal facies (4888–4897 m) including a single breccia bed, from the low-porosity zone at the bottom of the wedge reservoir. **D)** Crudely bedded, porous lower slope rudstones and fine breccias representing lower slope lithofacies toward the base of the wedge reservoir. **E)** Massive middle slope boundstone breccia with low matrix porosity in core from an interval identified on BHI logs as boundstone or breccia. **F)** BHI of massive slope boundstone breccia or boundstone, wedge reservoir (4556–4565 m). Tengiz BHI logs are generally unable to distinguish the tightly compacted boundstone clasts in massive breccia from massive in situ boundstone. Core plug holes are ~3.5 cm. BHI clips represent a borehole circumference of ~20 cm. See Figure 15 for image locations.

in the Capitan platform margin of the Guadalupe Mountains (as noted in Hurley [1989]).

Upper Slope Facies

Toward the base of the outer platform zone, microbial boundstone facies become more continuous vertically and more abundant in the wedge reservoir. The transition to dominantly microbial boundstone marks the top of the upper slope facies zone, although precise placement of the boundary can be somewhat arbitrary or subjective. Tengiz microbial boundstones form a spectrum between two end-member types in cores: (1) skeletal–microbial boundstones with large crinoids and occasional brachiopods, corals, or sponges (Fig. 19C) and skeletal grains derived from the platform-top and (2) massive microbial boundstones generally devoid of microfauna and megafauna (Fig. 19D). Both types have massive or patchy micritic matrix texture that is usually invisible at the core scale. Some massive microbial boundstones display large-scale, irregular, cauliflower-shaped fabrics formed by microbial filaments and masses. Other features present in both kinds of boundstone include large growth-framework cavities lined with marine cement and small, irregular subhorizontal fenestral voids. The larger voids may also contain geopetal sediment including micrite, fossiliferous sediment, and clay. The skeletal–microbial boundstones are interpreted to represent shallower upper slope environments and host a variety of smaller in situ and allochthonous grain types, notably algae, foraminifers, bryozoans, and brachiopods. In situ foraminifera include a diverse array of benthic types as well as micritic and agglutinating forms. Algae include deeper-water varieties such as Donezella and *Calcifolium* sp. Calcimicrobes, and other skeletal enigmata are also present. Fenestellid bryozoans are the only locally abundant fauna in massive microbial boundstones that are interpreted to represent deeper upper slope settings. Biomicrite in Tengiz boundstones is observed in three primary forms: (1) laminar filaments, (2) peloidal to clotted masses, or (3) amorphous micritic masses. Biomicrite is commonly associated with inclusion-rich, fibrous early calcite cement interpreted as marine in origin at Tengiz (Collins et al. 2006). The total cement volume varies greatly and can make up anywhere from 10 to 75% of the local rock volume.

Middle Slope Facies

Middle slope facies in the wedge reservoir consist of massive to poorly bedded microbial boundstone breccias. Cored examples contain continuous breccia intervals with subangular microbial

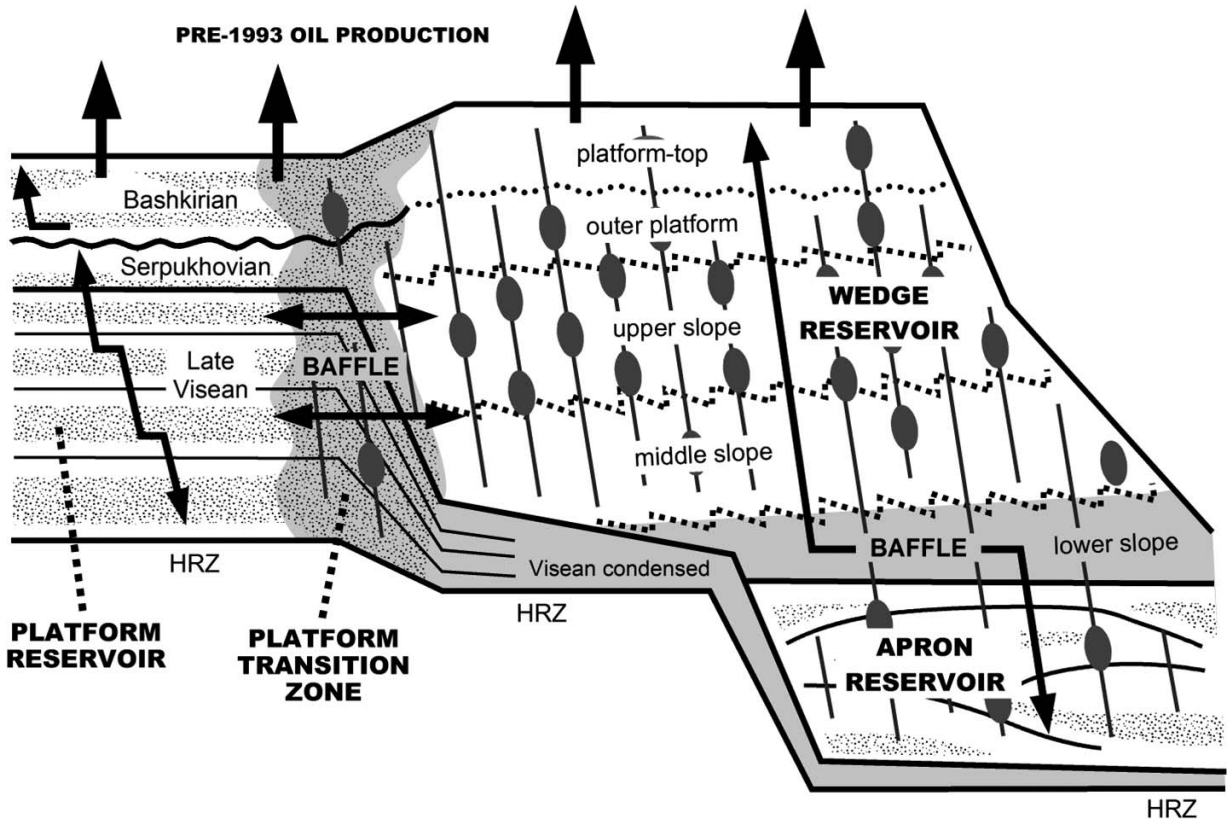

FIG. 17.—Schematic illustration of reservoir quality themes in the platform, wedge, and apron reservoir subcompartments based on field dynamic data, lithofacies, and outcrop analog concepts discussed in the text: The platform reservoir is characterized by stratigraphically baffled matrix permeability (stippled pattern). The wedge reservoir consists of well-connected nonmatrix permeability (enlarged fractures, caverns) controlled by the early mechanical properties of diachronous horizontal lithostratigraphic zones. The apron reservoir is characterized by a mix of matrix porosity and nonmatrix permeability, both interpreted to be limited by lithofacies heterogeneity or discontinuities. Short double arrows indicate inferred baffled communication between the platform and wedge reservoir subcompartments. Longer double arrows in each subcompartment indicate the behavior of the oil gradient with time during production. One-way arrows at the top of the buildup indicate unknown production quantities from the platform and wedge reservoirs prior to 1993.

boundstone clasts transported from the upper slope ranging in size up to more than a meter (Fig. 19E). Where there is matrix between clasts, it typically consists of crinoidal rudstone with small lithoclasts similar to the larger boundstone fragments. Cores exhibit vertical variations in matrix relative to clasts, but there is insufficient coverage to determine if these variations represent cyclicity, bedding, or just stochastic spatial differences. Thin sections reveal that clasts are dominantly upper slope microbial boundstones but with considerable mixing of biomicrite types. Grainstone lithoclasts transported or eroded from shallow platform-top environments are only occasionally observed. Matrix skeletal grains also represent a mixture of shallow and deeper assemblages. In addition to crinoids the matrix also contains brachiopod fragments, various types of bryozoans, and allochthonous foraminifera.

Lower Slope Facies

Lower slope facies have been identified in only a few short cored intervals near the base of the wedge reservoir. They contain alternating intervals of boundstone breccia, lithoclast rudstone, and skeletal or crinoidal rudstone (Fig. 19F) less than a meter to several meters thick. Clasts in the breccias and rudstones are generally smaller compared to middle slope facies, ranging in size up to several centimeters, but they are still dominantly represented by upper slope microbial microfacies.

Synthesis and Outcrop Analog

If Tengiz fractures are concentrated in microbial facies, as indicated by cores and BHI logs, then the distribution of microbial facies in the wedge and apron subcompartments is important to know from a reservoir characterization standpoint. Cores and well logs alone are not sufficient to establish this distribution with certainty, and lithofacies zones are not generally recognizable on the Tengiz seismic data. Several well-documented outcrop examples that have steep-sided margins anchored by boundstones formed on the slope with assistance from microbes are potentially useful for insights into the distribution of microbial facies in the Tengiz wedge reservoir. These include the Permian margin in West Texas and New Mexico (Babcock 1977; Yurewicz 1977; Bebout and Kerans 1993; Osleger 1998; Tinker 1998, figs. 6, 8; Playton et al. 2010), Triassic carbonate platforms in the Italian Dolomites (e.g., Bosselini 1984, Keim and Schlager 2001), and the previously cited Devonian Lennard shelf system in the Canning

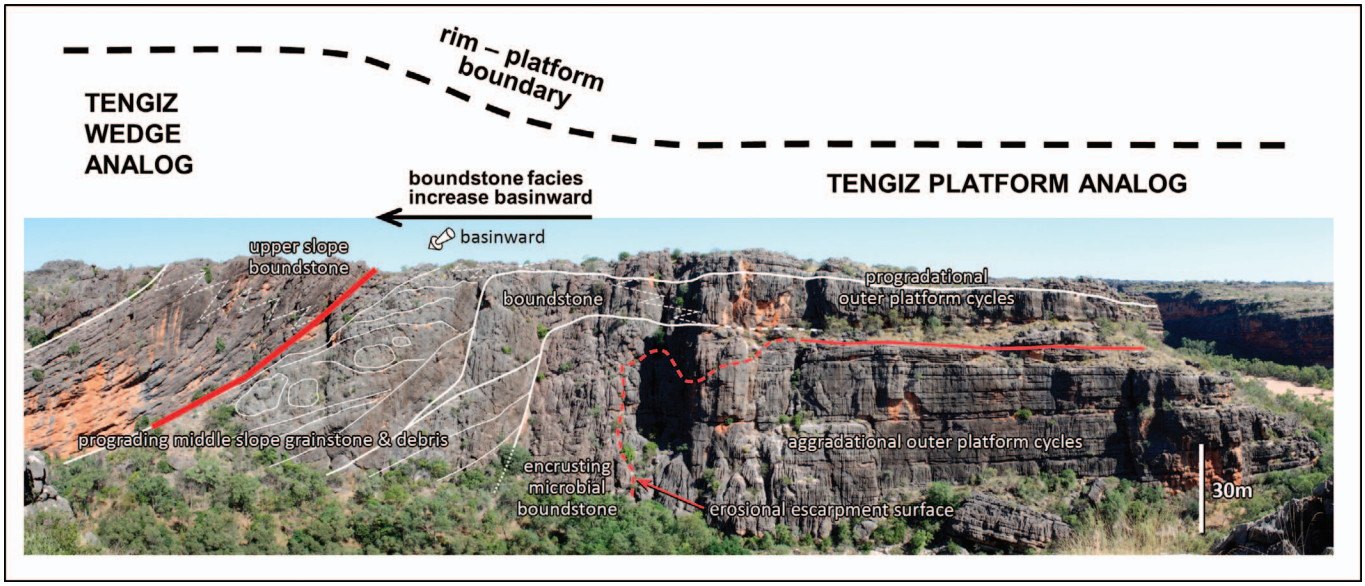

FIG. 18.—Interpreted photomosaic of the "Classic Face" in Windjana Gorge, Western Australia, showing depositional facies heterogeneity across the turnaround from aggradation to progradation: The outcrop includes an erosional escarpment at the margin of the aggradational cycles (dashed red line), a transitional "healing sequence" (solid red line) of boundstone masses and onlapping allochthonous sediment wedges, followed by systematic basinward progradation of middle and upper slope clinoforms. This panel represents a possible analog for stratigraphic and lithofacies relationships between the Tengiz wedge reservoir and the adjacent late Visean platform margin, as indicated by the stippled line above the outcrop panel. The stippled line is a schematic representation of the structural elevation difference across the Tengiz rim–platform boundary as it might relate to the underlying stratigraphy in the outcrop, based on the hypothetical premise that the same outcrop lithofacies are also present at Tengiz and that the boundstones in the outcrop have greater resistance to burial compaction than do other facies. In the outcrop, encrusting microbial boundstones are locally present in the healing sequence before becoming more continuous in the upper slope (mostly eroded in the outcrop) of the prograding clinoforms. This basinward increase in microbial facies accounts for the postcompaction slope of the rim–platform boundary in the schematic drawing. The outcrop interpretation is compiled from Playton (2008), Playford et al. (2009), and Frost and Kerans (fig. 9, 2010).

Basin. A Carboniferous progradational margin from the Asturias region in northern Spain (e.g., Bahamonde et al. 1997, 2000; Kenter et al. 2002; Della Porta et al. 2004) was chosen over the others as an analog for facies distribution within the Tengiz wedge reservoir because of the close similarity of lithofacies in hand specimen, similar gross depositional thicknesses of the slope environments, and because of the proximity in geologic age of the two systems.

The Asturias margin also consists of diachronous horizontal lithostratigraphic zones representing platform-top, outer platform, upper slope, middle slope, and lower slope environments and lithofacies (Fig. 20A). Aggradational shallow platform-top lithofacies occur at the top of the succession, with depositional cycles clearly visible in the outcrop as alternating recessive and resistant layers. These are analogous (in terms of the aggradational stacking pattern but not in terms of depositional thickness) to the Bashkirian interval at the top of the Tengiz wedge reservoir, which also has prominent depositional cyclicity (Kenter et al. 2006). The Asturias outer platform zone contains facies transitional between the aggradational platform-top cycles and progradational upper slope facies (Della Porta et al. 2002, 2003). It weathers more evenly but is still bedded, with occasional resistive layers that gently dip basinward (fall-in beds sensu Hurley 1989) and merge with the underlying slope facies. The lower 600 m of the Asturias outcrop contains mainly of massive in situ upper slope microbial boundstone and massive middle slope microbial boundstone breccia (Fig. 20B). Both facies have similar weathering characteristics, however, and form a thick continuous recessive zone with irregular or chaotic hummocky resistive ridges (Fig. 20C). The base of the outcrop contains a thin interval with a few continuous resistive beds representing allochthonous lower slope to toe-of-slope facies. The thickness of the outer platform and slope lithofacies belts at Asturias is 900 to 1150 m compared, with 650 to 800 m for the Serpukhovian progradational sequence within the Tengiz wedge reservoir. More important than the direct thickness comparison is the number of lithofacies zones, their lateral continuity in the direction of progradation, and their relative proportions within the vertical succession at Asturias. Tengiz rim wells potentially could provide more information about lateral facies continuity in the strike direction because of the narrow width of the rim relative to its total length (see Fig. 2). Applying the lithofacies concept from Asturias, namely that Tengiz wedge lithofacies zones should be continuous and nearly horizontal in the direction of progradation, well logs patterns were then examined for indications of lithofacies zone thicknesses and continuity in the strike direction.

The wells on the cross section in Figure 21 effectively form a north-to-south strike section. The correlations shown represent iterations between consideration of lithofacies thicknesses represented by the Asturias slope environments and the attempted use of Tengiz well logs (including BHI) to identify lithofacies zones in the wedge reservoir. The wedge reservoir commonly displays three distinct zones on gamma ray (GR) logs: (1) an upper zone consisting of low overall radioactivity but with numerous sharp, high-radioactivity spikes; (2) a middle interval marked by relatively pervasive elevated radioactivity;

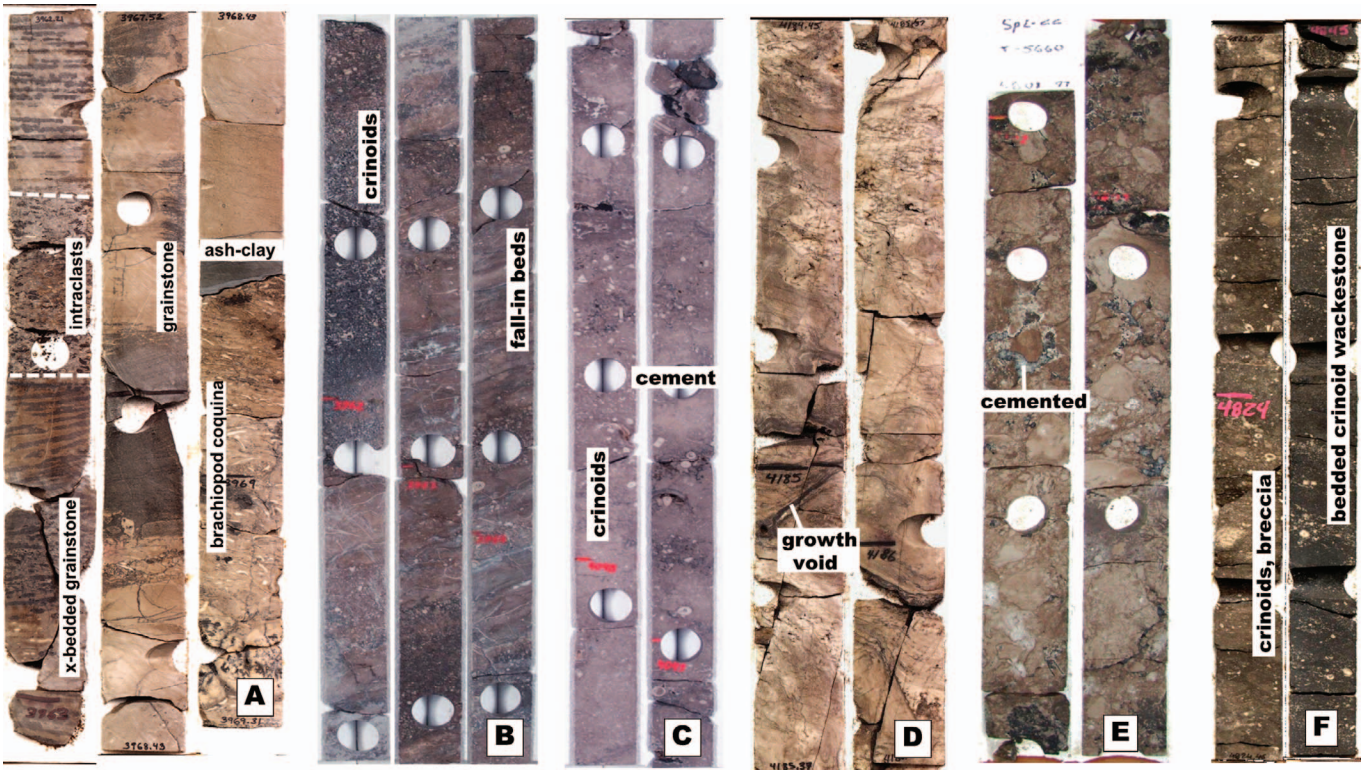

FIG. 19.—Typical facies types from the major diachronous lithofacies zones of the wedge reservoir: **A)** Bashkirian platform-top facies (T-5056). These facies are cyclic, with frequent exposure surfaces (marked by ash/clay beds) and rapid vertical lithofacies changes. Lithofacies shown include laminated and cross-bedded grainstones, massive grainstone, brachiopod shell coquinas, and thin beds containing coarse intraclasts. **B)** Gently dipping "fall-in" beds characteristic of the Serpukhovian outer platform lithofacies zone (T-4556) containing layers of mudstone, crinoid rudstone, and occasional breccias or intraclast conglomerates. **C)** Cemented, skeletal-rich microbial boundstone (T-4556) with large floating crinoids, brachiopods, and occasional corals or sponges. The patchy matrix texture is due to biomicrite masses or thick early cements associated with increased microbial influence. **D)** Massive in situ upper slope microbial boundstone (T-5056) with chaotic microbial fabrics revealed by dark bitumen staining. A large cement-lined primary growth–framework void with geopetal sediment fill is indicated. **E)** Massive middle slope boundstone breccia (T-5660). Clasts are tightly packed and well-cemented, angular to subangular slope microbial boundstone fragments up to a meter or more in size. **F)** Lower slope facies (T-7252) characterized by meter-scale beds or coarse layers of small-clast boundstone conglomerates alternating with crinoid-lithoclast rudstones. Core plug holes are ~3.5 cm across.

and (3) a basal interval with reduced total radioactivity and fewer radioactive spikes. Spectral GR indicates that most of the radioactivity in these zones is due to uranium rather than clay. The Serpukhovian–Bashkirian unconformity occurs in the middle of the upper zone, and the cored intervals indicated in Figure 21 suggest that continuous in situ upper slope microbial boundstone occurs no higher than the 150 to 300–m middle interval with elevated uranium radioactivity. The top of this radioactive interval is therefore interpreted to indicate the base of the Serpukhovian outer platform lithofacies zone. The thickness variations for the outer platform zone indicated in Figure 21 could be attributed to the erosion at the Serpukhovian unconformity or to stepped progradation, with boundstone tongues onlapping the outer platform during minor transgressions.

Cores from the 200 to 300–m zone of reduced radioactivity toward the base of the wedge reservoir each contain middle slope massive microbial boundstone breccia or lower slope bedded breccias and rudstones. These cores also suggest that the lower slope facies may form a thin zone at the base of the wedge reservoir, as they do in the Asturias example, but lower slope facies cannot be recognized specifically because they have the same general GR characteristics as the overlying middle slope breccias. Based on its proportional thickness within the Asturias outcrop, the Tengiz lower slope interval is represented as a thin interval toward the base of the wedge reservoir, in lieu of a characteristic defining log marker.

The GR log lithofacies associations described above are generalizations, and in some of the wells on Figure 21 the GR contrasts are suppressed. In these cases, facies interpretations from BHI logs were used to constrain the correlations, but zone thicknesses were largely based on the overall outcrop pattern. The reason for the elevated radioactivity associated with upper slope facies is unknown, but it could indicate uranium fixation by microbes during deposition. If so, the absence of elevated radioactivity in some wells may indicate reduced microbial contribution to the upper slope facies. It is recognized, however, that uranium redistribution and contamination of the depositional signal might have occurred during later diagenesis. The Asturias outcrop zones were therefore used to guide an interpretation of continuously distributed slope microbial facies within the wedge reservoir regardless of the GR log signature. From a distance the horizontal erosional pattern produced by the diachronous lithostratigraphic zones is the most distinctive feature of the Asturias

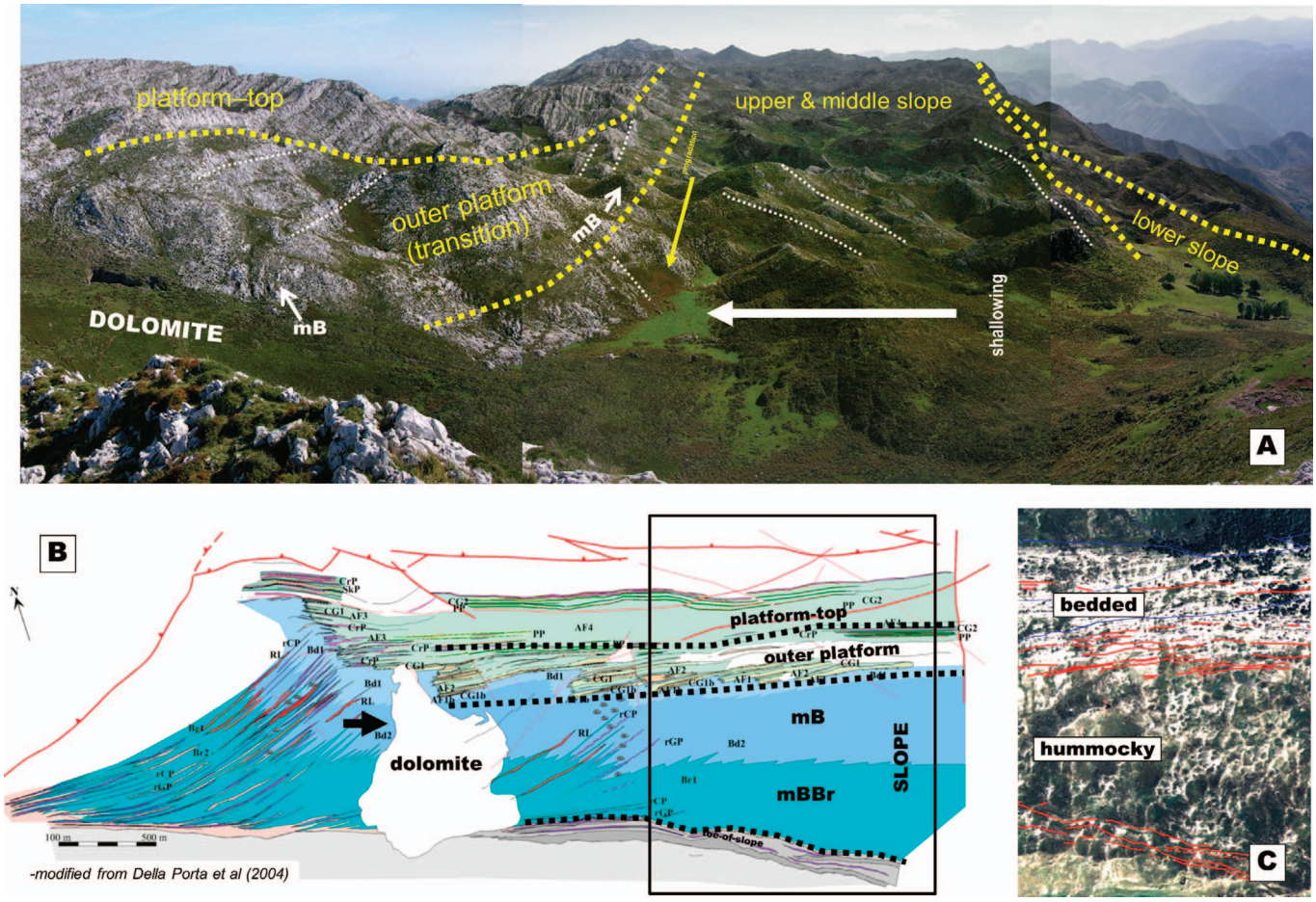

FIG. 20.—Analog elements of the progradational margin at Asturias, northern Spain, applied to the Tengiz wedge reservoir: **A)** Photo pan of the Asturias margin, showing the high lateral continuity of horizontal diachronous lithofacies, as indicated by overall surface erosional patterns. The 1200 m of near-vertically dipping strata represent several kilometers of progradation with four continuous lithostratigraphic zones: (1) a thin basal lower slope zone; (2) a thick zone containing middle to upper slope microbial boundstone breccia (mBBr) and microbial boundstone (mB) facies; (3) an outer platform facies transition with fall-in beds; and (4) platform-top cycles of shallow marine facies. Each zone has a distinct erosional pattern determined by internal stratigraphic and facies heterogeneity. The dashed yellow lines identifying these zones are diachronous lithostratigraphic boundaries that intentionally cut across individual bedding surfaces. Dashed white lines indicate known fall-in beds and slope clinoforms, and mB (arrows) indicate resistive tongues of microbial boundstone in the outer platform zone interpreted to have resulted from stepped progradation. **B)** Detailed stratal geometries and facies in the lithofacies zones based on field mapping of the outcrop. Note that in situ mB and massive mBBr have equal thickness within the slope lithofacies zone. Stepped progradation and fall-in geometries are evident throughout the outer platform zone, and cyclic platform-top facies are associated with increased aggradation. The black arrow shows the location from which A was taken. **C)** Ortho-rectified aerial photograph of the eastern portion of the outcrop (black rectangle in B) showing a hummocky erosional pattern for the slope facies contrasting with the bedded erosional pattern for the platform-top facies. The in situ boundstone and boundstone breccia facies are indistinguishable from only the erosional pattern.

outcrop. Outcrop erosional patterns are partly controlled by rock hardness, and for the portions of the Asturias outcrop containing limestone, this hardness may also be correlated with mechanical resistance to fracturing that also gave these two different lithologies similar responses to erosion. The in situ microbial boundstones and the massive boundstone breccias comprising the Asturias upper and middle slope zones display evidence of early lithification in thin section (Vanderkooij et al. 2007, fig. 12), and syndepositional fractures are present in the upper slope (Della Porta 2003; Della Porta et al. 2003, fig. 4). The in situ boundstones and boundstone breccias of the Tengiz wedge reservoir show similar evidence of early lithification (Fig. 22), suggesting that both facies might be more prone to fracturing relative to other lithofacies.

APRON RESERVOIR SUBCOMPARTMENT

The depositional system representing the apron reservoir was originally intended to take into account downslope allochthonous deposits visible on seismic data (e.g., Fig. 3). These seismic features vary in thickness but are laterally continuous within the Bashkirian–

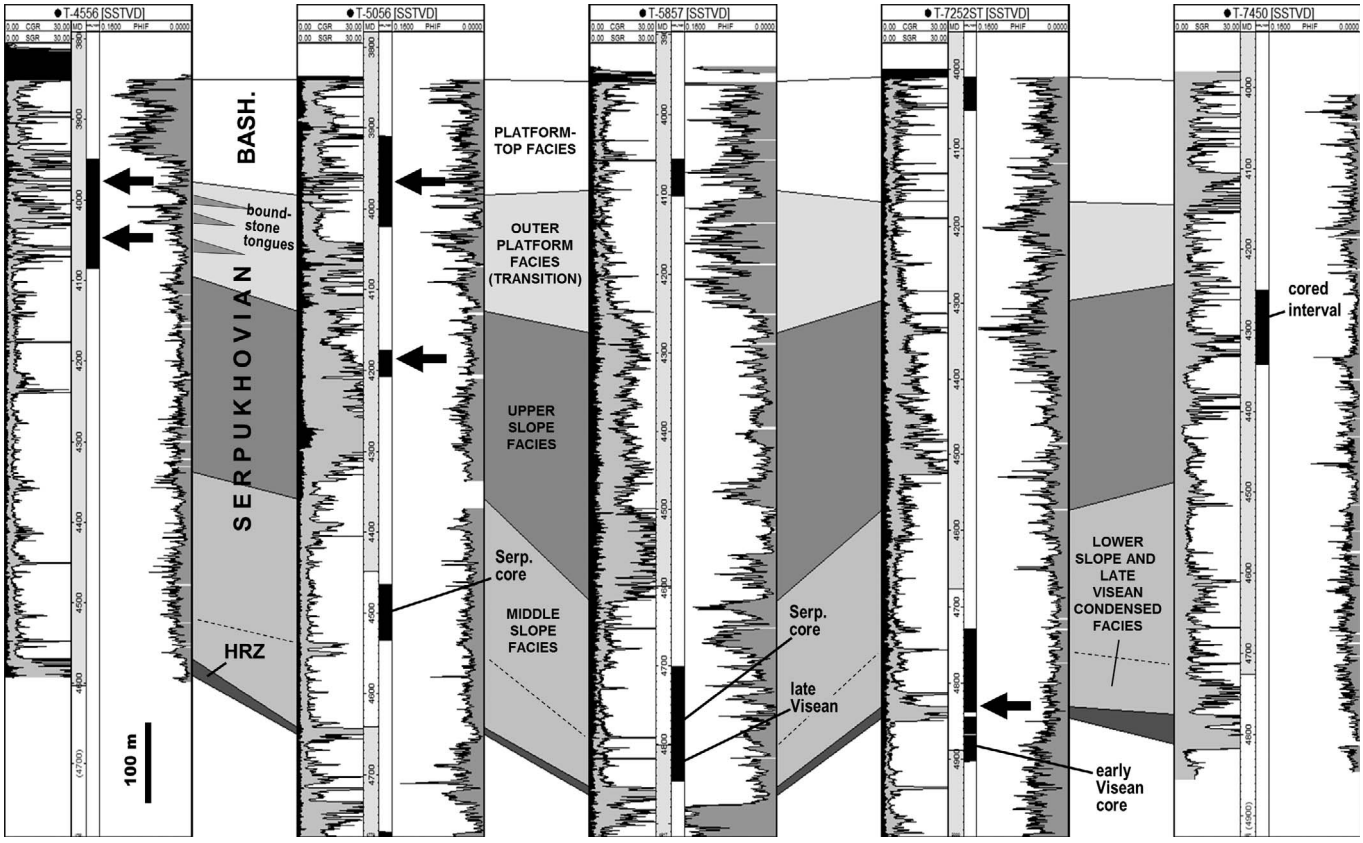

FIG. 21.—North–south strike section using cored wells from the wedge reservoir along the eastern Tengiz margin (see Fig. 2 for well locations): Well panels show two GR logs in the left track, SGR (gray-filled curve, total radioactivity) and CGR (solid black curve, potassium–thorium radioactivity). The difference between the curves indicates uranium radioactivity. The Bashkirian correlation is known from core biostratigraphy. Lithostratigraphic correlations within the Serpukhovian are derived from Asturias outcrop themes (lithofacies zone thickness proportions and continuity) and constrained by core and BHI facies interpretations from the field. These lithostratigraphic zones are partly conceptual and have the best tie to vertical variations in uranium activity (see text for discussion). The lower slope facies and the late Visean basinal zone indicated at the base of the interval are known to be thin from limited age control but have no distinctive log characteristic. The porosity logs (PHIF, right track, scale from 0 to 16%, increasing to the left) show that matrix porosity is generally low in the slope facies, with only thin, noncorrelative intervals of higher porosity. The outer platform or platform-top lithofacies zones have elevated porosity in T-5857 and T-4556. Arrows indicate locations of core slab photos in Figure 19A–D and F.

Serpukhovian sequence along the western and northern margins of the rim and flank areas (Collins et al. 2008, Poster 1). Core and BHI log facies from the seismic bulges demonstrate that the allochthonous deposits contain coarse material transported from the slope mixed with finer-grained basinal facies.

Coarse Allochthonous Facies

Coarse allochthonous material in the apron reservoir consists of bedded facies at one end of the spectrum and large olistostromes or detached blocks at the other end. Coarse bedded lithologies include mainly coarse skeletal-lithoclast rudstones, massive skeletal grainstones, and boundstone breccias (Fig. 23A, B). Microbial boundstone lithoclasts are generally dominant in rudstone and breccia beds. Skeletal grains in grainstones and rudstones are represented by abundant allochthonous algae, foraminifera, and crinoids. Algae and foraminifera are generally more abundant in the massive or thicker grainstone beds, while crinoids are abundant in thinner beds. Bedding thickness, grain composition, and clast size in the coarse facies all display considerable heterogeneity. Cores and BHI logs indicate that individual beds range in thickness from a few centimeters to more than 10 m and that clasts occur in sizes up to 1/3 or 1/2 m (Collins et al. 2008, Poster 4). The base of the coarse allochthonous facies has been cored in the three wells shown in Figure 24, and in each case they form a sharp contact with underlying thin-bedded to laminated basinal shales, mudstones, and fine skeletal packstones. In the T-3938 well the dominant basal clasts were lithified grainstone and packstone fragments (Fig. 23D) rather than microbial boundstones. These beds were also rich in crinoids and other shallow marine skeletal grains, suggesting they may have originated from erosion of platform-top facies rather than from failure of a prograding upper slope.

Olistostromes and Detached Blocks

A few anomalously thick intervals of microbial boundstone have been encountered in cores from the apron reservoir that are interpreted

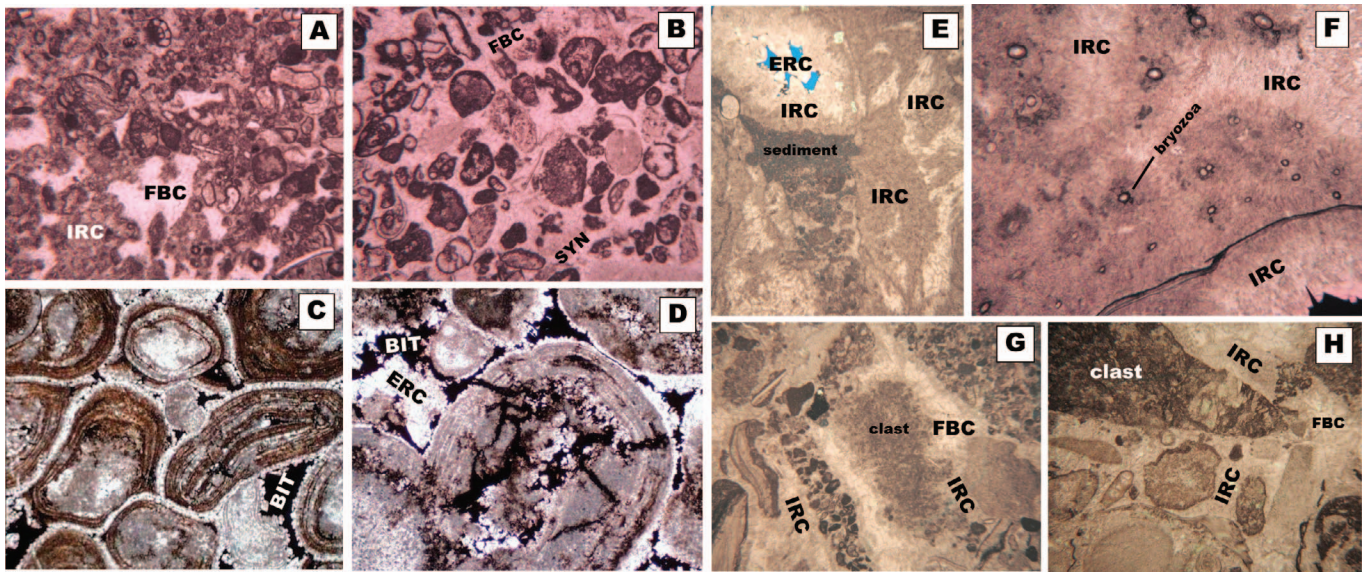

FIG. 22.—Lithification patterns indicated by cement history in the wedge reservoir lithofacies zones: The platform-top and outer platform lithofacies **(A–D)** were lithified over a longer period by a combination of early and late cementing agents, including microbial binding and inclusion-rich calcite **(A)**, early syntaxial and blocky cements **(B)**, grain compaction **(C)**, and burial cements **(C, D)**. Microbial boundstones and boundstone breccias **(E–H)** on the slope were early lithified by microbial binding and marine cement. Examples shown include massive microbial boundstone with early voids containing geopetal sediment and masses of microbial or cloudy marine cement **(E)**, thick cloudy to fibrous marine cements around bryozoans **(F)**, and thick isopachous cloudy or fibrous marine cements around clasts and grains in breccias **(G, H)**. Cement abbreviations are listed in Figure 6. Thin-section photos represent low magnification and are ~1 to 2 mm wide.

as olistostromes from the upper slope, although they may simply represent the high end of a general clast size spectrum. A single such clast measuring more than 100 m thick was interpreted in the T-3948 well, based on lithologic continuity over the interval, the presence of facies out of overall depositional context (upper slope boundstone in a distal setting). The interval contains well-preserved microbial fabrics (Fig. 23C) similar to those in the in situ upper slope facies in the wedge reservoir. Ironically, this example may represent the longest core recovery of continuous microbial boundstone facies representing the upper slope environment. The olistostrome demonstrates textural heterogeneity in biomicrite fabrics and in the proportion of skeletal material mixed with biomicrite. It also contains some minor brecciated intervals, but changes in texture and fabric are generally gradational and do not appear to represent bedding or layering related to transport and redeposition. Unfortunately, the T-3948 olistostrome contains few definitive geopetal fabrics that would indicate how much rotation it underwent during transport. Another continuous boundstone interval was cored in the T-6337 well representing a 39-m clast. In this case, geopetal structures are present throughout the interval and indicate internally consistent rotation of more than 10° from horizontal. The T-3948 olistostrome occurs within an interval interpreted to belong to the Serpukhovian. The T-6337 olistostrome, however, yielded an anomalous Serpukhovian age within the Bashkirian interval (Collins et al. 2008, Poster 2), indicating that at least locally, failure of the Serpukhovian slope continued during the Bashkirian.

"*Fine-Grained*" *Basinal Facies*

Interbedded with coarse allochthonous facies are thin-laminated or thin-bedded facies that represent a mix of allochthonous and pelagic sediment. These facies accumulated around the base of the buildup during aggradation of the late Visean and Bashkirian sequences and when slope failure was inactive during the Serpukhovian. Typical lithologies include allochthonous skeletal packstones or grainstones, silicified skeletal packstone beds, dark-colored lime mudstones, and dark-gray to brown shales and clays. An example of these thin-bedded facies occurs above 4960 m in depth in Figure 23A. Fine-grained basinal facies are common toward the base of the apron interval (above the HRZ) and were noted more frequently in core from the Bashkirian compared to the Serpukhovian within the apron interval.

Synthesis and Well Log Characteristics

The Tengiz apron reservoir can be more than 600 m thick in complete well penetrations. In most wells, it can be divided into three zones based on spectral GR character: (1) A basal zone up to 150 m thick that consists of elevated radioactivity due to clay or shale, (2) a 200 to 300–m middle zone of elevated uranium radioactivity that is virtually devoid of clay, and (3) an upper zone with reduced overall radioactivity that also contains distinctive spikes near the base, with elevated potassium–thorium radioactivity indicating clay. The uranium pattern within the middle zone shows a distinct upward-increasing trend in some wells. The Serpukhovian–Bashkirian boundary was identified in core from T-6337 near the top of the middle radioactive zone, 30 m below some shale-rich beds at the base of the upper zone (Fig. 24). The shales at the base of the upper zone are associated with basinal facies in core similar to those identified in Figure 23A. The Serpukhovian interval in this core includes at least some of the late Serpukhovian interval missing from the platform and wedge reservoirs (Collins et al. 2008, Poster 2), with no obvious interruption in facies or sedimentary style across the boundary. The shaly beds at the base of the upper GR zone were therefore interpreted to signify deepening and reduced sediment supply from the shallow platform associated with transgression early in the Bashkirian that eventually flooded the

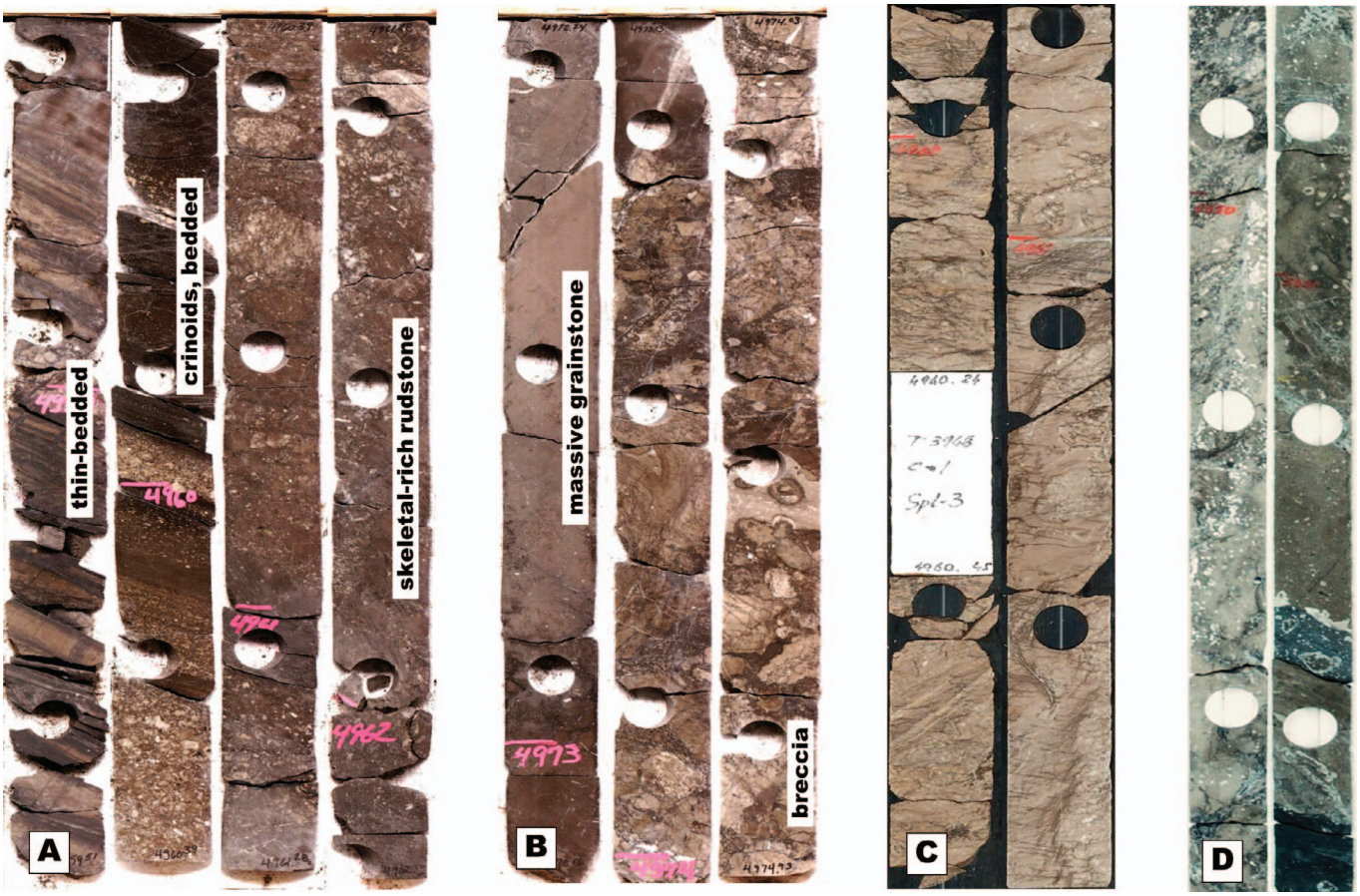

FIG. 23.—Coarse allochthonous facies of the apron reservoir: **A)** Coarse crinoidal and skeletal-lithoclast rudstones containing occasional boundstone clasts interbedded with basinal thin-laminated mudstone and fine-grained skeletal beds near the Serpukhovian–Bashkirian boundary in T-6337. **B)** Massive allochthonous grainstone interbedded with a poorly sorted microbial boundstone breccia (T-6337). **C)** Part of an olistostrome of massive microbial boundstone derived from the upper slope (T-3948, compare with Fig. 19D). **D)** Bedded breccia near the base of the apron interval containing nonboundstone clasts and crinoids (T-3938), possibly derived from an early stage of platform-top erosion. Plug holes are ~3.5 cm across.

platform-top above the Serpukhovian unconformity. They were therefore used as a proxy for approximate correlation of the Serpukhovian–Bashkirian boundary within the apron reservoir. Despite having an overall vertical pattern of high and low GR radioactivity similar to that of the wedge reservoir, the three zones in the apron do not correlate with the three zones in the wedge reservoir. The upper two zones in the apron reservoir are separated by the Serpukhovian–Bashkirian boundary, whereas in the wedge reservoir the upward transition from high to low radioactivity is associated with the appearance of outer platform facies within the Serpukhovian, below the boundary.

The correlations in Figure 24 are based on age control from bedded facies (as opposed to olistostromes or large transported clasts). While the age control is limited, the GR correlation suggests the Bashkirian and Serpukhovian intervals vary in thickness within the apron interval. The Serpukhovian age obtained for the olistostrome in the T-6337 Bashkirian interval demonstrates the age mixing between the Serpukhovian and Bashkirian due to continued failure of the Serpukhovian slope after deposition. The previously described stratigraphic relationship between the apron and wedge reservoirs at T-5660 was used as evidence for an early failure phase followed by a stable progradational phase. If Serpukhovian olistostromes turn out to be common in the Bashkirian, it is possible that a more substantial Serpukhovian progradational system was once present along the western margin but was later destroyed. A total of only 430 m of core has been described from the apron reservoir. The olistostromes interpreted in T-6337 and T-3948 total 140 m; the remaining 290 m consist of bedded allochthonous facies or basinal facies. Facies interpreted on BHI logs from the apron interval in T-5660 indicate an additional 250 m of bedded allochthonous facies (Collins et al. 2008); thus, interpreted olistostromes account for ~21% of the total thickness from the apron with reliable facies data. The T-6337 core that spans the Serpukhovian–Bashkirian boundary shows the Bashkirian to have a higher proportion of thick, allochthonous grainstone beds, while the Serpukhovian contains more frequent boundstone breccia and skeletal-lithoclast beds, with thinner and less abundant allochthonous grainstones. While the GR patterns described above suggest a crude systematic vertical lithologic pattern could exist within the apron, the variety of bedded facies so far found in core also suggests lateral variability is probably higher than for the wedge reservoir. The

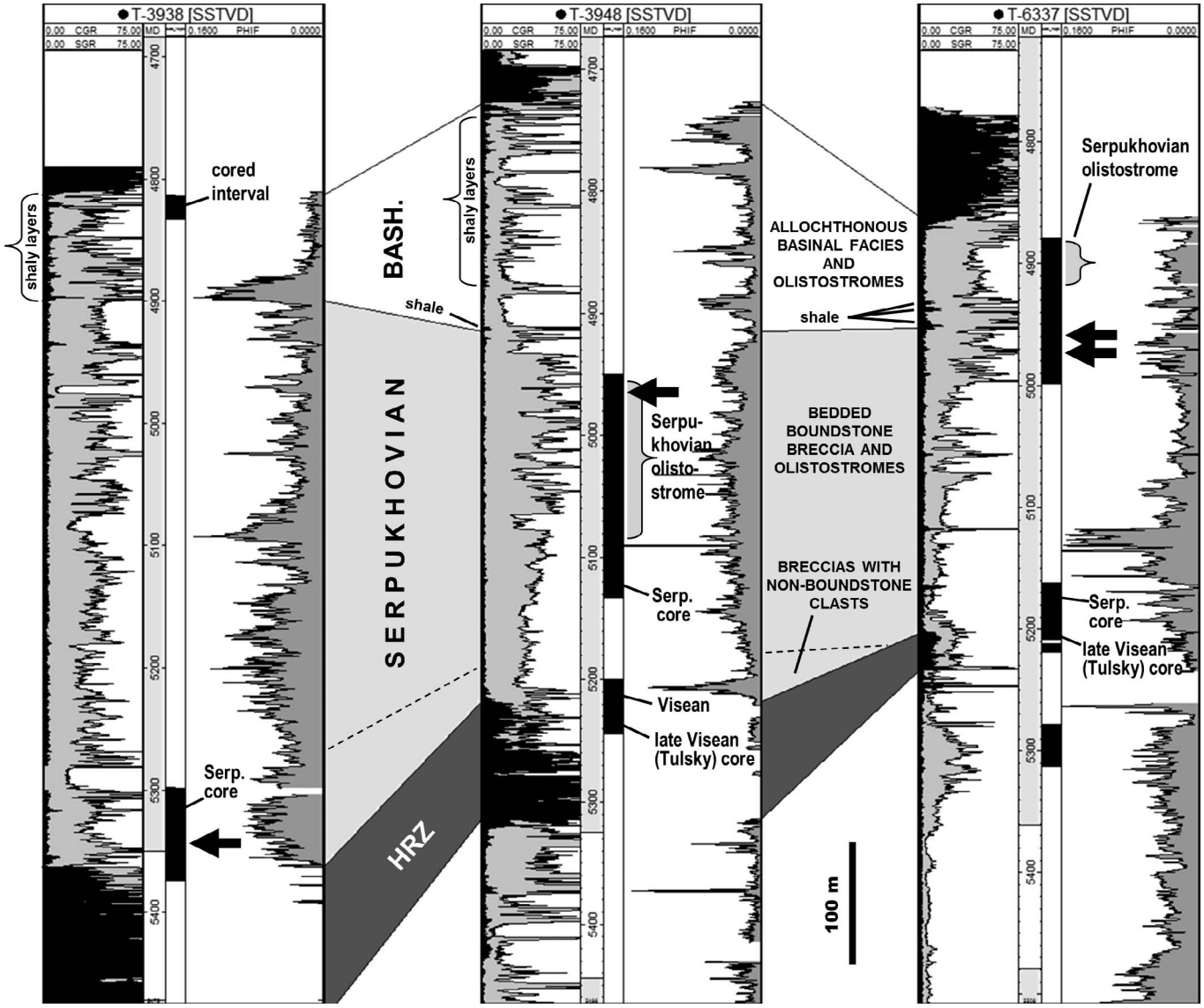

FIG. 24.—Cross section through the apron reservoir along the western buildup margin: Wells are selected to represent a dip profile but do not actually lie on a line (see Fig. 2 for locations). Distance from the buildup increases to the left. Well panels show two GR logs in the left track, SGR (gray-filled curve, total radioactivity) and CGR (solid black curve, potassium–thorium radioactivity). The difference between the curves indicates uranium radioactivity. The Serpukhovian–Bashkirian correlation is based on the appearance of clay beds near the base of the Bashkirian in the T-6337 well. Cored intervals representing interpreted olistostromes are noted. Note that an interval containing crinoid-rich breccias without boundstone clasts is absent in the T-6337 core above the HRZ but present in the other wells. PHIF porosity logs (right track, scale from 0 to 16%, increasing to the left) suggest considerable heterogeneity in the vertical and lateral distribution of higher-porosity zones. Arrows indicate locations of core slab photos in Figure 23. See Figure 2 for well locations.

olistostromes and large upper slope clasts display early lithification by marine and other calcite cements, similar to that of their in situ counterparts in the wedge reservoir, but most of the bedded, coarse-grained allochthonous material became lithified as a result of grain compaction or the presence of micrite matrix (Fig. 25).

Well-exposed outcrops of coarse allochthonous carbonate facies are readily available (e.g., Braithwaite and Heath 1992; Eberli et al. 1993; George et al. 1997; Vecsei et al. 1998; Janson et al. 2007, 2011; Phelps and Kerans 2007; Playton 2008; Playton et al. 2010; Goldstein et al. 2012), but themes that could be used to quantify vertical and lateral lithofacies variations to demonstrate possible limits of internal reservoir continuity within the Tengiz apron or themes that describe stratigraphic and lithofacies relationships with an overlying progradational unit that could be used as an analog for the boundary between the Tengiz apron and the wedge reservoirs are not emphasized or are not adequately exposed. In general, lithofacies variability and continuity appear to vary considerably between these outcrop areas. The examples cited therefore provide little specific quantitative constraints for the Tengiz apron reservoir, but they suggest that a

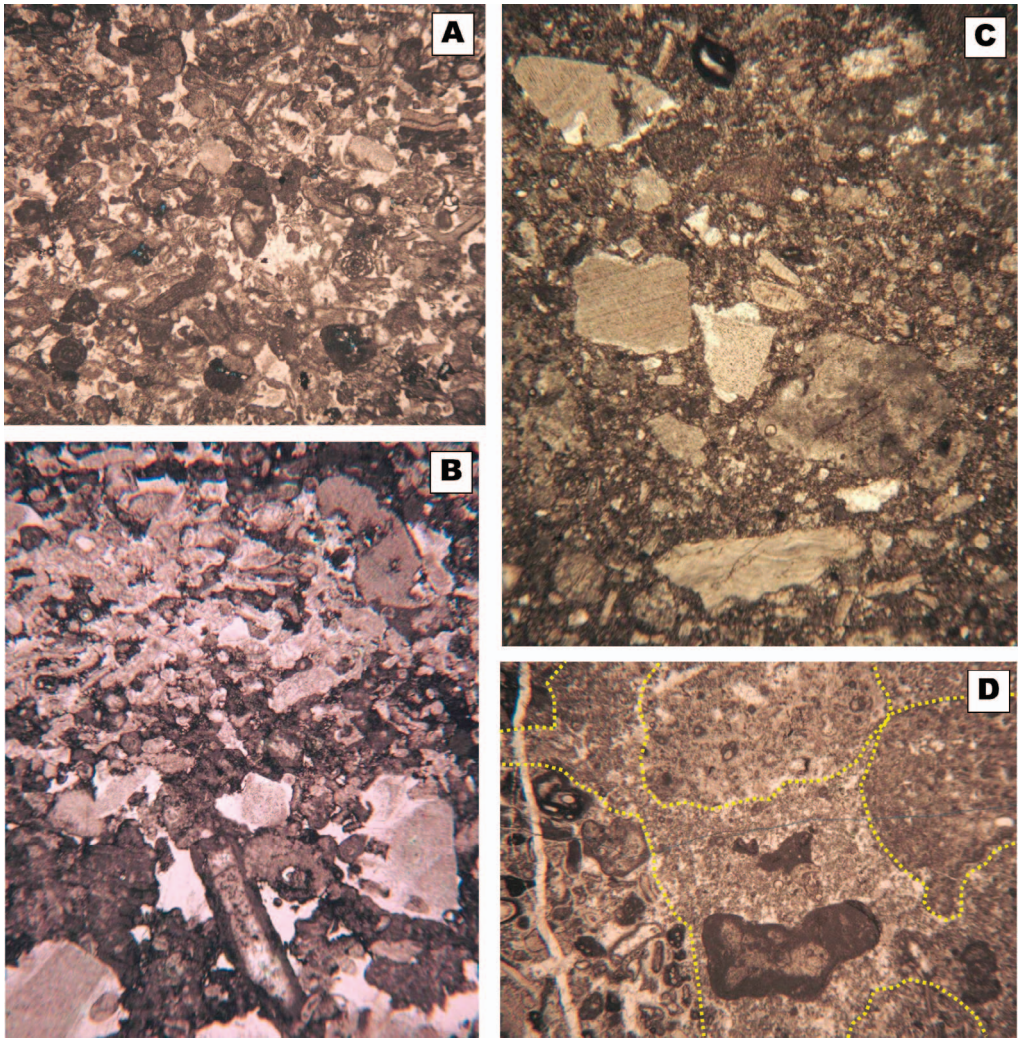

FIG. 25.—Lithification in coarse allochthonous facies of the apron reservoir: These facies generally lack early marine cements, with compaction influenced mainly by grain support. **A)** Compacted grainstone with discontinuous cements around and between grains; **B)** Highly compacted grainstone with interpenetrating grain contacts and only minor syntaxial cement; **C)** Matrix-supported breccia with micrite between clasts; **D)** Clast-supported breccia with micrite and fine skeletal material between clasts. Thin-section photos represent low magnification and are ~1 to 2 mm wide.

general theme of high vertical and lateral lithofacies heterogeneity exists within the apron reservoir.

DISCUSSION: IMPACT OF BURIAL DIAGENESIS ON FRACTURES AND ON RESERVOIR CONTINUITY AND COMMUNICATION IN SUBCOMPARTMENTS

Subsurface reservoir quality is an attribute that encompasses both porosity and permeability. The impact of burial diagenesis on Tengiz reservoir quality does not have to be judged by the size of a porosity increase, and negative or positive changes can have equal status in terms of whether an impact is important. The impact of burial diagenesis on the Tengiz reservoir has three main themes: One is physical or visual presence; another theme is the actual net amount of pore space created or destroyed; the third and more important theme is its possible effects on reservoir permeability, connectivity, and communication. In both the wedge and apron reservoirs the physical aspect of burial diagenesis is a visually conspicuous overprint that in fact contributes to the low overall matrix porosity measured by well logs. However, burial diagenesis is also associated with fracture enlargement in a reservoir for which fracture and cavernous porosity represent major elements of permeability. It is more of a challenge to state from the Tengiz core and BHI data that the observed burial diagenetic overprint transformed an otherwise less effective or ineffective fracture system into an more effective or effective system of fractures and caverns, let alone to demonstrate that the communication between the Tengiz reservoir subcompartments indicated by the pressure data would not exist in the absence of burial diagenesis.

The observed association between burial diagenesis and fractures or caverns in cores and BHI logs includes halos around enlarged

fractures that contain the burial overprint (equant calcite, bitumen, microporosity) accompanied by evidence of dissolution along fracture walls (see Figs. 11E, 12). More specifically, burial overprint halos occur around solution-enlarged fractures in facies with low matrix porosity that are common in the wedge reservoir, while facies with higher matrix porosity, mainly from the PTZ and the apron reservoir, tend to have enlarged fractures and rubble zones in intervals where a pervasive burial overprint exists in the matrix. An outcrop analog is presented in comparison with Tengiz data from the wedge reservoir that illustrates how selective dissolution of fractures, regardless of differences in the dissolution mechanism, might result in a well-connected wedge reservoir subcompartment containing cavernous porosity, as suggested by the Tengiz pressure data. A feedback mechanism by which fracture permeability and fracture connectivity increases during dissolution is described in association with certain textures and dissolution fabrics that have been identified in the outcrop and in the Tengiz reservoir. By this mechanism, an increase in permeability and connectivity can be achieved through fracture dissolution without necessarily dramatically increasing total reservoir pore volumes. Average matrix porosity in slope facies of the wedge reservoir (see Fig. 9) is too low for matrix permeability to be a factor in the high productivity of rim wells (Sullivan et al. 2006, Tankersley et al. 2010). On the other hand, there are well-documented instances of nonmatrix voids (fractures and caverns) contributing directly to multi-darcy wellbore inflow and general summaries indicating the influence of nonmatrix porosity on the high production rates of Tengiz rim and flank wells (Narr et al. 2004, Sullivan et al. 2006, Tankersley et al. 2010). Production rates from the wedge reservoir are variable (Fig. 13), and in the absence of high matrix permeability, the uniform pressure decline for the wedge reservoir implies that the nonmatrix pore system must be internally well connected.

The nonsystematic pressure decline in the apron reservoir and the lower production rates could be interpreted as an indication of increased internal reservoir quality heterogeneity in general as well as of reduced fracture permeability. Coarse allochthonous facies show a greater contribution of mechanical compaction over cementation to early lithification (Fig. 25), and early fractures are likely to be less abundant in these facies, relative to the cemented microbial facies on the slope. The pressure data give no indication that enlarged fractures in the apron reservoir are as well developed or as well connected as those in the wedge reservoir.

Fracture Outcrop Analog

Flow simulation of Tengiz reservoir models currently employs a dual porosity–dual permeability numerical approach that does not contain discrete fracture objects but that nevertheless uses fracture size and spacing information (Tankersley et al. 2010). Size and spacing data for the solution-enlarged fractures and other nonmatrix voids identified in cores, BHI logs, or during drilling operations are limited and associated with a large degree of uncertainty, especially as they relate to fracture height and length. Tengiz fracture heights cannot be quantified because the cores and borehole images almost never follow along a fracture surface for more than a few meters, but height data are important in reservoir simulations for control of gravity drainage, recovery efficiency, and vertical permeability. Fracture length is significant for controlling horizontal permeability, permeability anisotropy, and connectedness throughout regions. Solution-enlarged fractures from the Windjana Gorge outcrops in the Canning Basin provided a source of input data and constraints for effective fracture height and a range of fracture spacing for comparison with values determined from well data in these models.

Fractures in platform-top and adjacent slope facies of these outcrops were studied (Narr and Flodin 2012). Specifically, apertures, height distributions, and spacing characteristics of open fractures were measured across the transition from aggrading platform-top facies to prograding slope facies exposed in Windjana Gorge, noting also the control on fracture orientation imparted by the shape of the depositional margins. Fracture porosity was estimated from average apertures, height, and spacing in 75-m-long measurement bins. Fracture apertures ranged from zero to several tens of centimeters, and aperture variability is likely nonlinear; therefore, average apertures provide only porosity range estimates. Estimated fracture porosity values ranged from 0% to about 5%, with the average for the entire Windjana Gorge traverse (Fig. 26) in the range of 1 to 2%. Many present-day apertures are partially filled by calcite cement, and if it is assumed that all of the enlarged fractures observed today were once filled by calcite prior to dissolution, then 1 to 2% represents an upper limit for the total amount of material dissolved.

Fracture height data from the outcrop were derived from a set of "tall" fractures (fractures >2 m) ranging in height up to at least 90 m (the extent of the exposed outcrop) that have been interpreted as early (syndepositional) fractures (Frost and Kerans 2009). Playford (1984), Hurley (1986), and Frost and Kerans (2010) have pointed out that facies exert a strong measure of control over the orientation of syndepositional fractures in the Canning Basin. Like many previous workers cited elsewhere in this article, we noted that the syndepositional fractures in the prograding slope facies of Windjana Gorge are predominantly parallel and perpendicular to the depositional margin and follow its strike trend. Fracture orientations in the aggradational platform margin to the east show greater variability (Fig. 26A), likely as a result of large-scale collapse of this margin prior to progradation and increased mechanical heterogeneity in the platform-top facies (Frost and Kerans 2010). A similar orientation change from the rim into the platform margin is suggested at Tengiz (compare Figs. 10 and 26), but it is poorly constrained around the field by borehole image data. As is the case with the Tengiz fractures, early fractures in the Canning Basin have various types of early fill, such as coeval sediments, marine cements, and microbial encrustations (e.g., Kerans 1985, Kerans et al. 1986, Frost and Kerans 2009, Playford 2009). Early fractures in the Lennard shelf of the Canning Basin were potentially solution-enlarged twice after burial, once during extensive karst development, when the Devonian Lennard shelf carbonates were uplifted and covered by Permian continental glaciers of the Gondwanda supercontinent (Playford 2002, Playford et al. 2009), and again during telogenetic dissolution by surface waters (Wallace et al. 1991). Despite their early fills the fractures were targets for dissolution, suggesting that the fracture fills included material more soluble than the adjacent matrix or that the fractures were incompletely filled or that they were reactivated. Based on the data in Figure 26B, average fracture height and frequency in the slope facies of the Windjana Gorge are both approximately double the values in the reef flat and outer platform. Unfortunately, fracture lengths were not studied as a result of difficulties in obtaining reliable data on this dimension from the field.

Fracture Dissolution Sequence and Implications for Tengiz Field

We focused on solution-enlarged fractures in Windjana Gorge because of the evidence from Tengiz BHI logs and cores indicating that solution-enlarged fractures represent most of the effective nonmatrix porosity controlling fluid flow and reservoir connectivity in the Tengiz wedge reservoir. Although dissolution of the Lennard and Tengiz fractures occurred by different mechanisms and at different times relative to their respective burial histories, selective dissolution of early fractures (over other types of fractures) occurred in both places. For the solution-enlarged fractures, similar stages of enhancement are evident in both areas that show qualitative size and

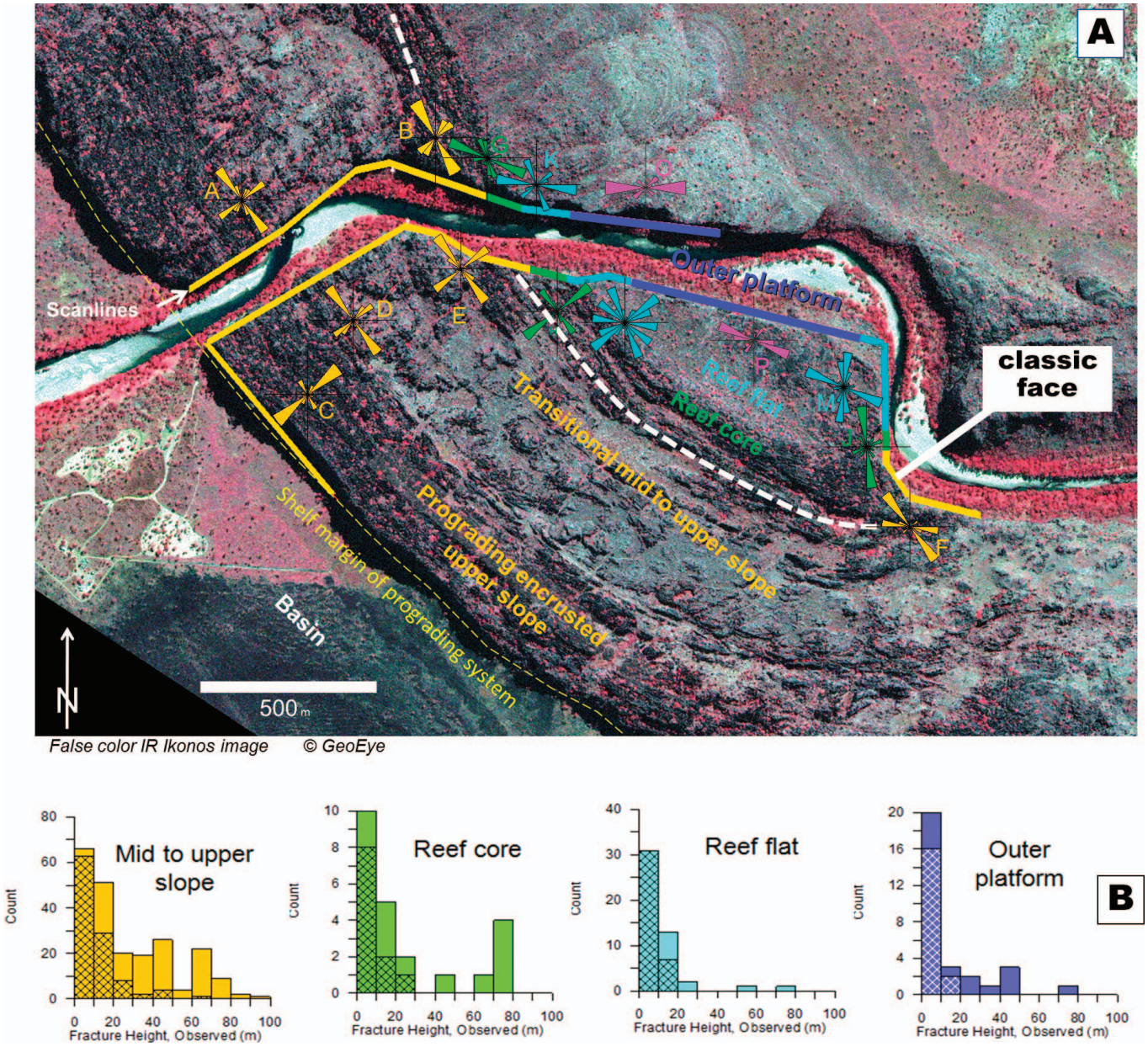

FIG. 26.—Orientation patterns of enlarged tall fractures by depositional environment in Windjana Gorge, Western Australia: **A)** Satellite image of Windjana Gorge showing traverse paths and bias-corrected (Terzaghi 1965) fracture orientations in the slope, reef core, reef flat, and outer platform environments. The slope includes middle to upper slope prograding facies in the outer zone (south and west of the dashed white line) analogous to the Tengiz wedge reservoir. Fracture orientations are parallel and normal to the margin in the slope facies. Fracture orientations become less systematic in the reef flat and outer platform facies. The reef flat and outer platform facies in the outcrop are analogous to cyclic platform-top facies in the Tengiz late Visean sequence, but the reef core facies are likely not present in Tengiz (after Narr and Flodin [2012]). **B)** Fracture height distributions according to the facies illustrated in A for early fractures in Windjana Gorge. Hachures indicate fractures, the upper terminations of which are visible in the cliff face; the solid pattern indicates fractures that extend beyond the outcrop (after Narr and Flodin [2012]).

other physical attribute similarities. Both the enlarged fractures on Tengiz BHI logs from different wells and the enlarged fracture system in Windjana Gorge illustrate similar stages of small cavern development from fracture dissolution. In the initial stages of dissolution, the fractures developed enhanced corrosion streamlines or "worm tubes" that show a "string of pearls" appearance (Fig. 27A). Progressive enlargement led to increasingly wide fracture apertures with approximately parallel walls (Fig. 27B, C). In some cases fracture dissolution forms small caverns in which the walls are not parallel (Fig. 27D) and have irregular shapes.

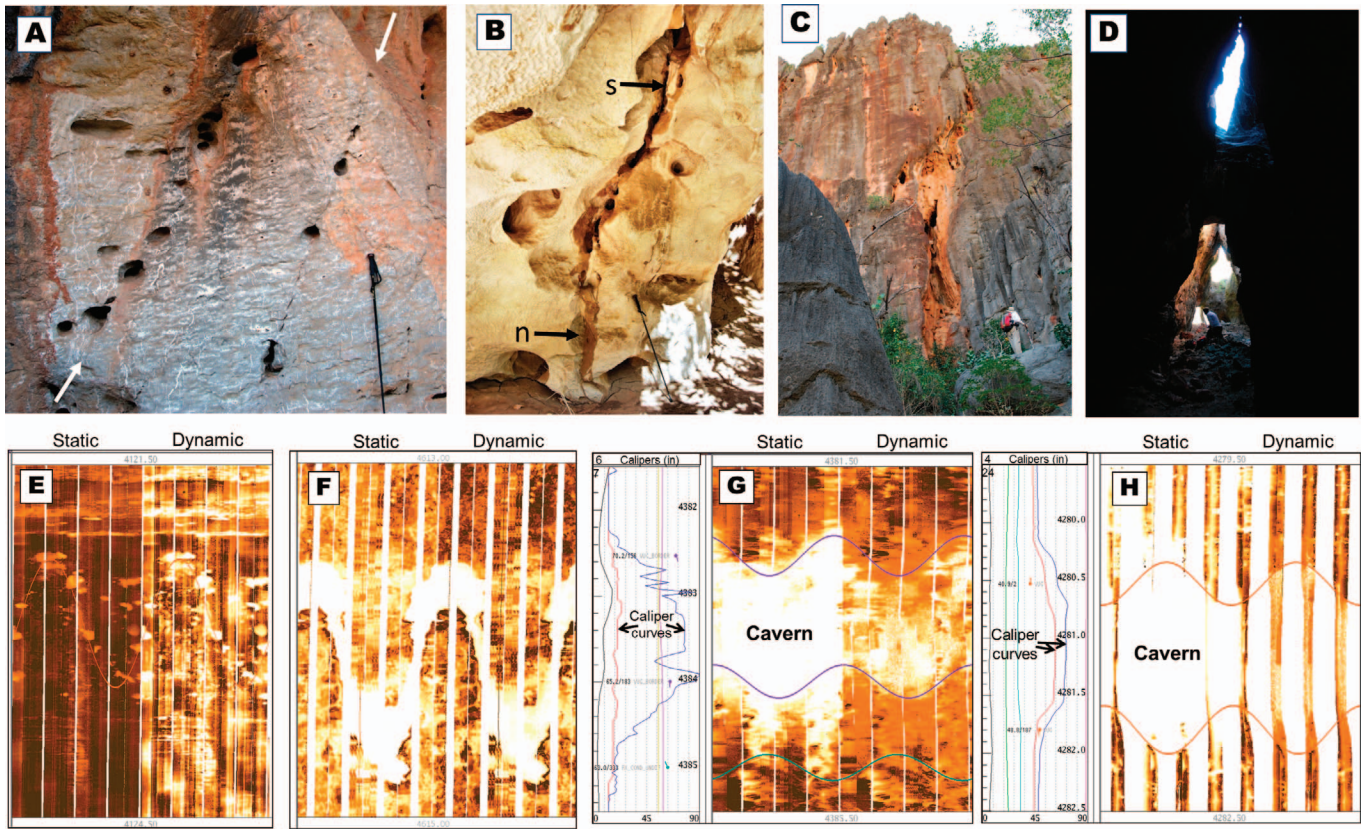

FIG. 27.—Similar stages of cavern development from selective dissolution of fractures in Windjana Gorge **(A–D)** and in the Tengiz Field **(E–H)**: Enlargement of the fracture system occurs by initial formation of "string-of-pearls" features representing corrosion-induced streamlines (worm tubes) developed along a fracture **(A)**, which become a continuous enlarged fracture **(B)**. Dissolution progresses in the enlarged fractures, forming wider fractures with irregular to nonparallel wall shapes **(C)** and eventually small caverns **(D)**. Borehole image and caliper logs reveal a similar sequence of fracture enlargement and cavern formation for Tengiz: **E)** BHI log image of "string-of-pearls" dissolution along a fracture in T-5442 from the platform region, about 1 km from the late Visean platform margin; **F)** Enlarged fracture from the wedge reservoir, middle slope facies (T-5660); **G)** Small (∼1.5-m) cavern from the wedge reservoir (T-7450, upper slope facies) with parallel walls, indicating origin from fracture enlargement; **H)** Cavern with nonparallel walls from the wedge reservoir (T-5454, probably middle slope facies with elevated matrix porosity). Tengiz wells were drilled with oil-based mud, with open features expressed as resistive features (brighter colors) on BHI logs. Caliper logs are not shown for E and F because they indicated no borehole enlargement across the fractures. Static and dynamic BHI each represent a borehole circumference of ∼20 cm and depth intervals of 2 to 4 m.

The enlarged fractures in the Lennard shelf outcrops have several implications for the Tengiz reservoir. Tengiz fractures are interpreted to be most abundant in early-lithified in situ upper slope microbial boundstones and massive middle slope boundstone breccias because the large volumes of early marine cement observed in core promoted mechanical rigidity and increased early fracturing (Narr et al. 2004, Carpenter et al. 2006, Tankersley et al. 2010). Frost and Kerans (2009, 2010) suggest that maximum fracture height in the Lennard shelf is related to similar large-scale mechanical units that track early lithification patterns: for example, early cemented progradational slope facies, which contrasts with shorter fractures in facies representing aggradational platform cycles. The Asturias outcrop (Fig. 20) was used to predict that the Tengiz slope boundstone facies form a continuous mechanical unit, reflecting an early lithification pattern. The Asturias and Windjana Gorge outcrop analogs can be combined to predict that more frequent and taller fractures are also likely present throughout the slope boundstone facies of the Tengiz wedge reservoir. No data were collected comparing fracture height/length relationships in the Windjana outcrops, but qualitatively the outcrops suggest that taller fractures (measured normal to bedding) will tend to be relatively longer fractures (measured parallel to bedding). For Tengiz, these relationships mean that the early fractures in the slope facies, after solution enlargement, are the most likely candidates to contribute to the high connectivity indicated by the field pressure data.

The heights of early fractures suggested by the Windjana Gorge example were therefore used as a reservoir characterization parameter for Tengiz flow simulations because both the Lennard fractures and the early Tengiz fractures initially formed in similar boundstone facies with similar geometries and depositional circumstances (progradation) and because of observed similarities in the widths of enlarged fractures and the thickness of enlarged fractures and small caverns on Tengiz BHI logs. While we noted the size similarity, no attempt was made to apply fracture apertures or cavern sizes from the Canning

system to Tengiz reservoir volumes; only the height data was used. Fracture spacing interpretation for the Tengiz reservoir is derived mainly from BHI logs using the approaches of Narr (1996) and Tankersley et al. (2010). It is nevertheless useful to consider the increase in total porosity that fracture dissolution might represent at Tengiz. The aperture increase represented by a single enlarged fracture in core or in outcrop compared to its original state represents a dramatic increase in local porosity. The statistics from the Windjana Gorge traverse suggest that a well-developed, solution-enlarged fracture system has a fracture porosity of only 1 to 2%. The fracture porosity estimated for the Tengiz wedge reservoir is even smaller (0.4%); hence, the major impact of burial diagenesis on Tengiz reservoir quality relates primarily to changes in fracture permeability and connectivity, not to changes in total pore volume.

Another implication is related to the circumstances that favored dissolution of syndepositional fractures over other fractures that may be present. The Tengiz fractures studied in cores appear to have been extensively filled by pre-bitumen cements or sediment, whereas many of the effective fractures appear to lack the early cement phases. However, even well-cemented early fractures may retain enough residual porosity that they represent the most soluble and most fluid-accessible conduits, and some fractures may have been reactivated prior to dissolution. Under these circumstances, fracture dissolution may be sufficient to eliminate evidence of previous fill phases or evidence of reactivation, and an early fracture may be interpreted as a later fracture on the basis of cements precipitated after dissolution. Based on Figure 6, reactivation of Tengiz early fractures, if it occurred, may have been possible during either the late Paleozoic burial phase or even later, during the Mesozoic burial associated with reservoir depressurization and bitumen formation.

A third implication is related to the degree that fracture systems enlarged by fundamentally different dissolution processes can be compared. Dissolution and maintenance of an open fracture system such as the one at Tengiz would have required flux of a substantial volume of fluid through the fractures (Palmer 1991). In the case of the Windjana Gorge analog, the flux during either the Permian or present-day exposures was a direct supply of meteoric fluids across the breadth of the fracture system. In order to produce similar cavernous porosity associated with selective fracture dissolution during burial in the subsurface, the Tengiz fracture system would need to have experienced a comparable flux per rock volume of undersaturated fluids across the fracture system, either by subsurface migration or by continual large-scale circulation through fractures in the subsurface. We interpret the burial overprint observed near enlarged fractures in each of the PTZ, the wedge, and the apron reservoirs to indicate that efficient fracture pathways provided access for whatever burial fluid flux operated within or between the Tengiz reservoir subcompartments.

The Windjana exposures demonstrate how the dissolution-enlarged fracture system at Tengiz might look across the transition between the wedge and platform reservoirs. The scenario provides a conceptual explanation for the apparent dynamic communication between the two reservoirs that is beyond the capability of current well data to confirm or refute. The observation of burial diagenesis associated with enlarged fractures in the PTZ, wedge, and apron reservoirs indicates that the formation of the Tengiz enhanced fracture system involved different types of undersaturated fluids than were involved at Windjana Gorge. Despite the different dissolution histories and processes, the application of data from the solution-enlarged fracture system in the Canning outcrops to Tengiz encompassed only the lowest common denominators: selective dissolution of the same genetic set of fractures from similar depositional environments and facies and data that are not obtainable from wells in the field (fracture height).

Mechanisms of Fracture Dissolution

The process of selective fracture network dissolution in either the Canning Basin example or in the Tengiz reservoir is a positive feedback system that entails circulation or migration of an undersaturated fluid or fluids that causes enlargement of enough fractures to then establish the fractures as preferred pathways for subsequent fluid flow, resulting in continual maintenance of an open fracture system (Palmer 1991). In addition to this general constraint, the enlarged fracture apertures and sizes of any associated caverns formed during enlargement also reflect the size of the supply and type(s) of undersaturated fluid in terms of the amount of calcite it (they) can dissolve or carry away. Another constraint, specific to Tengiz, is the observed concentration of enlarged fractures and the associated matrix burial diagenetic overprint in the PTZ, wedge, and apron reservoirs. Here we make no specific interpretations of a mechanism for Tengiz that explains all the observations presented; instead we qualitatively evaluate various proposed scenarios for burial diagenesis in the rim and flank in terms of these constraints. These scenarios include geothermal groundwater convection; sulfuric acid formation during H_2S buildup; variations in calcite solubility controlled by organic acids in the presence of hydrocarbons; charge by an external hydrothermal or basinal fluid; or one or more of these processes acting in concert with active groundwater convection.

The potential for large-scale geothermal circulation of groundwater in the rim and flank driven mainly by temperature was illustrated by Jones and Xiao (2006, fig. 8) and Jones et al. (2008). Although this mechanism was modeled for depositional and shallow burial conditions, it may be appropriate during later burial as long as similar fracture permeability existed and as long as an equally strong temperature driver was present. The amount of local dissolution they report for convection cells in the Serpukhovian slope facies (up to 1.6%) compares favorably with the fracture pore volumes estimated for both Tengiz and the Windjana Gorge fractures. The convection scenario has the appeal of being naturally restricted to the rim and flank by fracture permeability. The reservoir forms a closed diagenetic system in which contemporaneous dissolution and precipitation of calcite occur within the convection cells; therefore, the permeability structure of the fractured reservoir could be altered without any change to the total pore volume. Their closed convection models were limited by conditions of local undersaturation, however, and indicated contemporaneous calcite precipitation within the same fracture system being dissolved. It is not certain, therefore, that a well-connected fracture network could be formed and maintained under these conditions.

Large-scale flux of an external hydrothermal fluid has also been proposed, both for the origin of bitumen and for dissolution and burial diagenesis in the rim and flank (Hallager 1997, personal communication cited in Warner et al. [2007]). While theoretically possible, there is little evidence for or against this scenario. Hydrothermal temperatures have been reported from calcite cements in the reservoir (Collins et al. 2013), and exotic cements or replacement phases (chalcedony, barite, fluorite, fluoroapatite, dickite, and saddle dolomite) are occasionally observed in thin section that can form in hydrothermal settings, but their presence does not imply large-scale dissolution of calcite.

Formation of sulfuric acid during buildup of H_2S in the reservoir has also been proposed as a dissolution mechanism for Tengiz (Collins et al. 2006). H_2S levels greater than a few percent in subsurface sour gas accumulations are generally attributed to deep burial thermochemical sulfate reduction (TSR) (Orr 1977, Machel 1987), and the concentrated H_2S in Tengiz oil (13.4%) is thought to have migrated to the reservoir after being generated by TSR off structure, based primarily on the scarcity of reactive sulfate within the reservoir (Warner et al. 2007). Fracture dissolution is possible because sulfuric

acid can form by mixing with an external fluid of higher H_2S concentration than the reservoir groundwater (Hill 1992, 1995; Stoessel 1992). However, the local petroleum system in which Tengiz is located is not sufficiently understood to know whether the H_2S migrated to the reservoir through an aquifer alone or whether it was dissolved in the oil of the primary charge. Figure 6 also suggests that the 100 to 140° C temperatures normally required for TSR (Machel 1998, 2001) were not achieved until after the bitumen formed. H_2S-related dissolution can more readily explain observed instances of postbitumen dissolution, but not the earlier burial overprint related to bitumen and calcite co-precipitation. H_2S-related dissolution could be restricted to the rim, flank, and PTZ by fractures as well and if these areas served as a chemical buffer zone within which acidity was ultimately reduced and dissolution ceased.

The large reservoir pressure fluctuations indicated on Figure 6 interpreted as the main mechanism for bitumen formation suggest an alternative dissolution process involving transient fluid flow triggered by the natural reservoir depressurization. The formation of bitumen means that hydrocarbons were present during the fluctuations, but they were also in the process of evacuating the reservoir as a consequence of the fluctuations. Figure 6 also indicates that new hydrocarbons representing the primary charge were being delivered to the reservoir at around the same time. As previously discussed, calcite solubility would have varied as a result of the pressure changes alone. A contemporaneous flux of hydrocarbons within the reservoir could have also formed organic acids in the groundwater (Helgeson et al. 1993, Morad et al. 2000) in connection with pressure and $CO_2(g)$ solubility fluctuations, increasing the chances for calcite dissolution. This explanation has the attraction of linking a number of disconnected observations, such as bitumen–calcite co-precipitation, in situ microporosity enhancement, and the dissolution progression feedback sequence observed on BHI logs (Fig. 27E–H). Initial fracture corrosion would have occurred mostly in situ, driven by the paleo-pressure decline that was also the source of the burial overprint in the matrix. The magnitude of the pressure fluctuations (~7000 psi) likely would have induced large temporary pressure transients across the field. Depending on the size and extent of the aquifer, these transients may have been sufficient to activate groundwater flow within the reservoir, which was now more susceptible to diagenesis as hydrocarbons evacuated. At this point, several options could have led to selective fracture dissolution, including (1) reactivation of fractures in response to pressure changes and fluid flow; (2) increased local undersaturation–supersaturation disequilibrium arising from increasingly fast circulation or perhaps even initiation of geothermal convection throughout the fracture system via the fracture-enlargement feedback mechanism; (3) injection of additional undersaturated external fluids via the pressure transient; and (4) contemporaneous migration of new hydrocarbons into the reservoir, forming organic acids available to be circulated in fractures. Equant calcite and bitumen cements are common in secondary microfractures from the Tengiz rim and flank (Collins et al. 2008, Poster 6). Many of these fractures are associated with stylolites, which may have even formed during brief accelerated compaction in response to pressure declines, possibly accompanied by reactivation of some of the early fractures. A reactivated early Tengiz fracture system, especially if it became a more efficient fluid conduit with time through self-perpetuating progressive enlargement, would also tend to confine burial dissolution and related diagenesis to the rim and flank areas.

SUMMARY AND CONCLUSIONS

The integration of field dynamic data with stratigraphy, facies, fracture systems, and diagenetic patterns allows the Tengiz late Visean to Bashkirian interval to be grouped into three geologically defined reservoir subcompartments or material balance regions. These subcompartments—the platform, wedge, and apron subcompartments—are separated primarily by stratigraphic boundaries, with burial diagenesis interpreted to have played a role in both internal connectivity and communication across their boundaries. Each subcompartment is characterized by different large-scale internal lithofacies distributions, and their respective dynamic behaviors are functions of lithofacies continuity and its influences on the distribution of nonmatrix permeability.

The boundary between the platform and wedge reservoirs occurs where the aggradational late Visean platform margin joins the progradational Serpukhovian slope sequence, with baffled communication between them interpreted to be provided by an early fracture system enhanced during burial diagenesis across the PTZ. The boundary between the wedge and apron reservoirs is interpreted to be a stratigraphic baffle related to an early depositional phase of frequent slope failure and accumulation of allochthonous debris that underlies a later depositional phase dominated by progradation. Subsurface data and outcrop analogs are consistent with the presence of continuous slope facies prone to early fracture formation in the progradational sequence.

Outcrop analogs were especially useful for predicting the lithofacies thicknesses and continuity in the wedge reservoir beyond the ability of current well and seismic data, and, based on the presence of more frequent open fractures in early-lithified slope microbial lithofacies, the analogs further predict that connected, facies-controlled, solution-enlarged fractures are the reason for the high degree of pressure communication within the wedge subcompartment. Supplemental core observations were interpreted to indicate that burial diagenesis could be responsible for improved fracture permeability and reservoir connectivity in the wedge reservoir without necessarily dramatically increasing the total reservoir pore volume. In more detail, the observations from the field and from the outcrops included the following.

1. The wedge reservoir is predicted to consist of laterally continuous, diachronous horizontal lithofacies zones created during progradation based on fits of outcrop analogs to field data but that cannot unequivocally be extrapolated from the field data alone. Nonmatrix porosity (fractures and small caverns) was preferentially developed in slope microbial facies (in situ boundstone and downslope massive boundstone breccia) because of early fractures concentrated in this facies that were selectively enlarged during burial dissolution. The enlarged fractures may have been reactivated during burial prior to dissolution, thereby overcoming early cement fills and making them targets for late burial dissolution.
2. The wedge reservoir and the PTZ both have the burial diagenetic overprint in the matrix adjacent to enlarged fractures. These fractures display a dissolution sequence on BHI logs suggesting progressive enlargement to form a well-connected fracture network. An outcrop analog displaying the same dissolution sequence in enlarged fractures across similar environments and facies and with similar overall fracture apertures and small cave sizes was used to supplement poorly constrained data for fracture height in reservoir simulations of the field.
3. The erratic dynamic behavior of the apron reservoir is interpreted to be in part due to heterogeneous distribution of bedded coarse allochthonous facies derived mainly from upper slope failure. Bedded lithofacies controlled and localized the distribution of matrix porosity, including the effect of the burial overprint. Bedded facies also limited the size, frequency, and distribution of both early and secondary fractures, thereby limiting their contribution to flow, even after solution enlargement. The uneven depletion may also reflect regions of greater and lesser communication with the wedge reservoir across the stratigraphic baffle. As illustrated in Collins et al. (2006, 2008), the areal extent of the aprons and the

width of the wedge reservoir both vary irregularly around the buildup. In some areas, the extent of the apron reservoir is largely unknown as a result of complete burial by the wedge, and in other areas there is no connection because the wedge reservoir is absent by complete failure. The full effects of the stratigraphic baffle will be revealed only when more details about how slope failure and apron deposition are related around the buildup become known.

4. Late burial dissolution influenced reservoir quality in the Tengiz apron and wedge reservoirs mainly by improving fracture permeability. The increase in fracture permeability occurred via a fracture flow-dissolution feedback mechanism, without necessarily creating large new pore volumes. The absence of the burial overprint in the central platform (except for bitumen precipitation) is further evidence that the rim and flank fractures became better connected during burial dissolution, restricting fluid circulation and associated diagenesis to the apron, wedge, and PTZ reservoirs. The enhanced fracture connectivity is manifested today as an extremely uniform production pressure decline observed in the wedge reservoir.
5. For matrix porosity, burial diagenesis is mainly a physical presence, as an overprint on pre-bitumen diagenetic sequences throughout the PTZ, wedge, and apron subcompartments. The matrix burial overprint is interpreted to represent mainly in situ diagenesis resulting from large-scale reservoir paleo-pressure fluctuations in the presence of hydrocarbons. It created microporosity locally while resulting overall in average matrix porosity reduction, but it provides a key to recognizing the overall distribution of burial diagenesis in the field.

REFERENCES

Babcock JA. 1977. Calcareous algae, organic boundstones, and the genesis of the upper Capitan Limestone (Permian, Guadalupian), Guadalupe Mountains, West Texas and New Mexico. *In* Hileman ME, Mazzullo SJ (Editors). *Upper Guadalupian Facies, Permian Reef Complex, Guadalupe Mountains, New Mexico and West Texas*, Publication 77-16: SEPM Permian Basin Section, Midland, Texas. p. 3–44.

Bahamonde JR, Colmenero JR, Vera C. 1997. Growth and demise of Middle Carboniferous carbonate platforms in the eastern Cantabrian Zones, Asturias, NW Spain. *Sedimentary Geology* 110:99–122.

Bahamonde JR, Vera C, Colmenero C. 2000. A steep-fronted Carboniferous carbonate platform: clinoformal geometry and lithofacies (Picos de Europa, NW Spain). *Sedimentology* 47:645–664.

Bathurst RGC. 1975. *Carbonate Sediments and their Diagenesis*, Developments in Sedimentology 12: Elsevier, New York. 658 p.

Bebout DG, Kerans C (Editors). 1993. *Guide to the Permian Reef Geology Trail, McKittrick Canyon, Guadalupe Mountains National Park, West Texas*, Guidebook 26: Bureau of Economic Geology, University of Texas–Austin. 48 p.

Braithwaite CJR, Heath RA. 1992. Deposition and diagenesis of debris flows in Upper Ordovician limestones, Hadeland, Norway. *Sedimentology* 39:753–767.

Brenckle PL, Milkina NV. 2003. Foraminiferal timing of carbonate deposition on the Late Devonian (Famennian)–Middle Pennsylvanian (Bashkirian) Tengiz platform, Kazakhstan. *Revista Italiana di Paleontologia e Stratigrafia* 109(2):131–158.

Bridges PH, Gutteridge P, Pickard NAH. 1995. The environmental setting of early Carboniferous mud-mounds. *In* Monty CLV, Bosence DWJ, Bridges PH, Pratt BR (Editors). *Carbonate Mud Mounds, Their Origin and Evolution*, International Association of Sedimentologists, Special Publication 23: Wiley-Blackwell, New York. p. 171–190.

Carpenter DG, Guidry SA, DeGraff JD, Collins J. 2006. Evolution of Tengiz rim/flank reservoir quality: new insights from systematic, integrated core fracture and diagenesis investigations (Abstract). Annual Meeting Abstract, Vol. 15: American Association of Petroleum Geologists, Tulsa, Oklahoma. p. 18.

Choquette PW, James NP. 1990. Limestones—the burial diagenetic environment. *In* McIlreath IA, Morrow DW (Editors). *Diagenesis*, Geoscience Canada Reprint Series 4: Geological Association of Canada, St. Johns, Newfoundland. p. 75–112.

Collins JF, Katz D, Harris PM, Narr W. 2013. Burial cementation and dissolution in Carboniferous platform-top, slope and basinal facies, Tengiz Field, Kazakhstan (Abstract): American Association of Petroleum Geologists Annual Meeting, May 19–22, Pittsburgh, Pennsylvania, USA.

Collins JF, Kenter JAM, Harris PM, Kuanysheva GD, Fischer DJ, Steffen KL. 2008. Facies and reservoir quality variations in the late Visean to Bashkirian outer platform, rim, and flank of the Tengiz buildup, Pricaspian Basin, Kazakhstan: American Association of Petroleum Geologists, Search and Discovery Article 20052. http://www.searchanddiscovery.com/documents/2008/08035collins/index.htm

Collins JF, Steffen KL, Kenter JAM, Harris PM, Kuanysheva GD, Fischer DJ. 2006. Facies and reservoir-quality variations in the late Visean to Bashkirian outer platform, rim and flank of the Tengiz buildup, Precaspian Basin, Kazakhstan. *In* Harris PM, Weber LJ (Editors). *Giant Hydrocarbon Reservoirs of the World: From Rocks to Reservoir Characterization and Modeling*, Memoir 88: American Association of Petroleum Geologists/SEPM (Society for Sedimentary Geology), Tulsa, Oklahoma. p. 55–95.

Della Porta G. 2003. Depositional anatomy of a Carboniferous high-rising carbonate platform (Cantabrian Mountains, NW Spain) [PhD thesis]: Vrije Universiteit, Amsterdam, 250 p.

Della Porta G, Kenter JAM, Bahamonde JR. 2002. Microfacies and paleoenvironment of Donezella accumulations across an Upper Carboniferous high-rising carbonate platform (Asturias, NW Spain). *Facies* 46:159–168.

Della Porta G, Kenter JAM, Bahamonde JR. 2004. Depositional facies and stratal geometry of an Upper Carboniferous prograding and aggrading high-relief carbonate platform (Cantabrian Mountains, NW Spain). *Sedimentology* 51:267–295.

Della Porta G, Kenter JAM, Bahamonde JR, Immenhauser A, Villa E. 2003. Microbial boundstone dominated carbonate slope (Upper Carboniferous, N Spain): microfacies, lithofacies distribution and stratal geometry. *Facies* 49:175–208.

Eberli GP, Bernoulli D, Sanders D, Vecsei A. 1993. From aggradation to progradation: the Maiella Platform, Abruzzi, Italy. *In* Simo JAT, Scott RW, Masse JP (Editors). *Cretaceous Carbonate Platforms*, Memoir 56: American Association of Petroleum Geologists, Tulsa, Oklahoma. p. 213–232.

Flugel E. 2004. *Microfacies of Carbonate Rocks (Analysis, Interpretation and Application)*: Springer, Berlin. 976 p.

Frost EL III, Kerans C. 2009. Platform-margin trajectory as a control on syndepositional fracture patterns, Canning Basin, Western Australia. *Journal of Sedimentary Research* 79:44–55.

Frost EL III, Kerans C. 2010. Controls on syndepositional fracture patterns, Devonian reef complexes, Cannng Basin, Western Australia. *Journal of Structural Geology* 32:1231–1249.

George AD, Playford PE, Powell C McA, Tornatora PM. 1997. Lithofacies and sequence development on an Upper Devonian mixed carbonate–siliciclastic fore-reef slope, Canning Basin, Western Australia. *Sedimentology* 44:843–867.

Goldstein RH, Franseen EK, Dvoretsky R, Sweeney RJ. 2012. Controls on focused-flow and dispersed-flow deepwater carbonates: Miocene Agua Amarga Basin, Spain. *Journal of Sedimentary Research* 82:499–520.

Gutteridge P. 1995. Late Dinantian (Brigantian) carbonate mud-mounds of the Derbyshire carbonate platform. *In* Monty CLV, Bosence DWJ, Bridges PH, Pratt BR (Editors). *Carbonate Mud Mounds, Their Origin and Evolution*, International Association of Sedimentologists, Special Publication 23: Wiley-Blackwell, New York. p. 289–307.

Hallager WS, Suisinov K, Baskin DK, Garber RA, Harris PM, Warner JL. 1997. Two-stage hydrocarbon migration model for the Tengiz Field, Kazakhstan (Abstract). *American Association of Petroleum Geologists Bulletin* 81:1380.

Helgeson HC, Knox AM, Owens CE, Shock EL. 1993. Petroleum, oil field waters, and authigenic mineral assemblages: are they in metastable equilibrium in hydrocarbon reservoirs? *Geochemica et Cosmochemica Acta* 57:3295–3339.

Hill CA. 1992. Sulfuric acid oil-field karst. *In* Candelaria MP, Reed CL (Editors). *Paleokarst, Karst-Related Diagenesis, and Reservoir Development*, Field Trip Guidebook 92-33: SEPM Permian Basin, Midland, Texas. p. 192–194.

Hill CA. 1995. H_2S-related porosity and sulfuric acid oil-field karst. *In* Budd DA, Saller AH, Harris PM (Editors). *Unconformities and Porosity in Carbonate Strata*, Memoir 63: American Association of Petroleum Geologists, Tulsa, Oklahoma. p. 301–313.

Hurley NF. 1986. Geology of the Oscar Range Devonian Reef Complex, Canning Basin, Western Australia [PhD thesis]: University of Michigan, Ann Arbor, 269 p.

Hurley NF. 1989. Facies mosaic of the lower Seven Rivers Formation, McKittrick Canyon, New Mexico. *In* Harris PM, Grover GA (Editors). *Subsurface and Outcrop Examination of the Capitan Shelf Margin, Northern Delaware Basin*, Core Workshop Notes 13: SEPM (Society for Sedimentary Geology), Tulsa, Oklahoma. p. 325–346.

Janson X, Kerans C, Bellian JA, Fitchen W. 2007. Three-dimensional geological and synthetic seismic model of Early Permian redeposited basinal carbonate deposits, Victorio Canyon, West Texas. *American Association of Petroleum Geologists Bulletin* 91:1405–1436.

Janson X, Kerans C, Loucks R, Marhx MA, Reyes C, Murguia F. 2011. Seismic architecture of a Lower Cretaceous platform-to-slope system, Santa Agueda and Poza Rica Fields, Mexico. *American Association of Petroleum Geologists Bulletin* 95:105–146.

Jones GD, Collins JF, Xiao Y, Kenter JAM, Harris PM, Assaubaeva A. 2008. Geothermal convection in the Tengiz reservoir: a mechanism for generating burial karst? *In* Sasowsky ID, Feazel CT, Mylroie JE, Palmer AN, Palmer MV (Editors). *Karst from Recent to Reservoirs*, Special Publication 14: Karst Waters Institute, Leesburg, Virginia. p. 104.

Jones GD, Xiao Y. 2006. Geothermal convection in the Tengiz carbonate platform, Kazakhstan: reactive transport models of diagenesis and reservoir quality. *American Association of Petroleum Geologists Bulletin* 90:1251–1272.

Keim L, Schlager W. 2001. Quantitative compositional analysis of a Triassic carbonate platform (Southern Alps, Italy). *Sedimentary Geology* 139:261–283.

Kenter JAM, Harris PM, Collins JF, Weber LJ, Kuanysheva G, Fischer DJ. 2006. Late Visean to Bashkirian platform cyclicity in the central Tengiz buildup, Precaspian Basin, Kazakhstan: depositional evolution and reservoir development. *In* Harris PM, Weber LJ (Editors). *Giant Hydrocarbon Reservoirs of the World: From Rocks to Reservoir Characterization and Modeling*, Memoir 88: American Association of Petroleum Geologists/SEPM (Society for Sedimentary Geology), Tulsa, Oklahoma. p. 7–53.

Kenter JAM, Hoeflaken F, Bahamonde JR, Bracco Gartner GL, Keim L, Besems RE. 2002. Anatomy and lithofacies of an intact and seismic-scale Carboniferous carbonate platform (Asturias, NW Spain): analogues of hydrocarbon reservoirs in the Pricaspian Basin (Kazakhstan). *In* Zempolich W, Cook H (Editors). *Paleozoic Carbonates of the Commonwealth of Independent States (CIS): Subsurface Reservoirs and Outcrop Analogs*, Special Publication 74: SEPM (Society for Sedimentary Geology), Tulsa, Oklahoma. p. 185–207.

Kerans C. 1985. *Petrology of Devonian and Carboniferous Carbonates of the Canning and Bonaparte Basins*, Report 12: Western Australia Mining and Petroleum Research Institute, Perth. 203 p.

Kerans C, Hurley NF, Playford PE. 1986. Marine diagenesis in Devonian reef complexes of the Canning Basin, Western Australia. *In* Schroeder JH, Purser BH (Editors). *Reef Diagenesis*: Springer–Verlag, Berlin. p. 357–380.

King GR, Jones M, Tankersley T, Flodin E, Jenkins S, Zhumagulova A, Eaton W, Bateman P, Laidlaw C, Fitzmorris R, Ma X, Dagistanova K. 2012. Use of brown-field design methods for post-processing conventional history match results. *In Proceedings of the SPE Annual Technical Conference and Exhibition;* October 8–12, 2012; San Antonio, Texas. Society of Petroleum Engineers, Richardson, Texas. doi:10.2118/159341-MS. 12 p.

Machel HG. 1987. Some aspects of diagenetic sulphate-hydrocarbon redox reactions. *In* Marshall JD (Editor). *Diagenesis of Sedimentary Sequences*, Special Publication 36: Geological Society, London. p. 15–28.

Machel HG. 1998. Gas souring by thermochemical sulfate reduction at 140° C: discussion. *American Association of Petroleum Geologists Bulletin* 82:1870–1873.

Machel HG. 2001. Bacterial and thermochemical sulfate reduction in diagenetic settings—old and new insights. *Sedimentary Geology* 140:143–175.

Madi A, Bourque PA, Mamet BI. 1996. Depth-related ecological zonation of a Carboniferous carbonate ramp: upper Visean of Bechar Basin, western Algeria. *Facies* 35:59–80.

Madi A, Savard M, Bourque PA, Chi G. 2000. Hydrocarbon potential of the Mississippian carbonate platform, Bechar Basin, Algerian Sahara. *American Association of Petroleum Geologists Bulletin* 84:266–287.

Mamet BL. 1992. Paleogeographie des algues calcaires marines carboniferes. *Canadian Journal of Earth Science* 29:174–194.

Martindale W, Boreen TD. 1997. Temperature-stratified Mississippian carbonates as hydrocarbon reservoirs—examples from the foothills of the Canadian Rockies. *In* James NP, Clarke JAD (Editors). *Cool-Water Carbonates*, Special Publication 56: SEPM (Society for Sedimentary Geology), Tulsa, Oklahoma. p. 391–409.

Moore CH. 1989. *Carbonate Diagenesis and Porosity*, Developments in Sedimentology 46: Elsevier, New York. 338 p.

Morad S, Ketzer JM, De Ros LF. 2000. Spatial and temporal distribution of diagenetic alterations in siliciclastic rocks: implications for mass transfer in sedimentary basins. *Sedimentology* 47(Supplement 1):95–120.

Morse JW, Mackenzie FT. 1990. *Geochemistry of Sedimentary Carbonates*, Developments in Sedimentology 48: Elsevier, New York. 707 p.

Narr W. 1996. Estimating average fracture spacing in subsurface rock. *American Association of Petroleum Geologists Bulletin* 80:1565–1586.

Narr W, Fischer DJ, Harris PM, Heidrick T, Robertson BT, Payrasyan K. 2004. Understanding and predicting fractures at Tengiz—a giant, naturally fractured reservoir in the Caspian Basin of Kazakhstan (Abstract): American Association of Petroleum Geologists International Meeting Abstracts volume, Cancun, Mexico, October 24–27, 2004.

Narr W, Flodin E. 2012. Fractures in steep-rimmed carbonate platforms: comparison of Tengiz Reservoir, Kazakhstan, and outcrops in Canning Basin, NW Australia (Abstract): American Association of Petroleum Geologists Annual Meeting Abstracts volume, Long Beach, California, April 22–25, 2012.

Narr W, Schechter DS, Thompson LB. 2006. *Naturally Fractured Reservoir Characterization*: Society of Petroleum Engineers (SPE), Richardson, Texas. 112 p.

Orr WL. 1977. Geological and chemical controls on the distribution of hydrogen sulfide in natural gas. *In* Campos R, Goni J (Editors). *Advances in Organic Geochemistry*: Enadisma, Madrid. p. 571–597.

Osleger DA. 1998. Sequence architecture and sea-level dynamics of upper Permian shelfal facies, Guadalupe Mountains, southern New Mexico. *Journal of Sedimentary Research* 68:327–346.

Palmer AN. 1991. Origin and morphology of limestone caves. *Geological Society of America Bulletin* 103:1–21.

Phelps RM, Kerans C. 2007. Architectural characterization and three-dimensional modeling of a carbonate channel-levee complex: Permian San Andres Formation, Last Chance Canyon, New Mexico, USA. *Journal of Sedimentary Research* 77:939–964.

Playford PE. 1980. Devonian "Great Barrier Reef" of Canning Basin, Western Australia. *American Association of Petroleum Geologists Bulletin* 64:814–840.

Playford PE. 1984. Platform-margin and marginal-slope relationships in Devonian reef complexes of the Canning Basin, Western Australia *In* Purcell PG (Editor). *The Canning Basin, WA:* Geological Society of Australia and Petroleum Exploration Society of Australia, Canning Basin Symposium Volume, Perth. p. 189–214.

Playford PE. 2002. Palaeokarst, pseudokarst, and sequence stratigraphy in Devonian reef complexes of the Canning Basin, Western Australia. *In* Keep M, Moss SJ (Editors). *The Sedimentary Basins of Western Australia*: Proceedings of the Petroleum Exploration Society of Australia Symposium, Perth. p. 763–793.

Playford PE. 2009. *Guidebook to the Geomorphology and Geology of Devonian Reef Complexes of the Canning Basin, Western Australia*, Record 2009/5: Geological Survey of Western Australia, Perth. 72 p.

Playford PE, Hocking RM, Cockbain AE. 2009. *Devonian Reef Complexes of the Canning Basin, Western Australia*, Bulletin 145: Geological Survey of Western Australia, Perth. 444 p.

Playford PE, Hurley NF, Kerans C, Middleton MF. 1989. Reefal platform development, Devonian of the Canning Basin, Western Australia. *In* Crevello PD, Wilson JL, Sarg JF, Read JF (Editors). *Controls on Carbonate Platform and Basin Development*, Special Publication 44: SEPM (Society for Sedimentary Geology), Tulsa, Oklahoma. p. 187–202.

Playton TE. 2008. Characterization, variations, and controls of reef-rimmed carbonate foreslopes [PhD thesis]: University of Texas at Austin, 283 p.

Playton TE, Janson X, Kerans C. 2010. Carbonate slopes. *In* James NP, Dalrymple RW (Editors). *Facies Models 4*, GEOtext 6: Geological Association of Canada, St. John's, Newfoundland. p. 449–476.

Pottorf RJ, Tseng H-Y, Hicks P, Putney K, Curry D, Mankiewicz P, Gray G. 2003. Timing, distribution and origin of bitumen formation at Tengiz Field, Kazakhstan. *In* Cubbitt J, England W, Larter S, Macleod G (Editors). *Geochemistry of Reservoirs II—Linking Reservoir Engineering and Geochemical Models*; February 3–4, 2003; Geological Society, London.

Schoellkopf NB, Hallager WS. 1998. Burial history and charge model, Tengiz Field, Kazakhstan (abstract): American Association of Petroleum Geologists Annual Meeting Abstracts volume, May 17–20, 1998; Salt Lake City, Utah.

Stephens NP, Sumner DY. 2003. Famennian microbial reef facies, Napier and Oscar Ranges, Canning Basin, Western Australia. *Sedimentology* 50:1283–1302.

Stoessel RK. 1992. Effects of sulfate reduction on $CaCO_3$ dissolution and precipitation in mixing zone fluids. *Journal of Sedimentary Petrology* 62:873–880.

Sullivan MJ, Belanger DL, Skalinksi MT, Jenkins SD, Dunn P. 2006. Permeability from production logs—method and application. *In* Proceedings of the SPE Annual Technical Conference and Exhibition; September 24–27, 2006; San Antonio, Texas; Society of Petroleum Engineers, Richardson, Texas. doi:10.2118/102894-MS. 16 p.

Tankersley T, Narr W, King G, Camerlo R, Zhumagulova A, Skalinski M, Pan Y. 2010. Reservoir modelling to characterize dual porosity, Tengiz Field, Republic of Kazakhstan. *In* Proceedings of the SPE Caspian Carbonates Technology Conference; November 8–10, 2010; Atyrau, Kazakhstan; Society of Petroleum Engineers, Richardson, Texas. doi:10.2118/139836-MS. 15 p.

Terzaghi R. 1965. Sources of errors in joint surveys. *Geotechnique* 15:287–304.

Tinker SW. 1998. Shelf-to-basin facies distributions and sequence stratigraphy of a steep-rimmed carbonate margin: Capitan depositional system, McKittrick Canyon, New Mexico and Texas. *Journal of Sedimentary Research* 68:1146–1174.

Tseng H-Y, Pottorf RJ. 2003. The application of fluid inclusion PVT analysis to studies of petroleum migration and reservoirs. *Journal of Geochemical Exploration* 78–79:433–436.

Tursinbayeva D, Lindsell K, Zalan T, Dunger D, Kassenov B, Howery R. 2012. Tengiz Field surveillance: planning strategy and implementation. *In* Proceedings of the Abu Dhabi International Petroleum Conference and Exhibition; November 11–14, 2012; Abu Dhabi, United Arab Emirates; Society of Petroleum Engineers, Richardson, Texas. doi:10.2118/160957-MS. 10 p.

Vecsei A, Sanders DK, Bernoulli D, Eberli GP, Pignatti JS. 1998. Cretaceous to Miocene sequence stratigraphy and evolution of the Maiella carbonate platform margin, Italy. *In* De Graciansky P-C, Hardenbol J, Jacquin T, Vail PR (Editors). *Mesozoic and Cenozoic Stratigraphy of European Basins*, Special Publication 60: SEPM (Society for Sedimentary Geology), Tulsa, Oklahoma. p. 53–74.

Wallace MW, Kerans C, Playford PE, McManus A. 1991. Burial diagenesis in the Upper Devonian reef complexes of the Geikie Gorge region, Canning Basin, Western Australia. *American Association of Petroleum Geologists Bulletin* 75:1018–1038.

Warner JL, Baskin DK, Hwang RJ, Carlson RMK, Clark ME. 2007. Geochemical evidence for two stages of hydrocarbon emplacement and the origin of solid bitumen in the giant Tengiz Field, Kazakhstan. *In* Yilmaz PO, Isaksen GH (Editors). *Oil and Gas of the Greater Caspian Area*, Studies in Geology 55: American Association of Petroleum Geologists, Tulsa, Oklahoma. p. 165–169.

Weber LJ, Francis BP, Harris PM, Clark M. 2003. Stratigraphy, lithofacies, and reservoir distribution, Tengiz Field, Kazakhstan. *In* Ahr WM, Harris PM, Morgan WA, Somerville ID (Editors). *Permo-Carboniferous Carbonate Platforms and Reefs*, Special Publication 78/Memoir 83: SEPM (Society for Sedimentary Geology) and American Association of Petroleum Geologists, Tulsa, Oklahoma. p. 351–394.

Yurewicz DA. 1977. Origin of the massive facies of the lower and middle Capitan Limestone (Permian), Guadalupe Mountains, New Mexico and West Texas. *In* Hileman ME, Mazzullo SJ (Editors). *Upper Guadalupian Facies, Permian Reef Complex, Guadalupe Mountains, New Mexico and West Texas*, Publication 77-16: SEPM Permian Basin Section, Midland, Texas. p. 45–92.